INTERFACIAL REACTION KINETICS AND MICROSTRUCTURAL EVOLUTION OF C/SiC COMPOSITES TO METAL JOINTS

A THESIS SUBMITTED TO
THE GRADUATE SCHOOL OF NATURAL AND APPLIED SCIENCES
OF
MIDDLE EAST TECHNICAL UNIVERSITY

BY

SİMGE SALTIK

IN PARTIAL FULFILLMENT OF THE REQUIREMENTS
FOR
THE DEGREE OF DOCTOR OF PHILOSOPHY
IN
METALLURGICAL AND MATERIALS ENGINEERING

SEPTEMBER 2021

Approval of the thesis:

INTERFACIAL REACTION KINETICS AND MICROSTRUCTURAL EVOLUTION OF C/SiC COMPOSITES TO METAL JOINTS

submitted by **SİMGE SALTIK** in partial fulfillment of the requirements for the degree of **Doctor of Philosophy** i**n Metallurgical and Materials Engineering, Middle East Technical University** by,

Prof. Dr. Halil Kalıpçılar
Dean, Graduate School of **Natural and Applied Sciences** _____

Prof. Dr. Cemil Hakan Gür
Head of the Department, **Metallurgical and Materials Eng.** _____

Prof. Dr. Arcan F. Dericioğlu
Supervisor, **Metallurgical and Materials Eng., METU** _____

Examining Committee Members:

Prof. Dr. Kadri Aydınol
Metallurgical and Materials Eng., METU _____

Prof. Dr. Arcan F. Dericioğlu
Metallurgical and Materials Eng., METU _____

Assoc. Prof. Dr. Ziya Esen
Materials Science and Eng., Çankaya Uni. _____

Assoc. Prof. Dr. Benat Koçkar
Mechanical Eng., Hacettepe Uni _____

Assist. Prof. Dr. Simge Çınar Aygün
Metallurgical and Materials Eng., METU _____

Date: 09.09.2021

I hereby declare that all information in this document has been obtained and presented in accordance with academic rules and ethical conduct. I also declare that, as required by these rules and conduct, I have fully cited and referenced all material and results that are not original to this work.

Name Last name : Simge Saltık

Signature :

ABSTRACT

INTERFACIAL REACTION KINETICS AND MICROSTRUCTURAL EVOLUTION OF C/SiC COMPOSITES TO METAL JOINTS

Saltık, Simge
Doctor of Philosophy, Metallurgical and Materials Engineering
Supervisor: Prof. Dr. Arcan F. Dericioğlu

September 2021, 171 pages

In the present study, joining of two dissimilar materials namely C/SiC composites and Ti6Al4V alloys by brazing using Ag-Cu based brazing filler alloys have been investigated. The effect of active Ti element content, additive particle size/amount in the filler alloy together with the reinforcement structure, material properties of the C/SiC composite on the interface evolution mechanism and resulting mechanical performance of the brazed joints have been examined. Additionally, apart from the brazing studies, the relationship between brazing performance and wetting behavior have been correlated by modeled wetting experiments conducted under actually applied brazing conditions.

According to the measured contact angle values obtained from the wetting experiments, it can be stated that Ticusil filler alloy with the highest amount of Ti considerably improves the wetting behavior of both monolithic SiC ceramic and C/SiC ceramic composite material with contact angles of 10° and 15°, respectively. 915 °C and 15 min were determined to be the optimized brazing parameters for this brazing filler alloy to ensure almost complete wetting and a uniform reaction layer for effective adhesion of the C/SiC composite surface. Resulting joints with ~1 μm

thick reaction layer, which were obtained using Ticusil brazing under this condition had the highest shear strength of ~33 MPa.

Varying amounts of SiC particles of two different sizes (nano and micro scale) were incorporated into the Ticusil brazing filler alloy to control and optimize its wetting characteristics on ceramic surfaces. In this regard, 2 wt% nano level SiC and 1 wt% micro level SiC particle addition led to the highest improvement in the shear strength of the joints by 35% and 8%, respectively, compared to their no additive containing versions. Although the recorded contact angle values were nearly same (42° for 2 wt% nano level and 37° for 1 wt% micron level), higher increment in the mechanical performance was achieved by the addition of nano level SiC particles due to more homogeneous reinforcement effect of the nanoparticles. Results indicated that the optimum contact angle for the highest joint performance is ~40° for both nano and micron level additive containing Ticusil filler alloy.

Composites reinforced by two different types of carbon fiber structures, namely 3D and 2D, had similar wettability characteristics, and hence showed similar reaction layer and interlayer morphologies. In addition to this, carbon nanotube (CNT) impregnation to the matrix of the 2D C/C-SiC composites improved the wettability of its surface by the brazing filler alloy. On the other hand, despite better wetting 2D C/C-SiC composites with or without CNT impregnation showed inferior mechanical characteristics which can be attributed to the level of residual stresses caused by material property variances as well as imperfections at the joint interlayer.

Keywords: Brazing, Wetting, C/SiC Composites, Microstructure, Mechanical Properties

ÖZ

C/SiC KOMPOZİT-METAL BAĞLANTILARDA ARAYÜZEY REAKSİYON KİNETİĞİ VE MİKROYAPISAL EVRİMİ

Saltık, Simge
Doktora, Metalurji ve Malzeme Mühendisliği
Tez Yöneticisi: Prof. Dr. Arcan F. Dericioğlu

Eylül 2021, 171 sayfa

Bu çalışmada, C/SiC kompozit ve Ti6Al4V alaşımı olmak üzere iki farklı malzemenin Ag-Cu bazlı dolgu alaşımı ile lehimlenmesi incelenmiştir. Aktif Ti element miktarı, katkı malzemesi partikül boyutu/miktarı, C/SiC kompozit takviye yapısı ve malzeme özelliklerinin arayüzey reaksiyon kinetiği ve lehimli bağlantıların mekanik performansına etkileri araştırılmıştır. Lehimleme çalışmalarına ek olarak lehimleme performansı ve ıslatma davranışı arasındaki ilişki, lehimleme koşulları altında gerçekleştirilen ıslatma deneyleri ile modellenmiştir.

Islatma deneylerinde ölçülen temas açısı değerlerine göre, dolgu malzemesi içeriğindeki aktif Ti elementi miktarının artması hem monolitik SiC seramik hem de C/SiC kompozit için sırasıyla 10° ve 15° gözlemlenen temas açısı değerleri ile önemli ölçüde iyileşme sağlamıştır. Bu dolgu malzemesi alaşımı için için 915 °C ve 15 dakika, C/SiC kompozit yüzeyinin etkin bir şekilde ıslatılması ve homojen reaksiyon katmanı oluşumu için optimum lehimleme parametreleri olarak belirlenmiştir. Bu koşullar ile Ticusil dolgu alaşımı kullanılarak elde edilen ~1 μm kalınlığında reaksiyon tabakasına sahip bağlantılar ~33 MPa ile en yüksek kesme mukavemetine sahiptir.

Seramik yüzeylerde ıslatma özelliklerini kontrol ve optimize etmek amacıyla Ticusil dolgu alaşımına iki farklı boyutta (nano ve makro ölçekli) değişen miktarlarda SiC partikülleri eklenmiştir. Bu kapsamda nano seviyede ağırlıkça %2 SiC ve mikro seviyede ağırlıkça %1 SiC eklenmesi, bağlantıların kesme mukavemetini katkız dolgu alaşımına kıyasla sırasıyla %35 ve %8 oranında iyileştirmiştir. Kaydedilen temas açısı değerleri neredeyse aynı olmasına rağmen (ağırlıkça %2 nano seviyesi için 42° ve ağırlıkça %1 mikron seviyesi için 37°), nanoparçacıkların daha homojen takviye etkisi sebebiyle nano seviyede SiC katkı içeren bağlantıların mekanik performansında daha yüksek artış gözlemlenmiştir. Mikron ve nano seviyedeki katkı içen Ticusil dolgu alaşımı koşullarında en yüksek bağlantı performansı için optimum temas açısı değeri ~40° tespit edilmiştir.

3B ve 2B olmak üzere iki farklı tipte karbon fiber yapı ile güçlendirilmiş kompozitler benzer ıslanabilirlik özelliklerine sahiptir ve bu nedenle benzer reaksiyon katmanı ve ara katman morfolojileri göstermişlerdir. Buna ek olarak, 2D C/C-SiC kompozitlerinin matrisine karbon nanotüp eklenmesi, dolgu alaşımı ile yüzeyinin ıslanabilirlik davranışı iyileştirmiştir. Diğer bir taraftan, CNT eklenmiş veya eklenmemiş 2D C/C-SiC kompozitler daha iyi ıslanma davranışı göstermelerine rağmen, arayüzeyde gözlemlenen boşluk oluşumları ve malzeme özelliklerinin farklı olması gerekçesiyle arayüzeyde oluşan kalıntı seviyelerinin farklılığı mekanik mukavemette gözlemlenen değişken değerler ile ilişkilendirilmektedir.

Anahtar Kelimeler: Lehimleme, Islatma, C/SiC Kompozit, Mikroyapı, Mekanik Özellikler

To my beloved family

ACKNOWLEDGMENTS

My sincere thanks goes to my supervisor Prof. Dr. Arcan F. Dericioğlu for his continuous encouragement to begin my graduate study. I am indebted to him for leading me to the field of research and shaping my academic vision and background with his endless academic experience.

I would like express my sincere appreciation to Assoc. Prof. Dr. Ziya Esen for spending his valuable time for reviewing my paper, providing feedback, supporting and motivation throughout the study.

I would like to thank Dr. Olcay Elmalı Meço and Barış Akgün for their support and guidance.

I must also acknowledge ‘Nablatar” for sharing good and bad times through my master and phd period.

I would like also to express my deep appreciation to my mother, my father and my brother who have been patient through the doctorate period. I owe a depth to my family for their endless love, support and encouragement throughout my life.

I am also grateful to Saltık family for their support and encouragement.

Last, but not least, I would like to express my sincere appreciation to my husband, Ege Cem, for his love, endless support and encouragement. He has always motivated me to overcome difficulties and he has never left me alone.

TABLE OF CONTENTS

LIST OF TABLES

TABLES

LIST OF FIGURES

FIGURES

LIST OF ABBREVIATIONS

1D	One-dimensional
2D	Two-dimensional
3D	Three-dimensional
ABA	Active Brazing Alloy
ASTM	American Society for Testing and Materials
C/C	Carbon/Carbon Preform
C/C-SiC	Carbon Fiber Reinforced Carbon-Silicon Carbide Matrix
C/SiC	Carbon Fiber Reinforced Silicon Carbide Matrix
CCD	Charged Coupled Device
CMC	Ceramic Matrix Composite
CNT	Carbon Nano Tube
CTE	Coefficient of Thermal Expansion
CVI	Chemical Vapour Infiltration
DSC	Differential Scanning Calorimeter
EDS	Energy Dispersive X-ray Spectroscopy
FEM	Finite Element Analysis
LSI	Liquid Silicon Infiltration
SEM	Scanning Electron Microscope
TC4	Ti6Al4V Alloy
XRD	X-ray Diffraction

LIST OF SYMBOLS

A	contact area
Cp	specific heat
K	reaction rate constant
k_0	pre-exponential factor
P	applied force
Q	activation energy
R	gas constant
t	time
T	temperature
X	reaction layer thickness
α	thermal diffusivity
θ	contact angle
λ	thermal conductivity
ρ	density
τ	lap-shear strength

CHAPTER 1

INTRODUCTION

Carbon fibre reinforced silicon carbide (C/SiC) matrix ceramic composites presents low density, high mechanical strength and oxidation resistance. Since these materials maintain their mechanical properties at extreme temperatures, they are candidate materials to be used in hot structural parts of the rocket systems exposed to high thermal stresses at high temperatures and advanced friction systems. Ti6Al4V alloy, on the other hand, is used in aerospace, automotive, and marine applications for extremely demanding structural parts because it has outstanding specific mechanical properties, as well as strong corrosion resistance, free machining, and workability.

Complex-shape C/SiC composite part production is difficult because manufacturing process demands a long production time and a high cost. Furthermore, due to the absence of effective integration methods to other ceramic matrix composites or metallic parts, the use of C/SiC composite parts is limited. The use of these materials is limited due to problems that emerge during joining, which often leads to the search for alternative materials that fulfill the desired material standards. As a result, developing C/SiC composite joining techniques to other ceramic matrix composites or metals in order to construct large-scale complicated structural components is critical.

Among the traditional integration methods, brazing stands out as a beneficial technique due to its ease of use, low cost, and versatility for generating complicated forms and diverse joint geometries at a high rate of reproduction. To achieve precise joining during brazing, filler alloys used for brazing must have good wetting on the

base material surfaces. Because of their ionic/covalent bonding characters, ceramics have low wettability when compared to metallic parts. Wettability is also affected negatively by chemical and structural inhomogeneity of the ceramic matrix composite surfaces. Alternative strategies for improving the wettability of ceramic matrix composites have been offered, including surface metallization and the use of active brazing fillers. Surface-active elements (Ti, Zr, Hf, or Nb, for example) are present in active brazing filler alloys, which promote not only wetting but also adhesion and bonding. Interfacial reactions between the brazing filler alloy and the ceramic matrix composite in active brazing systems result in the production of reaction layers, which affect wettability, brazing performance, and the mechanical properties of brazed parts. Therefore, type and quantity of phases formed in reaction layer as well as the thickness of the layer are important factors controlling the mechanical properties. In order to have a homogenous and continuous reaction layer formation in the brazed parts, the brazing alloy should wet to surfaces of brazed parts adequately.

In this regard, the present study investigates the effects of active Ti element content, additive particle size/amount, reinforcement direction and material properties of the C/SiC composite on the interface evolution mechanism and resulting mechanical performance of the brazed joints. Additionally, apart from the brazing experiments, it is aimed to simulate the relationship between brazing performance and wetting behavior by performing all the conditions in brazing conditions in the wetting experiments.

To the best of authors' knowledge, for C/SiC composite and active brazing alloy system, there is no detailed work about the correlation between the reaction layer thickness/composition and the mechanical properties of C/SiC composite-Ti6Al4V alloy joints brazed using Ticusil brazing filler alloy. There is also limited information on the wetting and spreading behaviour of Ticusil brazing alloy on C/SiC composites at high temperatures, which in turn affect the homogeneity and continuity of the

reaction layer that has direct influence on the mechanical properties. Moreover, the relationship between the reaction layer formation, the wettability of the C/SiC composite surface and the mechanical properties of the brazed joints have not been discussed comprehensively. Therefore, to fill the research gap in the literature about the joining of C/SiC composite and Ti6Al4V, current study has focused upon the effect of processing parameters on the thickness/microstructure of the reaction layer has been investigated and discussed in detail by comparing the experimental reaction layer thickness values with those obtained from theoretical diffusion models. Moreover, many studied in the literature have been devoted to understand the additive content-joint performance relationship. Although the wetting behavior of the brazing filler alloy is the most important characteristic for effective joining, the effects of additive amount and size on the wetting behavior of the brazing filler alloy are not thoroughly researched. Therefore, the relationship between additive particle size/content and wetting behaviour of the brazing filler alloy is simulated and optimum wetting conditions for the high mechanical performance of the joint is analyzed.

This thesis is divided into five main chapters that give information about the topics covered in the study. Chapter 2 is subdivided into various parts to present a detailed background about the main components of the study. First of all, properties of the base materials as well as the requirements for engineering applications are being explained, basically. Additionally integration techniques of ceramic matrix composites to metals, their advantages and disadvantages are discussed, especially, brazing method is explained briefly. Furthermore, crucial parameters for the brazing process, as well as the specifics of active brazing, are examined in detail. Apart from these, Chapter 2 discusses wetting mechanisms and factors that influence wetting behavior. In Chapter 3, properties of materials used in the current study, details of brazing process utilized in production of C/SiC composite/metal joints and wetting experiments are explained in detail. In addition, the characterization approaches employed in the current study are covered in this chapter. Chapter 4 presents the

interface evolution mechanism and mechanical performance of the C/SiC composite/Ti6Al4V alloy brazed joints using different brazing filler alloys to understand the effects of the active titanium (Ti) element on the brazing performance of the brazed joints. Furthermore, the influence of the brazing filler composition on the contact angle morphology and its change with time is also investigated. Secondly, this chapter has focused upon the effect of brazing parameters on the reaction layer formation at the interface region of C/SiC composite and Ti6Al4V alloy when Ticusil brazing alloy is used. Additionally, spreading behavior of the Ticusil brazing alloy on C/SiC composite surfaces has been examined at various temperatures and holding time via wetting tests to enhance the joining performance of C/SiC composite to Ti6Al4V alloy. Thirdly, influence of particle addition to the filler alloy on the interfacial reaction and resulting mechanical properties of the brazed joints has been investigated. The microstructural evolution and mechanical strength as well as the wetting behavior of the additive containing C/SiC composite/Ti6Al4V alloy joints are analyzed in detail. Finally, effects of various material characteristics and reinforcing structures of the ceramic matrix composite on the wetting behavior and related brazing performance of the C/SiC composite/ Ti6Al4V alloy joints have been discussed. Finally, Chapter 5 summarizes the concluding remarks obtained during the study and the recommendations for future research.

CHAPTER 2

LITERATURE REVIEW

This chapter is subdivided into various parts to present a detailed background about the main components of the study. Firstly, properties of the base materials as well as the requirements for engineering applications are being explained, basically. Additionally integration techniques of ceramic matrix composites to metals, their advantages and disadvantages are discussed, especially, brazing method is explained briefly. Moreover, crucial parameters for the brazing process, as well as the specifics of active brazing, are examined in detail. Apart from these, wetting mechanisms and factors that influence wetting behavior will be mentioned in this chapter.

2.1 Ceramic Matrix Composites (CMC)

Advanced materials with high mechanical strength and temperature resistance, are required for engineering and industrial applications. Ceramics materials are known to have higher temperature tolerance than metals and polymers. Despite having desirable properties, monolithic ceramics lack plasticity and exhibit brittle behavior when subjected to thermal and mechanical loading [1]. Reinforcements materials are used to improve the toughness behavior of ceramics in ceramic matrix to overcome this disadvantage [2]. A composite is a material made up of a reinforcing material and a matrix material that work together to offer qualities that neither single item can provide [3,4]. The reinforcement material increases the mechanical performance of the matrix, in parallel, the matrix material protects the reinforcement from failure and supply mechanical stability under load conditions [2,5]. Stress-strain behavior comparison for ceramics and CMCs is presented in Figure 2.1.

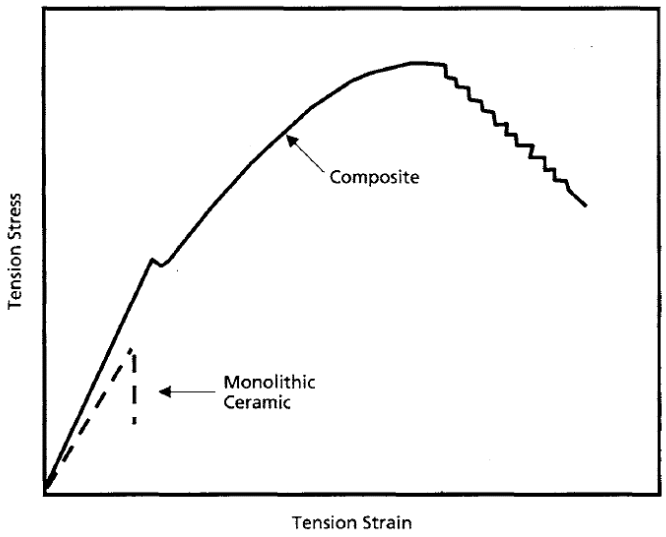

Figure 2.1 Stress-strain behavior comparison for ceramics and ceramic matrix composites [3].

2.2 C/SiC Composites

When compared to other engineering materials, C/SiC composites present the highest specific strength at high temperatures. Therefore, these materials are frequently used in parts that require high temperature resistance, high mechanical performance and low density [6,7]. C/SiC composites are extensively employed in structural parts instead of monolithic ceramics due to their improved mechanical capabilities at high temperatures and oxidation resistance. C/SiC composites have a wide variety of applications that are influenced by service temperature and time (Figure 2.2) [8-10].

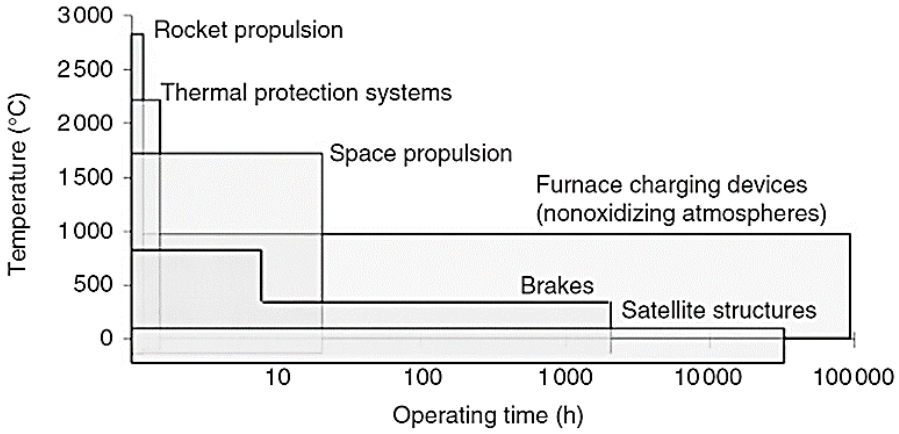

Figure 2.2 Service temperature and time-dependent application areas of C/SiC [10].

The microstructure of the C/SiC composite and its composition are determined by the manufacturing process, the materials used in the manufacturing, and the quantity and dimension of the reinforcement material [11]. Chemical vapor infiltration (CVI), polimer infiltration and pyrolysis (PIP) and liquid silicon infiltration (LSI) are the production methods of the C/SiC composites. Among these methods, the CVI method produces stoichiometric and uniform SiC matrix, while the PIP and LSI processes rely on a precursors to convert the polymeric matrix to SiC [12]. SEM microstructures based on different production methods are given in Figure 2.3.

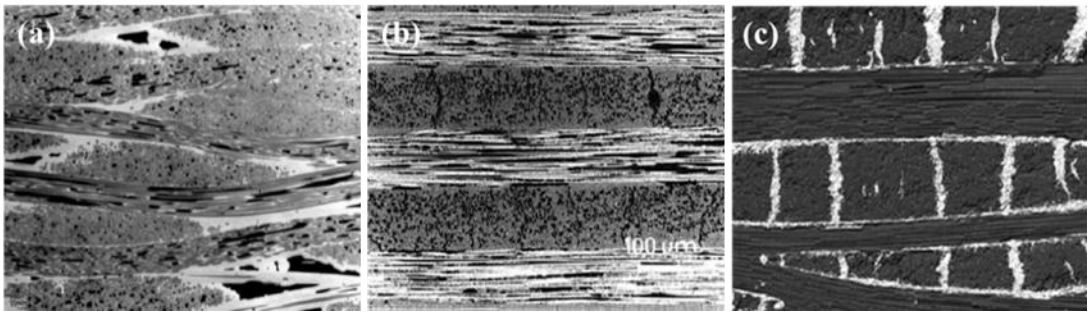

Figure 2.3 Microstructures of C/SiC composites depending on manufacturing methods a) Chemical vapor infiltration (CVI), b) Polymer infiltration and pyrolysis (PIP) and c) Liquid silicon infiltration (LSI) [13].

Density and porosity content of the C/SiC composites are also influenced by the manufacturing process. Density and porosity contents are in the interval of 1.8–2.4 g/cm^3 and 1-12 %, respectively. The highest porosity content with 8-12 % is observed for the CVI, although LSI makes the porosity content up to 1-4 % levels [13,14].

In addition to manufacturing method, material properties of the C/SiC composites are affected from the dimension of the reinforcement structure (1D, 2D and 3D etc.) and volume percentages of the carbon fibers [15]. The material property change of the C/SiC composites in accordance with the manufacturing method and reinforcement direction is given in Table 2.1. The C/SiC composites manufactured using the LSI process reveal less lower mechanical strength than CVI and PIP methods, as shown in Table 2.1.

Table 2.1 Material of C/SiC composites manufactured by different methods [16,17].

Property	**CVI**	**PIP**	**MI**
Fiber Architecture	3D fabrics	2D fabrics	2D fabrics
Fiber Content (vol.%)	45	50	60
Density (g/cm^3)	2.1	1.8	>1.8
Porosity	10	8	2
Tensile Strength (MPa)	350	260	110
Strain to failure (%)	0.9	0.53	0.25-0.3
Young's Modulus (GPa)	90	110	50-55
Flexural Strength (MPa)	500	240	80-140
Thermal Conductivity (W/m.K)	14.3	14	28-33
CTE$_\perp$ (10^{-6} K^{-1})	3	5	6-6.5
CTE$_\parallel$ (10^{-6} K^{-1})	5	2	1.0-1.5

Comparing with the C/C composite materials, C/SiC composites present higher oxidation resistance because SiC matrix results in a proper oxygen barrier [18,19].

2.3 Ti6Al4V Alloys

Titanium can be the form of pure element and alloy. Alloy forms are usually classified as alpha (α), near α alloys, alpha-beta (α-β), near β alloys and beta (β) [20,21]. Material properties of Titanium alloys are given in Figure 2.4 and the key features of the titanium alloys are shared in Figure 2.5. As presented in Figure 2.4, with increasing content of the β phases, density of the alloy, strain rate sensitivity and manufacturability increase [22,23]. However, creep strength and weldability of the part mainly improve with high content of α phases.

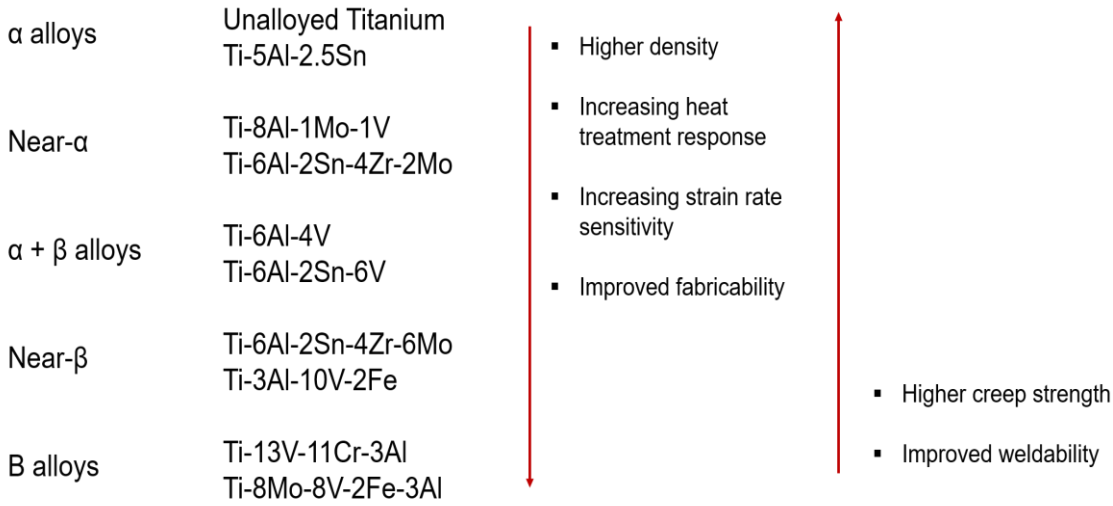

Figure 2.4 Material properties of Titanium Alloys [24].

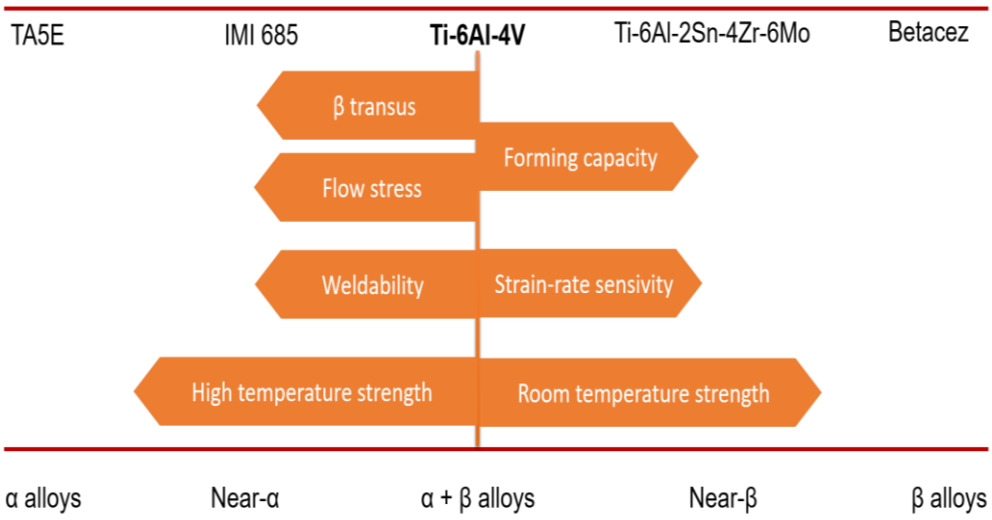

Figure 2.5 The key features of Titanium alloys [25].

The Ti6Al4V alloy is the α-β alloy that includes a phase stabilizer of 6 wt.% aluminum and 4 wt.% vanadium. The quantities of α-β phases, as well as the microstructure, differ depending on the form of heat treatment and cooling rate of the alloy. α-β phases result in higher strength and better creep resistance. Furthermore, α-β alloys are classified as heat treatable alloys [23]. Having lower content of β stabilizer makes the Ti6Al4V alloy be welded easily to other materials [21]. Another advantage of Ti6Al4V alloy is being compatible with carbon fiber reinforced polymer matrix composites (CFRP). Ti6Al4V alloy and carbon fibers are compatible in terms of galvanic corrosion [26].

The low density Ti6Al4V alloy presents high mechanical strength, high fracture toughness, high corrosion resistance [21,27]. In addition to outstanding material properties it also classified as biocompatible material. In the 1950s, this alloy was designed for aircraft structural applications [27]. Ti6Al4V alloy is ideal material for jet vane, static and rotating parts of the gas turbines, and structural part of the airframe applications because it has both a low density and a high mechanical strength. These alloys are employed in dental materials, surgical equipment, and other applications because of their biocompatibility and superior corrosion resistance.

Approximately 80 % of the aircraft applications are based on Ti6Al4V alloy. For instance, fuselage, nacelles, landing gear, wing, and empennage parts of the aircrafts are produced by this alloy [28].

Ti6Al4V alloy is available in a variety of cast and wrought forms. Generally, Ti6Al4V components are obtained by machining and hot working wrought materials. In this cases, process temperature and strain rate of deformation have the greatest impact on the final microstructure and the performance of the material. The material properties of the Ti6Al4V alloy is given in Table 2.2 [29].

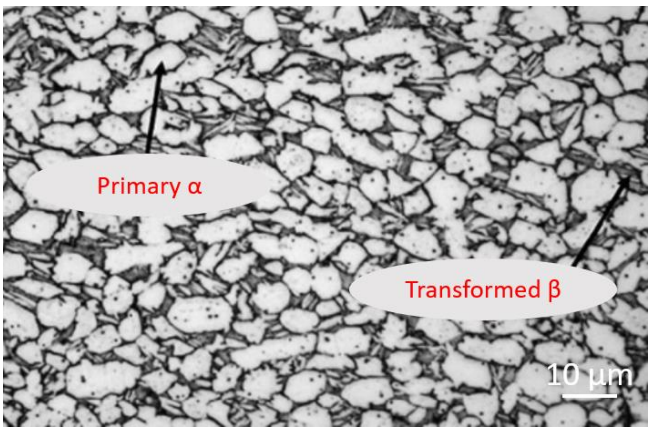

Figure 2.6 Microstructure of the Ti6Al4V alloy [30].

Table 2.2 The material properties of Ti6Al4V alloy [29].

Density (g/cm^3)	4.3
Hardness (HV)	300-400
Yield Strength (MPa)	800-1100
Tensile Strength (MPa)	900-1200
Elastic Modulus (GPa)	110-140
Beta Transus Temperature (°C)	995
Thermal Conductivity (W mC^{-1})	6.7

2.4 Ceramic Matrix Composites / Metal Joints

For aerospace and rocket applications, new processes to integrate ceramic matrix composites to metallic materials, ceramic materials and composite materials are required. Mainly the production of CMCs in a complex shaped geometry takes too much time and production cost. Moreover, difficulties faced in integration of CMCs to other materials limits their wide range usage application areas. Therefore, development of new joining technologies increases the utilization of the ceramic matrix composites [31,32].

CMC/metal joints can be used for leading edge applications, turbine engine components and air intake structures. The requirements for the CMC/metal joints can be summarized as follows [33]:

- Retaining high mechanical performance,
- Superior oxidation resistance,
- Stability under aggressive conditions,
- Low-cost manufacturing

Integration of CMC/metal joints can be categorized as four main methods: mechanical joining, adhesive bonding, diffusion bonding and brazing. Hence the only mechanical forces exist in joining, it is not reliable process for the extreme operating conditions. Adhesive bonding specially applied for polymer/polymer, polymer/CMC and CMC/CMC joints. Diffusion bonding and brazing techniques are applicable for the applications that are used to high temperature and aggressive environments. A list of the various joining techniques is given in Figure 2.7.

2.4.1 Mechanical Joining

Fastening or mechanical attachments are used to integrate the ceramic matrix composites into metallic materials. Although this method is the simplest way of integration, it is not reliable because of having only mechanical forces. Furthermore, stress concentration effects, hole positions, the usability of bolt materials at high

temperatures, bolt material - joint material property variations, and machining-related defects restrict the applicability of mechanical joints for CMC/metal components.

2.4.2 Adhesive Bonding

Adhesive bonding is the method of connecting materials by surface adhesion. The resulting forces that allow the joining can be classified as secondary bonding. Epoxies, acrylics, polyurethanes, silicones, and phenolics are some of the structural adhesive types available. Since all the types are made of polymeric materials, they have a low density, and they can be easily applicable to complex shape materials, they have advantages of sealing and insulating joints. Adhesive materials can not resist their material properties at high temperatures. As a matter of fact, the temperature-dependent destruction of the adhesive material may often result in an adhesive gap between the joint materials at operation conditions. Several environmental factors, such and solvent, can restrict the use and efficiency of adhesive materials [34].

2.4.3 Diffusion Bonding

Diffusion bonding allows joint materials to form a bond together by the interdiffusion of atoms. During the processing of the diffusion bonding method, pressure and temperature are applied simultaneously. The required temperature depends on the melting point of the joint materials. The pressure is needed to eliminate any voids that might exist due to the various surface properties of the joint materials. Although diffusion bonding results in good joint properties, the high temperatures and pressures required during processing restrict its use [35,36].

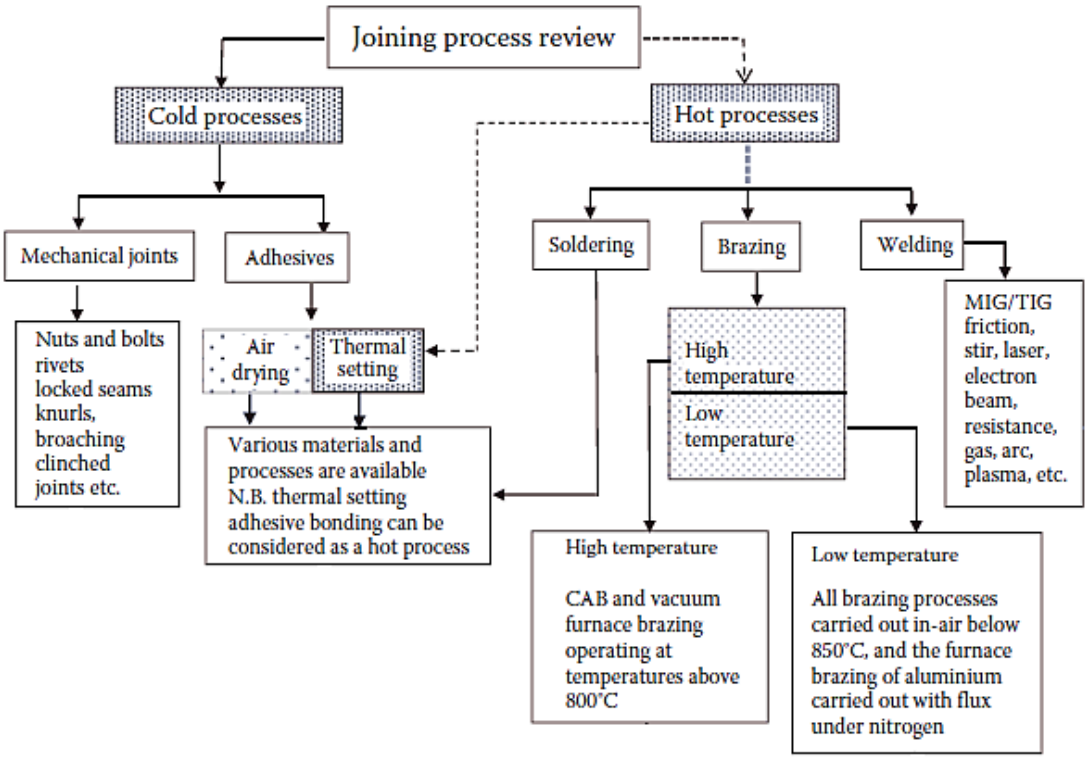

Figure 2.7 A list of the various joining techniques [37].

2.5 Brazing

Brazing is a joint technique in which a low-melting-point brazing alloy is used. Brazing alloy wets the surfaces of the joint materials as it melts, throughout the solidification process, a bond between the joint materials is produced. A brazed joint is depicted schematically in the diagram given in Figure 2.8.

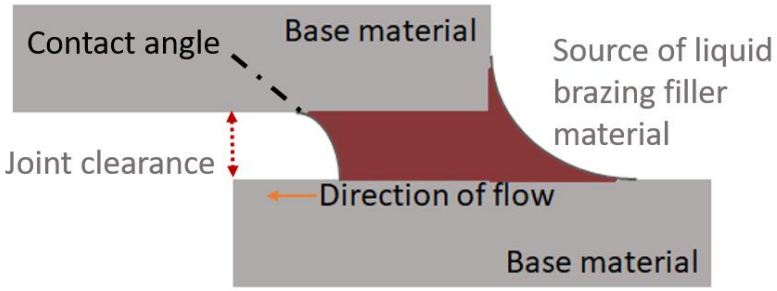

Figure 2.8 Schematic illustration of brazed joint.

The melting temperature of the filler material is what differentiates brazing and soldering. The procedure is known as soldering when the filler material's melting temperature is less than 450 °C. On the other hand, for brazing the filler material has a melting temperature higher than 450 °C. In welding metallic components are joined by applying heat to the base metal to cause melting or recrystallization. However, in brazing only the filler material melts during the joining application.

The following are the advantages of the brazing method [38,39]:

- simple method,
- high reproducibility,
- low cost,
- ideal joint size and shape adaptability,
- easy batch processing,
- low base material distortion,
- applicable to dissimilar materials,
- predictable thermal cycles.

2.5.1 Critical Factors for Brazing

While brazing appears to be a simple and straightforward procedure, the process often involves complex metallurgical and chemical processes both within the joint and on the surfaces of the materials involved. Braze joint configuration, type of brazing filler materials, and process variables in obtaining the desired properties in the brazing are the important factors to determine braze joint characteristics. These variables have a direct impact on the geometries and microstructures of braze joints, influencing their properties. Critical factors of the brazing process is summarized in Figure 2.9.

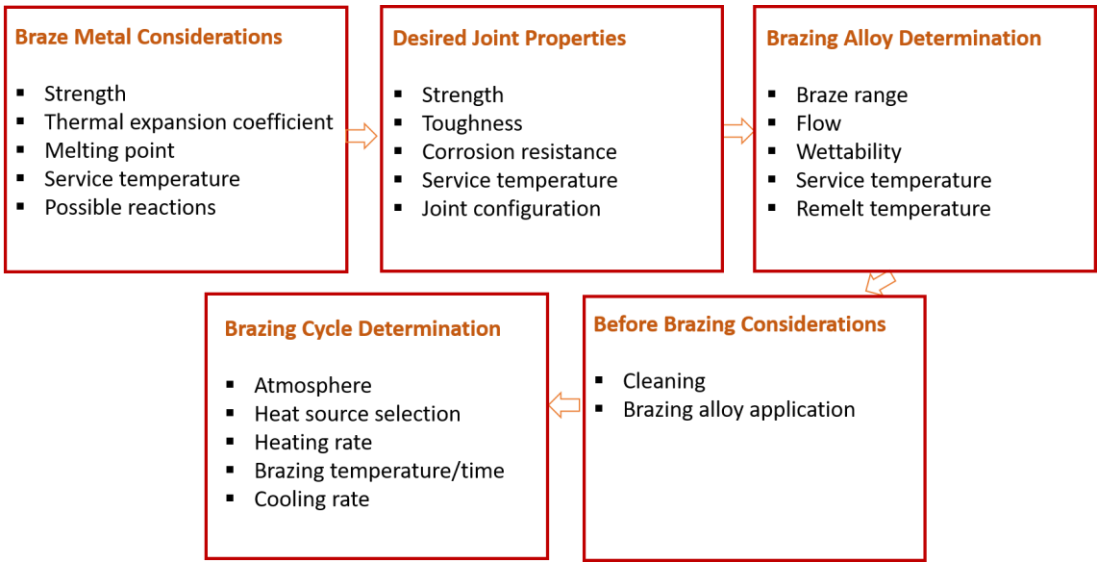

Figure 2.9 Critical steps for brazing process.

2.5.1.1 Surface Treatment

Surface preparation is critical to effective brazing. Surface of the base materials should be appropriately cleaned because impurities existing on the surface of the material prevent the adequate wetting and flow characteristics of the brazing material. Uniform capillary process and effective wetting can be achieved only after removing the oil based contaminations and oxides from the surfaces of the joint parts. Cleaning can be done by chemically and mechanically. Chemically cleaning methods of the surfaces based on solvent types (acetone, ethanol etc.), emulsions and water based alkalines. Grinding, machining, and grit blasting are examples of mechanical cleaning techniques.

2.5.1.2 Heat Source Selection

The brazing process can use a variety of heat sources. Torch brazing, induction brazing, vacuum brazing, continuous brazing, and batch furnace are only a few examples. Electric coils designed for cylindrical geometries are used to heat the component for induction brazing, while propane is used as a gas flame for torch

brazing. Both methods can be used for Silver and Copper-based brazing filler alloys. For continuous brazing, the parts are transported by the conveyor belts transport through each brazing cycle. For batch furnaces, any environment such as argon, hydrogen, nitrogen, etc., can be used. However, in vacuum brazing, brazing processes are performed under a vacuum environment to prevent brazing alloy from oxidation. The schematic of the vacuum-brazing furnace is given in Figure 2.10.

The following are some of the benefits of vacuum soldering over other techniques:

- Comparing with the other atmosphere-controlled furnaces, there exists a lower amount of oxygen to contaminate the base materials in a vacuum environment.
- Under vacuum and at high temperatures conditions, the oxide layer on the surface of the base material disintegrated. Elimination of the oxide layers enhances the base metal wetting properties and related mechanical properties of the joint.
- Since the components are heated and cooled at consistent rates, distortion is reduced.

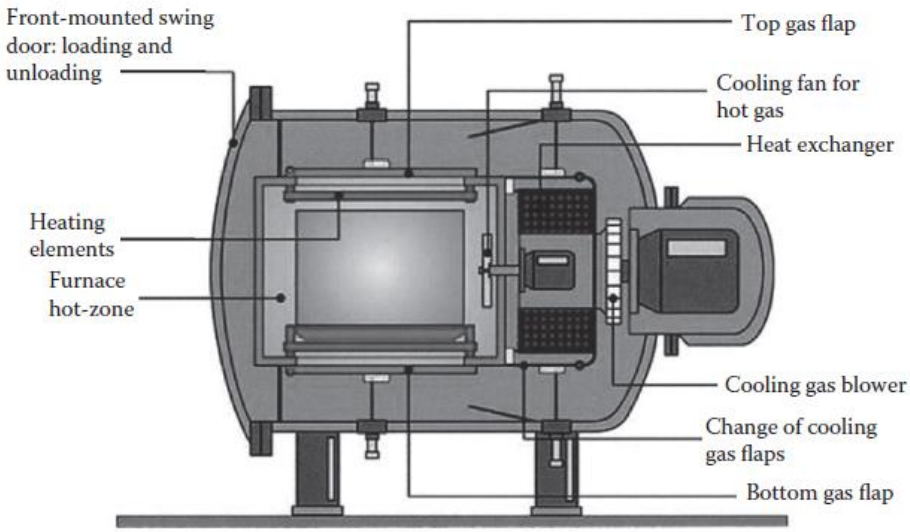

Figure 2.10 Schematic of the vacuum-brazing furnace.

2.5.1.3 Brazing Filler Material Selection

Brazing filler material selection is the most critical step to obtain the high performance braze joints. First of all, brazing filler material should wet the base material surfaces in order to obtain good chemical bonding. Secondly, melting point of the brazing material should not damage and/or erode the base material characteristics. In addition to that, appropriate melting and flow properties of the brazing filler material should enable proper capillary behavior. Then, in order to achieve sound joints, brazing filler materials should have capability of forming chemical and metallurgical bond with both base materials. The state of the brazing material during service condition is also a critical consideration. Mechanically, thermally, and otherwise, the brazing material should meet the operation requirements of the brazed component. Finally, brazing material should have homogenous structure in order to ensure identical liquidation and phase formation through the part.

Braze filler materials have a variety of elements. These alloying elements' functions and behaviors are outlined below.

- Nickel (Ni): presents good mechanical and thermal properties at high temperature conditions. Moreover, other alloying elements are very consistent with Nickel element.
- Cupper (Cu): it has a good wetting and flow behavior
- Silver (Ag): displays good corrosion characteristics and wetting behavior
- Cobalt (Co): similar to Nickel element, it shows good mechanical and thermal properties at high temperature conditions.
- Manganese (Mn): maintains the brazing filler alloy's melting point at low temperatures.
- Silicon (Si): increases the oxidation and corrosion resistance of the brazing material at high temperature conditions. Furthermore, it reduces the grain size grain with high tensile strength.

- Chromium (Cr): enhances the mechanical properties especially at high temperatures.
- Aluminum (Al): reduces the grain size and increases the oxidation resistance.
- Molybdenum (Mo): Reacting with carbon, strength improving carbides are formed. Moreover it eliminates the plastic deformation.
- Carbon (C): reduces the melting point of the brazing alloy.
- Titanium (Ti): forms carbide with the excess carbons which increases the high temperature strength and corrosion resistance.
- Germanium (Ge): reduces the melting point of the alloy.

Brazing temperature ranges for different type of brazing materials is given in Figure 2.11.

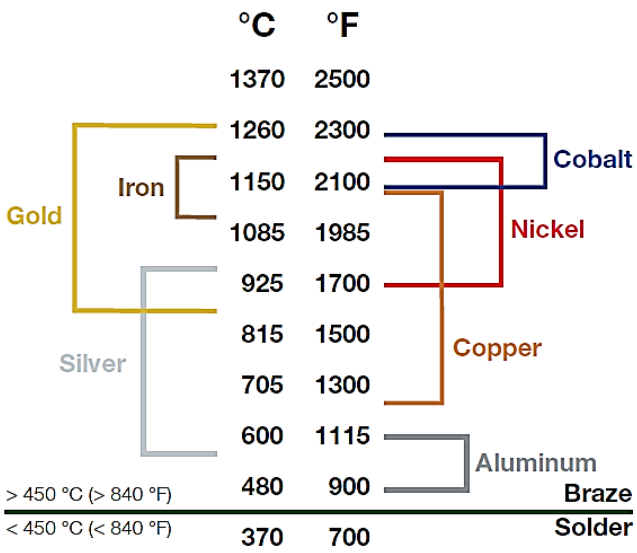

Figure 2.11 Brazing temperature ranges for different materials.

Brazing filler materials are in the form of powder, paste, tape, rod, and wire. Powder for braze materials contains homogeneously distributed spherical particles without containing any impurities. For the paste form brazing filler materials, one type or more type of brazing alloy powders are mixed with binder material to make paste shape. The organic or water-based binder content varies from 10-14% by weight, resulting in a consistent, easy-to-extrude braze filler alloy. Tape form filler alloys

include a homogeneous layer of brazing alloy, binder material, and adhesive at one or both sides of the tape material. This tape form results in easy handling for application and a wide range of brazing filler alloy thicknesses. Different from the brazing tape, brazing foils do not contain any binder or flux material. The brazing foils have the advantages of achieving uniform thickness by part brazing and being applicable to complex shape geometries. During the application, more than one foil can be used to achieve the desired thickness. Wire and rod form brazing materials are generally used for induction type brazing, and they do not include any binder material.

2.5.1.4 Joint Configuration and Clearance

For brazed joints to meet the specified standards, the design of the joint is critical. In operation, designed joint configuration has to fulfill the specifications. Butt, lapp, butt-lapp, scarf, and tee joints are the five major styles of the joints. Braze joint configurations for flat and tubular specimens are given in Figure 2.12.

Another critical parameter that affects the mechanical properties of the joint directly is joint clearance. Joint clearance can be defines as the distance between the base material surfaces of the joint during the brazing. Figure 2.13 presents the tensile strength of brazed stainless steel joints as a feature of joint clearance. The data demonstrate that tensile strength values are higher for the thicknesses of joints less than 0.150 mm compared to other joint thicknesses. Stretching of the brazing filler layer is diminished which allows obtaining higher joint strength values than the mechanical strength of the intrinsic brazing filler alloy. It can be stated that with increasing joint clearance, necking suppression decreases, and joint strength exceeds the strength of the brazing filler alloy. Therefore, joint clearance should be determined according to this considerations.

For the vacuum brazing of silver, copper and nickel based brazing filler materials, the recommended joint clearance is 0.0005- 0.004 inch intervals [40]. Vacuum

atmosphere affects the joint clearance design, therefore, to achieve maximum joint strength, vacuum brazing requires smaller joint clearance values than atmosphere controlled brazing processes.

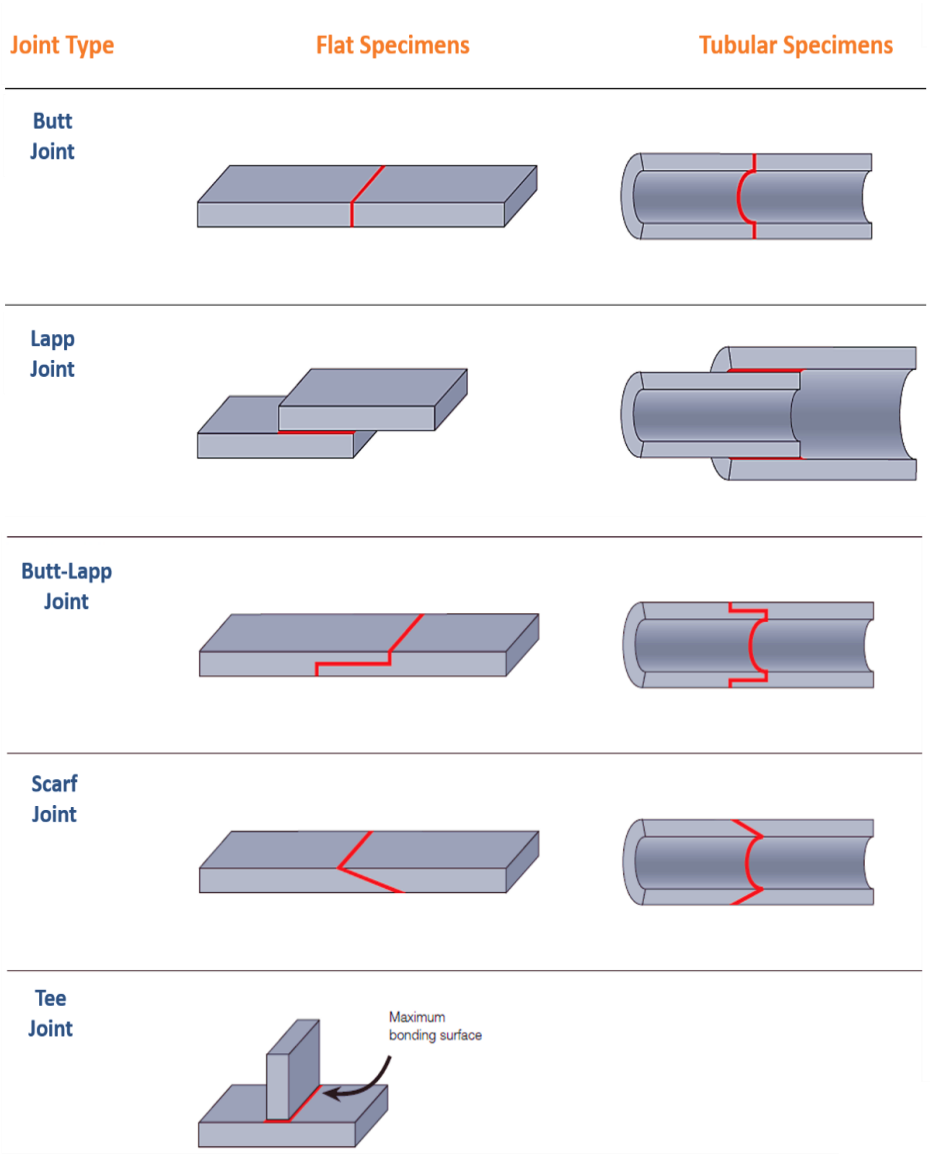

Figure 2.12 Braze joint configurations.

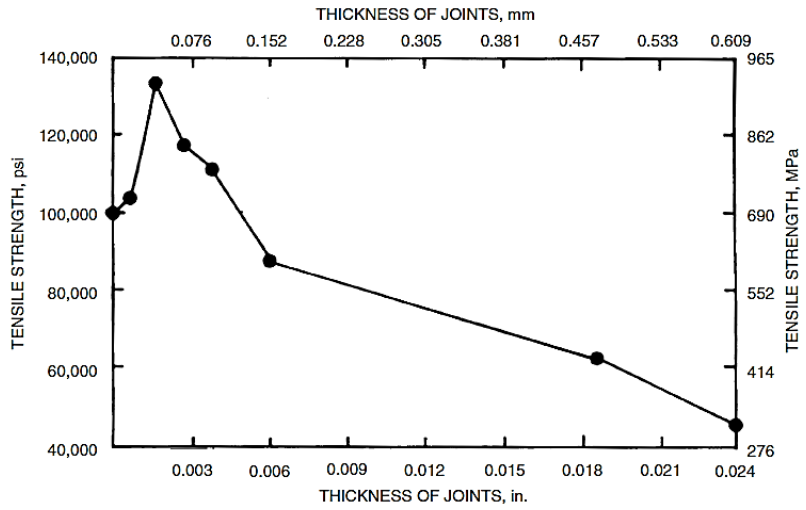

Figure 2.13 Effects of joint clearance on tensile strength of the brazed joints.

2.5.1.5 Brazing Parameters

Brazing temperature, brazing time, heating/cooling rate and surface preparation steps are the main brazing parameters [41]. Brazing temperature mainly depends on the liquidus temperature of the filler alloy. Optimized brazing temperature is needed because increase in the temperature may enhance the interactions between the base materials and brazing filler alloy. Furthermore, high brazing temperatures offer advantages in terms of penetration. However, the base materials may be destroyed and undesirable phases may occur at high temperature conditions. Since the brazing time impacts the thickness of the reaction layer, it should be optimized, also. Heating rate to brazing temperature and cooling rate of the parts after the brazing process are vital not just for preventing thermal stresses formation but also for forming secondary phases. Another major factor in brazing performance is surface characteristics. Comparing with the metallic surfaces, CMC base materials have higher surface roughness. Additional surface roughness conditions can be observed during the heating process under vacuum because of reopening of the closed pores [42].

2.6 Wetting

The wettability of the brazing filler alloy directly affects the efficiency of the brazing process. Sufficient wetting of the base materials is needed in order to ensure intimate contact and adequate bonding. Wetting is described as a liquid's capacity to maintain contact with a solid surface due to intermolecular interactions. The level of wettability is determined by the balance of adhesive and cohesive forces. The schematic of the equilibrium contact angle is presented in Figure 2.14. θ can be defined as Young contact angle θ_Y for even and uniform solid material surfaces [43].

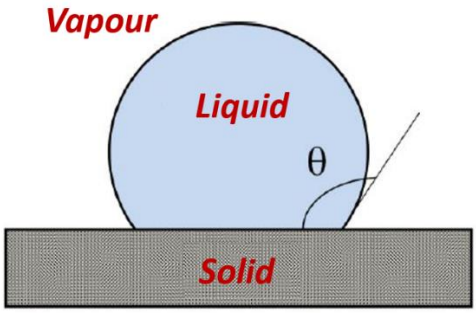

Figure 2.14 Schematic of the equilibrium contact angle.

The angle at which wetting and non-wetting terms are defined is $\theta_Y = 90^o$. As shown in Figure 2.15, the wetting condition is classified as weak for systems with a contact angle greater than the 90º; however, the wetting situation is strong for systems with a contact angle less than 90º.

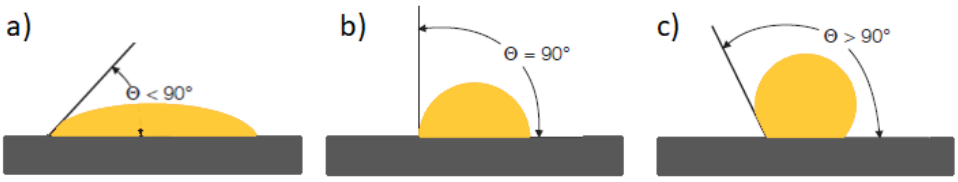

Figure 2.15 a) $\theta_Y < 90^o$; strong wetting situation, b) $\theta_Y = 90^o$; moderate wetting situation and c) $\theta_Y > 90^o$; weak wetting situation.

2.6.1 Non-reactive Wetting

The wetting of the solid by non-reactive liquid can be expressed by Young (Equation 2.1) and Young-Dupre (Equation 2.2) equations.

$$\cos\theta = \frac{\sigma_{sv}-\sigma_{sl}}{\sigma_{lv}} \quad (2.1)$$

$$\cos\theta = \frac{W_a}{\sigma_{lv}} - 1 \quad (2.2)$$

$$W_a = \sigma_{sv} + \sigma_{sv} - \sigma_{sl} \quad (2.3)$$

σ_{sv}: the surface energy of the solid,

σ_{sl}: interface energy of solid/liquid,

σ_{lv}: the surface energy of the liquid,

W_a: the adhesion energy of the system.

In accordance with Equation 2.2, the contact angle of the non-reactive system mainly depends on the adhesion and cohesion forces, even though the adhesion forces enhance the wetting, surface energy of the liquid functions in a reversible manner. As stated in Table 2.3, interaction forces are strong for the metallic materials due to the metallic bonding of the atoms. They have higher cohesion energy than the surface energy of the liquid form metals [44]. Therefore, good wetting conditions with 10°–30° contact angle can be observed for metallic systems. Semiconductor materials also present strong interaction. Although semiconductor materials have covalent bonding, they have metallic bonding properties at their surface. On the other hand, liquid metals can not sufficiently wet the carbon-based materials and ceramic due to their covalent bond character with a high bandgap. For these material groups, adhesion forces mainly depend on Van der Waals interactions [45].

Table 2.3 Variation in contact angle depending on different materials [46,47].

Substrate	Interaction	θ (degrees)	Examples
Solid Metals	Strong (Chemical)	$\theta_Y << 90^o$	Cu/Mo: 10°–30°
Semiconductors			Sn/Ge: 40°; Si/SiC: 35°–45°
Ceramics partially metallic character			Cu/WC: 20°; Au/ZrB_2: 25°
Carbon materials	Weak (Physical)	$\theta_Y >> 90^o$	Au/C: 120°–135°
Ceramics			Ag/Al_2O_3, Cu/SiO_2: 120°–140°; Au/BN: 135°–150°
Oxides	Moderate	$\theta_Y \sim 90^o$	(Ag+O)/Al_2O_3; Al/Al_2O_3

Young contact angle θ_Y is defined for even and uniform solid material surfaces as it is stated above. However, in most cases, the surfaces may include some heterogeneities and roughness. Young contact angle θ_Y is affected by the roughness of the solid surface in two ways: the improvement in the surface area and the pinning effect of the triple line.

The Wenzel Equation presents improvement in the surface area:

$$\cos \theta_w = S_R \cos \theta_Y \qquad (2.4)$$

S_R: actual area to planar area

In accordance with Equation 2.4, it can be stated that S_R>1. For the strong wetting condition of $\theta_Y < 90°$, less θ_w value will be observed than the θ_Y.

Sharp defects result in deviation of the contact angle. This deviation is presented in Equation 2.5.

$$\theta = \theta_Y + \alpha \qquad (2.5)$$

θ: observed contact angle due to deviation,

α: variation due to surface defect.

Wenzel Equation (Equation (2.4)) describes the surface roughness in systems with strong wetting. However, the pinning effect dominates when the $\theta_{Y.}$ value is close to 90° for poor wetting conditions.

2.6.2 Reactive Wetting

During the wetting of the solid material surface by the liquid material, dissolution or phase formation may occur due to the reactions take place at the interface. In agreement with Reaction Product Control Model, contact angle has two different stages: $\theta_{0,}$ initial contact angle and θ_F observed contact angle on the reaction product. The formed reaction layer on the solid material surface does not always improve wetting, in some cases it may increases the final contact angle [48]. The wetting behavior of liquid silicon on carbon surfaces has improved as a result of SiC formation, as shown in Figures 2.16 and 2.17.

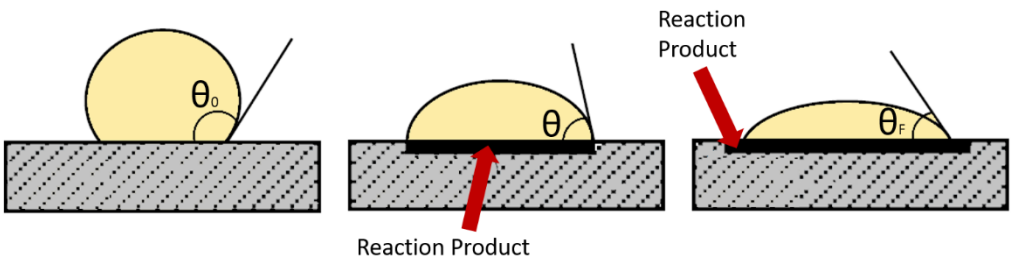

Figure 2.16 Schematic of the Reaction Product Control Model [43].

On the surface of the unreacted carbon, the initial contact angle θ_0 is higher than 140° as shown in Figures 2.16 and 2.17. The contact angle begins to decrease after SiC forms on the solid carbon surface. The final contact angle θ_F reaches a value of

approximately 40° at the end of the reaction. As a result, liquid silicon sufficiently wets the surface of carbon-based materials.

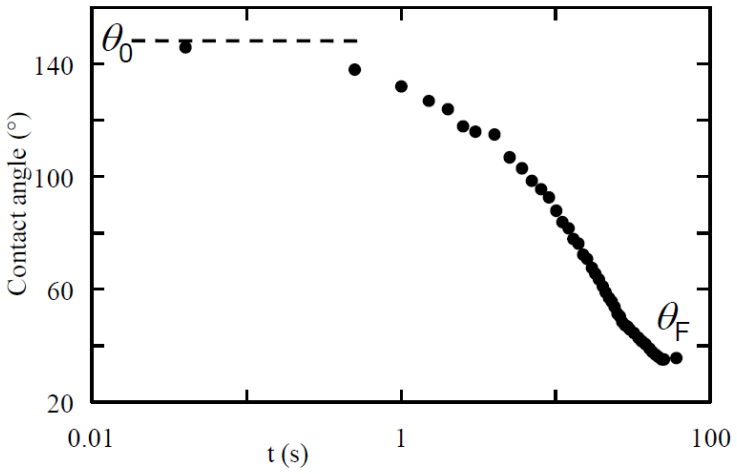

Figure 2.17 Contact angle versus time diagram of silicon on carbon [49].

2.6.3 Dissolution Wetting

During the liquid/solid interactions, the solid phase dissolutes in the liquid. This dissolution affects the obtained contact angle in two ways:

- Reduces the surface tension of the liquid material,
- Crater formation in which the observed contact angle lower is than the actual one.

Schematic of dissolution wetting is given in Figure 2.18. Liquid B has a curved morphology at the start of the wetting experiment, as shown in Figure 2.18. Then the pure liquid B forms a initial contact angle θ_0 on the surface of the solid A. After the dissolution and saturation of B in A, crater is formed on the surface of the A. As a result the observed contact angle θ_F increases comparing with the θ_0 [50].

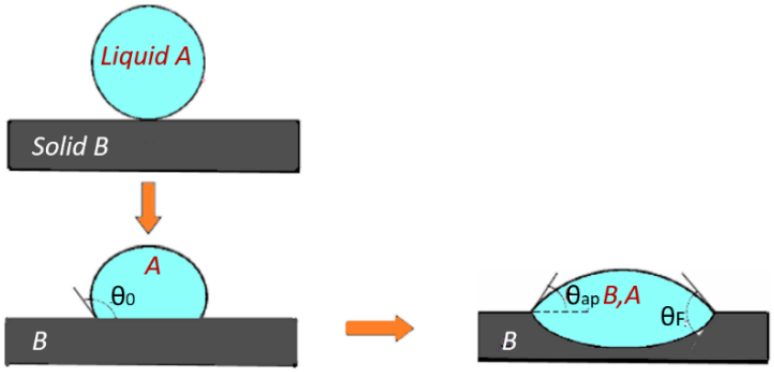

Figure 2.18 Schematic of dissolution wetting.

2.6.4 Wetting in Brazing

Interfacial reactions between the base materials and the brazing filler alloys directly affect the base materials' wettability. Therefore, the wettability of the base materials may be improved or worsened by the interfacial reactions.

When metal pieces exist on the top of the SiC surfaces, the reaction occurs between the liquid metal and SiC. As a result of this reaction, SiC dissolves in the liquid metal, and silicon and graphite flakes are formed at the interface. Compared with the SiC and graphite wettability, SiC can be easily wetted by liquid metals [51]. Therefore, it can be stated that the reaction between the SiC and liquid metal worsens the wetting. In order to increase wettability, silicon-containing alloys are utilized instead of pure metals. Hence the silicon in the alloy precludes the formation of graphite flake, and the system can achieve good wetting with approximately 40 degrees of contact angle [52].

The effect of Titanium concentration on the wetting behavior of Cupper-Silver alloy on the alumina surface is presented in Figure 2.19 [53]. The experiment is carried out in the Helium atmosphere at 900 °C. Two different compositions of Ti are placed on the top of the Cupper-Silver alloy during the investigation. As it is shown in Figure 2.19, with increasing the Ti concentration contact angle decreases from 65° to 10°. During melting, the non-wetting contact angle is observed, which is due to

the oxide behavior of the Alumina. However, the contact angle does not change for some time because the amount of time is required for Titanium to dissolve in the melt and diffuse to the metal–oxide boundary. Then, the contact angle begins to decrease, and at the end, it reaches 10° and 65° for 1.75 wt% Ti and 0.42 wt% Ti, respectively.

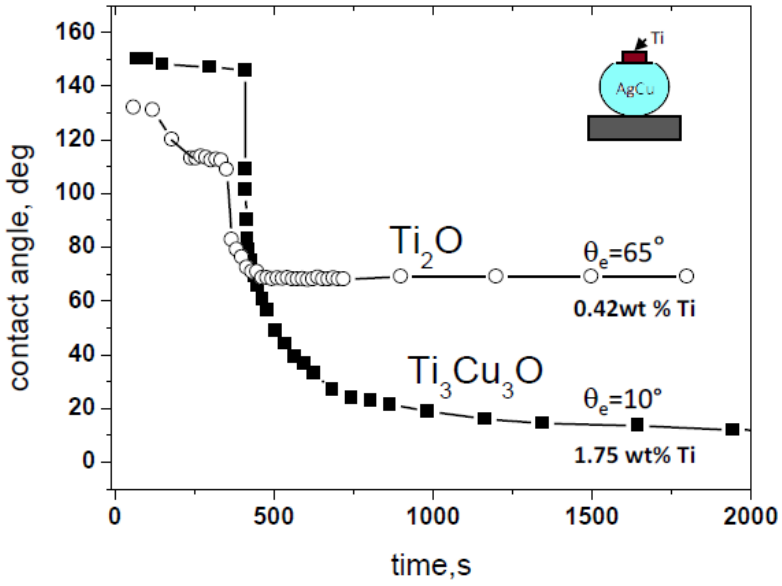

Figure 2.19 Ti concentration effect on the wetting behavior of Cupper-Silver alloy on the alumina surface [53].

The microstructure of the interface between Alumina and Cupper-Silver alloy after the wetting experiment is given in Figure 2.20. [42]. The interface contains Ti_3Cu_3O layer and Ti_2O layer. Although Ti_2O is an oxide, Ti_3Cu_3O presents a metallic character. For the low concentrations of Ti, 0.42 wt% Ti, only the Ti_2O layer can be observed in the interface. The predominant phase between the liquid melt and the interface for the 1.75 wt% Ti concentration is Ti_3Cu_3, and the Ti_2O layer is submicron, as illustrated in Figure 2.20. It can be stated that the metallic character of the Ti_3Cu_3O phase decreases the contact angle and results in a good wetting

condition. It can be noted from the experiment that brazing of Alumina ceramics should be carried out using Titanium active element containing brazing filler alloys. Furthermore, a higher Titanium concentration leads to better wetting and, as a result, better mechanically brazed joints [54].

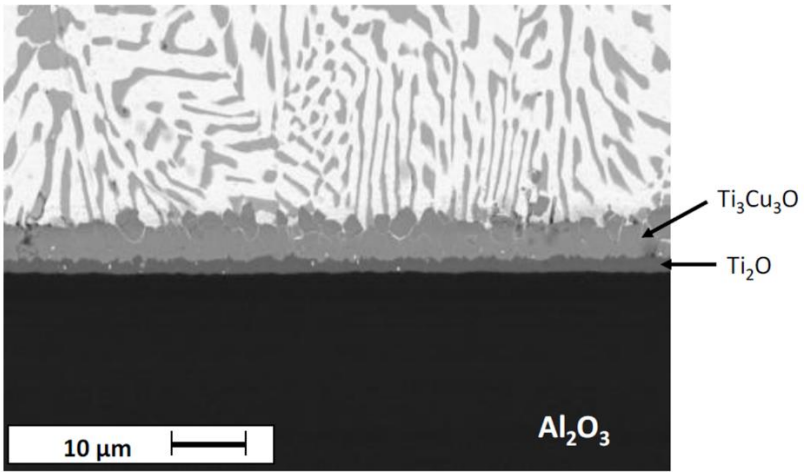

Figure 2.20 Microstructure of the interface between Alumina and Cupper-Silver alloy after the wetting experiment [53].

The interfacial reactions and interlayer microstructure are affected not only by the brazing filler composition but also by the joint metal type. Valette et al. investigated the joint material type on the interfacial reaction kinetics for the Alumina and Silver-Cupper-Titanium based brazing filler alloy [55]. In the study, for the same brazing filler alloy, Alumina-Alumina braze joint, and Alumina-CuNi braze joint are compared. According to Figure 2.21, interlayer microstructures and reaction layer thickness differ for both cases.

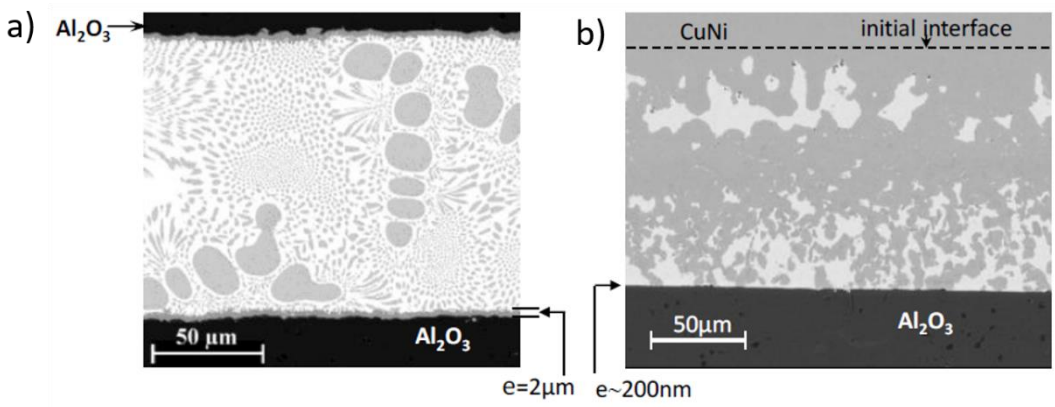

Figure 2.21 The interlayer of a) Alumina-Alumina braze joint, b) Alumina-CuNi braze joint where "e" presents the reaction layer thickness [55].

When the Alumina joint material is replaced with metallic CuNi alloy, the metallic alloy can dissolve in the molten filler material and reaches to equilibrium concentration during the brazing. However, increased Nickel and Copper concentration in the liquid braze affects the reactivity at the ceramic and braze filler material interface. Because of the reactivity change at the interface, variable microstructure and reaction layer thickness are seen at the interlayer. According to Figure 2.21, reaction layer thickness changes dramatically from 2 µm to 200 nm. Besides that, increased Nickel and Copper concentration suppressed the wettable Ti_3Cu_3O phase at the interlayer for the Alumina-CuNi braze system. Instead of Ti_3Cu_3O phase, the formation of Ti oxides results in a considerable rise in contact angle. In addition to changing the reaction layer composition, increasing contact angle has a negative impact on the mechanical strength of the brazed joint.

2.7 Active Brazing

Compared with the metallic materials, ceramic materials present poor wettability. In ceramic systems wettability can be enhanced by three different ways: Applying a wetting promoter to the ceramic surface, metallization of the ceramic surface before

the brazing and addition of active metal to the brazing filler [56-58]. To improve wettability in metal/ceramic systems, adhesion-active element, such as Ti, Hf, or Cr, is introduced into the liquid metal. Adhesion-active elements, such as Ti, Hf, or Cr, possess a high chemical affinity for the solid phase atoms [59,60].

Classification of the active elements for ceramic/metal brazing systems is given in Figure 2.22. As it is presented in Figure 2.22, adhesion-active elements can be divided into two groups: Type-1 adhesion-active elements include Ni, Co, Fe etc.; and type-2 adhesion-active elements include Zr, Ti, Hf, Mn, etc. Type-1 active elements react with only silicon. As a result of this reaction, brittle silicide phases and graphite layers appear. Although, type-2 adhesion-active elements react with both silicon and carbon. Consequently, carbides and silicides form at the interlayer [61,65].

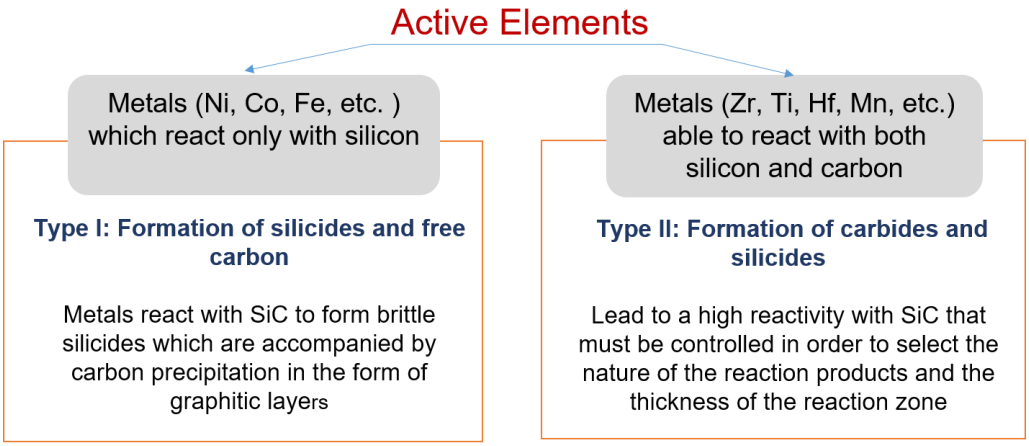

Figure 2.22 Classification of active elements for brazing.

Table 2.4 Composition of active brazing filler alloys used in CMC brazing [66].

Active-brazing filler metal	Chemical composition (wt.%)							Melting range (°C)
	Ag	Cu	Ti	In	Ni	Al	other	
AgCu26.5Ti3	70.5	26.5	3	–	–	–	–	780–805
AgCu34.2Ti1.8	64	34.2	1.8	–	–	–	–	780–810
AgCu25.2Ti10	64.8	25.2	10	–	–	–	–	780–805
AgCu34.5Ti1.5	64	34.5	1.5	–	–	–	–	770–810
Ag–Ti	96	–	4	–	–	–	–	970
AgIn1Ti0.6	98.4	–	0.6	1	–	–	–	948–959
AgIn1Ti1	98	–	1.0	1.0	–	–	–	948–959
AgCu19.5In5Ti3	72.5	19.5	3	5	–	–	–	730–760
NiTi67	–	–	67	–	33	–	–	942–980
CuNi15Ti70	–	15	70	–	15	–	–	910–970
AuNi3Ti0.6	–	–	0.6	–	3	–	96.4Au	1003–1030
SnAg10Ti4	10	–	4	–	–	–	86Sn	221–300
PbIn4Ti4	–	–	4	4	–	–	92Pb	320–325

Table 2.4 presents the elemental composition of active brazing filler alloys used in CMC brazing. As it is seen in the table, active element amount can reach up to 33 wt%. Generally, silver or silver-copper based alloys with low melting point are used.

In active brazing process, adhesion-active elements enhance the wettability of the ceramic or ceramic matrix base material surfaces. Adhesion-active elements increases the chemical reaction possibility between the filler material and base material. Metallic or metal-like phases are formed at the base material interface. Newly formed phases at the reaction layer considerably decreases the surface tension as a result the surface can be easily wetted [67-70].

Composition of the reaction layer products depends on the type of the base material, adhesion-active elements type and brazing parameters. For the reaction product forms, there are two alternatives:

1) AB + a → aB + A,
2) AB + a → aA + B where,

AB is the ceramic base material based on metallic and non-metallic compound and a presents the adhesion-active element.

2.8 Ag-Cu-Ti Phase Diagram

Ag-Ti and Cu-Ti phase diagrams are presented in Figure 2.23 and Figure 2.24, respectively. Although the Ag-Ti system only includes Ti_2Ag and TiAg intermetallic phases, the Cu-Ti system has six different intermetallic compound formations, as shown in Figures.

Ag-Cu-Ti system demonstrates two distinct characteristics. Firstly, between the Ti_2Ag and Ti_2Cu phases, there exist a constant solid solution. Secondly, miscibility gap exist between the silver rich and titanium rich liquids. Because the Ag-Cu system's eutectic temperature is 780 °C, this brazing alloy system is an excellent choice for low brazing temperatures of joint materials [71].

The activity of the Titanium element is increased by the presence of silver in the system. As a result, chemical possibility with the base materials increases and wetting behavior of the ceramic based material improves [72,73].

It is critical to evaluate the possible phases in relation to the brazing temperature in order to obtain high mechanical performance brazed joints. Eremenko et al. investigated the possible phases in Ag-Cu-Ti system [74]. In this study, possible phases for the Ag-Ti and Cu-Ti system, and related informations are given in Table 2.5.

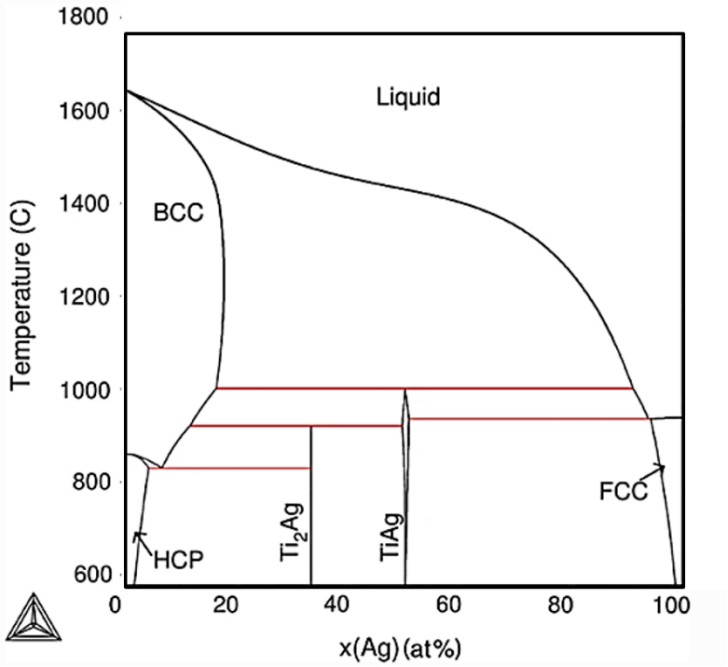

Figure 2.23 Ag-Ti Phase diagram [75,76].

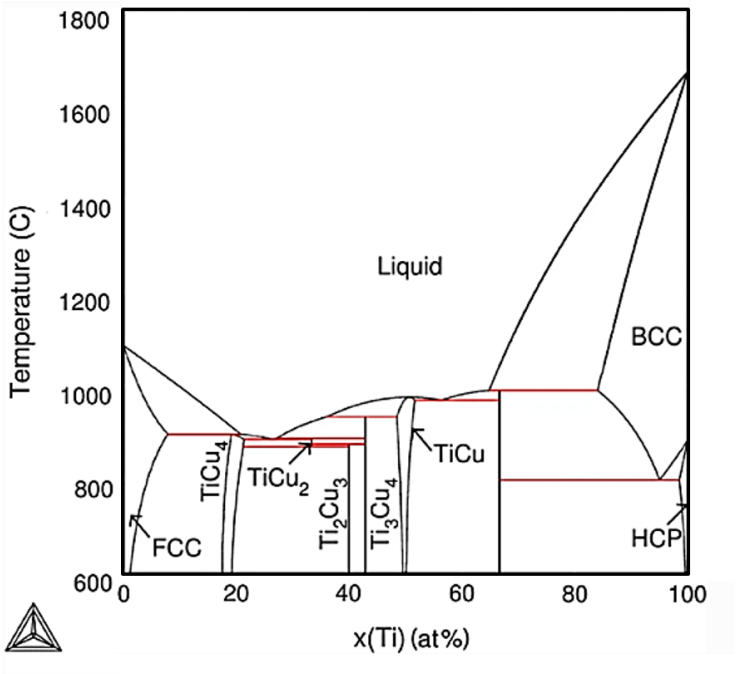

Figure 2.24 Cu-Ti Phase diagram [60].

Table 2.5 Crystal phase and symbol information of the phases existing in Ag-Cu-Ti system [74].

Structure report	Diagram symbol	Symbol used in thermo- data file	Pearson symbol/space group/prototype	Lattice parameter
A_1	(Ag)	FCC_Al	cF4	a = 408.57
	(Cu)	Fm3m	Cu	a = 361.46
A_3	α-Ti	HCP_A3	hP2	a = 330.65
			$p6_3/mmc$	
			Mg	
A_2	β-Ti	BCC_A2	cI2	a = 295.06
			Im3m	c = 468.35
			W	
	$TiCu_4$	$TiCu_4$	oP20	a = 452.5
			Pnma	b = 434.1
			$ZrAu_4$	c = 1295.3
	$TiCu_2$	$TiCu_2$	oC12	a = 436.3
			Amm2	b = 797.7
			VAu_2	c = 447.3
	Ti_2Cu_3	Ti_2Cu_3	tP10	
			P4/nmm	c = 1395
			Ti_2Cu_3	
	Ti_3Cu_4	Ti_3Cu_4	tI14	
			I4/mmm	a = 313
			Ti_3Cu_4Ti	c = 1994
$C11_b$		Ti_2M	tI6	a = 295.3
	Ti_2Cu		I4/mmm	c = 1073.4
	Ti_2Ag		$MoSi_2$	a = 295.2
				c = 1185
B11	TiAg	TiM	tP4	a = 290.3
	TiCu		P4/mmm	c = 574
			TiCu	a = 310.8–311.8
				c = 588.7–592.1

CHAPTER 3

EXPERIMENTAL PROCEDURE

3.1 Base Materials

In this study, initial materials to be joined were carbon fiber reinforced silicon carbide matrix (C/SiC) composite and Ti6Al4V alloy.

3.1.1 Carbon Fiber Reinforced Silicon Carbide Matrix (C/SiC) Composite

C/SiC composites reinforced by three-dimensional (3D) carbon fiber structure were used, where the carbon fiber volume fraction was in the range of 45-50%. The type of carbon fibers used in the C/SiC composite manufacturing was high modulus type with 7 μm diameter. As-received C/SiC composite had 10-15 vol.% porosity, and its elastic modulus was 40 MPa at room temperature. The microstructure of the C/SiC composite is shown in Figure 3.1. In this study, the XZ plane of the C/SiC composite (Figure 3.1(b)) was applied as the bonding surface in all experiments where Z direction is parallel to the C/SiC composite brazing filler interface. Sketch of reinforcement architecture in 3D C/SiC composite is given in Figure 3.2. The material properties of the C/SiC composite are presented in Table 3.1.

Table 3.1. The physical and mechanical properties of the 3D C/SiC composite.

Density (g/cm^3)	**Tensile Strength (MPa)**	**Tensile Modulus (GPa)**	**Thermal Conductvity ($W\ m^{-1}K^{-1}$)**	**CTE**
2.2	165	40	7-10	2.1

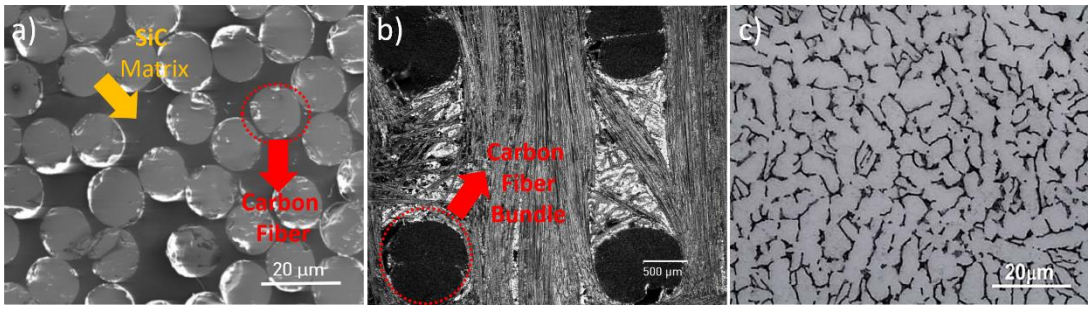

Figure 3.1 Microstructures of the initial materials used in the study a) XZ plane of the C/SiC composite, b) XZ plane view of the three-dimensional (3D) C/SiC composite and c) equiaxed microstructure of Ti6Al4V alloy containing α (bright) and β (dark) phases.

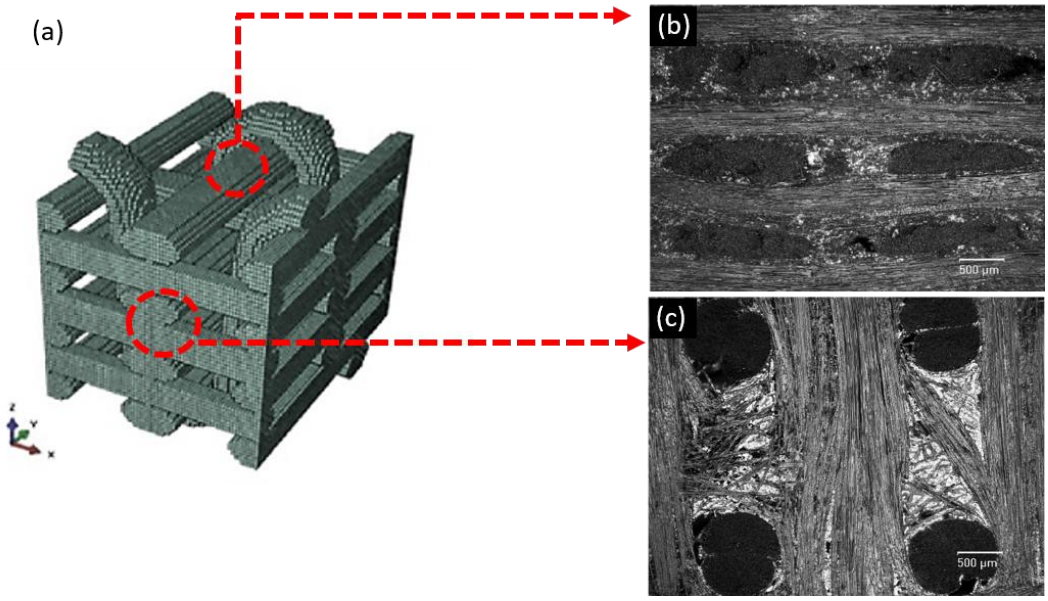

Figure 3.2 (a) Sketch of reinforcement architecture in 3D C/SiC composite (b) Micrograph of XY plane, (c) Micrograph of XZ plane.

In order to investigate the effect of varying material properties and reinforcement structure of the C/SiC composites on the wetting behavior and related brazing performance of the composites, 2D C/C-SiC composites manufactured by liquid silicon infiltration method in an earlier study [58] were also used during this study. Moreover, in order to improve the thermal properties of the C/C-SiC composites,

carbon nanotubes (CNTs) were also impregnated during the ceramic matrix composite manufacturing step [59].

2D C/C-SiC Composite Manufacturing

2D C/C-SiC composites were produced via liquid silicon infiltration method. Initial step of the C/C-SiC composite manufacturing is the carbon fiber-reinforced polymer (CFRP) matrix composite manufacturing. Therefore, CFRP composite composed of carbon fiber and phenol formaldehyde resin were used in the study. As the reinforcing structure, a 2D woven fabric with a volume percent of 45-55 was employed. Temperature of 1000 °C and time of 3 h were utilized as pyrolysis parameters to convert the polymeric matrix into carbon matrix, and hence to obtain the C/C preforms.

In an atmosphere-controlled vertical tube furnace, liquid silicon infiltration process was conducted. By the infiltration of liquid silicon into the C/C preform at a vacuum level of 10-3 mbar, carbon matrix of the preform was converted to SiC matrix. The preforms were held at 1650 °C for 1 h and cooled in the furnace under vacuum. Nevertheless, since the conversion of the C matrix to SiC could not be 100% completed, minor amount of C remains in the matrix of the resulting composites. Therefore, the matrix of the final 2D C/C-SiC composites is denoted as C-SiC where the presence of C fibers in this matrix is shown by C/ notation.

Carbon Nanotube (CNT) Incorporation to 2D C/C-SiC Composites

Multiwall CNTs incorporated to 2D C/C-SiC composites had a purity of over 96% and an exterior diameter of less than 8 nm. As an additional carbon source, CNTs were initially impregnated in a series of C/C preforms. Preparation of CNT containing propanol suspension was the first step. After that the ultrasonication was applied to the C/C preforms immersed in the CNT-propanol suspension. Following this, the beaker containing the C/C preform and the CNT-propanol suspension was kept in a vacuum desiccator for 1 h. As the final step, C/C preforms saturated with CNT were dried for 1 h at 50 °C. Consequently, above-described liquid silicon

infiltration process was applied to CNT impregnated C/C preforms to obtain CNT containing 2D C/C-SiC composites.

3.1.2 Ti6Al4V Alloy

In the present study, as a metallic joint material Ti6Al4V alloy was used (Grade 5, supplied by Timed, Turkey). Ti6Al4V alloy initially had density and elastic modulus values of 4.43 g/cm^3 and 110 MPa, respectively. The material properties and as received microstructure of the Ti6Al4V alloy are given in Table 3.2 and Figure 3.1(c), respectively.

Table 3.2 The physical and mechanical properties of the Ti6Al4V alloy.

Density (g/cm^3)	**Hardness (HRc)**	**Elastic Modulus (GPa)**	**Thermal Conductvity (W m^{-1}K^{-1})**	**Beta Transus (°C)**
4.3	35	110	6-8	996

3.1.3 Silicon Carbide (SiC) Ceramic

Monolithic SiC ceramics were also examined to concentrate on the matrix material only to understand the effect of carbon fibers on the wetting behavior of the molten brazing filler alloy. The material properties of the as-received SiC ceramic is given in Table 3.3.

Table 3.3 The physical and mechanical properties of the monolithic SiC ceramic.

Density (g/cm^3)	**Tensile Strength (MPa)**	**Elastic Modulus (GPa)**	**Thermal Conductvity (W m^{-1}K^{-1})**	**CTE**
3.1	300	380	150	4.0

3.2 Brazing Materials

In this study, Ag-Cu based active brazing alloys were used as filler material. Most commonly considered active brazing filler is a eutectic Ag–Cu alloy with a few percent of titanium (Ti). Active brazing filler alloys based on Ag-Cu and containing a small quantity of Ti have good wettability as well as low melting point. Because of the minimal deterioration of the metallic base material and loss of base-metal characteristics, a low melting point is necessary during the brazing application process. Melting temperatures of commercial Ti-Ni based filler alloys such as Tini and Ticuni are higher than 950 °C.

Throughout the study, to determine the effect of the titanium (Ti) content on the brazing performance of the joints three different brazing filler alloys were used namely, Cusil, Cusil-ABA, and Ticusil. Table 3.4 lists the properties of the brazing filler alloys utilized in this study.

3.2.1 Cusil Brazing Filler Alloy

Cusil brazing alloy was the eutectic composition of the Ag and Cu alloy with percentages of 72 wt% Ag + 28 wt% Cu (Table 3.4). Both sheet form and extrudable paste form of the alloy were used in the study. Both forms were supplied from Morgan Braze Alloys, USA. The thickness of the sheet formed Cusil brazing filler alloy was 50 µm. Correspondingly, thickness of the Cusil brazing filler alloy applied in the paste form on base material surfaces was also set to approximately 50 µm.

3.2.2 Cusil-ABA Brazing Filler Alloy

Cusil-ABA (supplied by Lot-Tek GmbH, Germany) brazing filler alloy differs from the Cusil brazing filler alloy in both Cu and Ag content, while it also contains 1.25 wt% Ti as the active element (Table 3.4). Cusil with the eutectic composition had a liquidus temperature of 780 °C; however, Cusil-ABA had a liquidus temperature of

816 °C with a small amount of Ti addition. Cusil-ABA was also supplied in the sheet form with a thickness of 50 µm.

3.2.3 Ticusil Brazing Filler Alloy

The brazing filler alloy called Ticusil was also supplied by Lot-Tek GmbH, Germany. According to its data sheet, 68.8 wt% Ag + 26.07 wt% Cu + 4.5 wt% Ti are the key elements in the brazing filler alloy (Table 3.4). Ticusil was in powder form with 325 mesh grain size. During the brazing experiments, it was turned into a paste by mixing it with ethanol and applied on ground C/SiC composite and Ti6Al4V alloy surfaces by a brush. The thickness of the Ticusil brazing filler alloy in paste form spread on both base material surfaces was approximately 50 µm.

Table 3.4 Physical and thermal properties of the brazing filler alloys used.

		Cusil	**Cusil-ABA**	**TiCusil**
Composition	Ag wt%	72	63	68.8
	Cu wt%	28	33.75	26.7
	Ti wt%	-	1.25	4.5
Liquidus (°C)		780	816	900
Solidus (°C)		780	780	780
Density (g/cm^3)		10	5.2	9.4
CTE (10^{-6} C^{-1})		10.9	18.5	18.5
Elastic Modulus (GPa)		83	83	83
Material Form	Sheet	+	+	-
	Paste	+	-	-
	Powder	-	-	+

3.3 Brazing of the C/SiC Composite-Ti6Al4V Alloy Joints

Brazing experiments of C/SiC composites and Ti6Al4V alloys were performed by vacuum brazing technique. Brazing furnace (NANOVAK VALES Brazing Systems, Turkey) which can operate within 100-1200 °C temperature range and had a capability of $1x10^{-7}$ Torr base pressure level was used in the study.

3.3.1 Material Preparation Steps before Brazing

As-received C/SiC composite and Ti6Al4V alloy were sectioned into two types of specimens with the size of 15 ×10 × 5 mm and 10 × 5 × 5 mm, respectively. Before bonding, base material surfaces were ground by 400 and 800 grit silicon carbide papers consecutively. After the surface grinding step, the base materials and filler alloy sheets were ultrasonically cleaned in ethanol for 15 minutes and dried at 60 °C.

Brazing filler alloys, which were in powder form, were turned into a paste by mixing them with ethanol and applied on ground C/SiC composite and Ti6Al4V alloy surfaces by a brush. The thickness of the brazing filler alloys in paste form spread on both base material surfaces were approximately 50 μm.

3.3.2 Temperature Profile for Vacuum Brazing

Determination of the vacuum brazing cycle parameters comprised of initial vacuum level, initial heating rate, stabilizing temperature, heating rate to brazing temperature, brazing temperature and cooling rate is very critical for the proper application of this technique.

Initial vacuum level: For materials which are easy to braze the vacuum level should be at 8×10^{-4} torr, while for materials which are difficult to braze the vacuum level should be under 5×10^{-4} torr before initiating the heating of the furnace.

Initial heating rate: In order to prevent part distortion and excessive outgassing, the heating rate should be 3-5 ºC/min.

Stabilizing temperature: The stabilization of the brazing filler material at a temperature approximately 100 °C below the solidus enables homogeneous heating; such that all materials in the joint can reach the brazing temperature simultaneously.

Heating rate to brazing temperature: The heating rate should be fast enough to avoid excessive liquefaction of the brazing filler alloy and erosion of the base materials.

Brazing temperature: The brazing temperature must be higher than the filler alloy's liquidus temperature. Moreover, enough time at that temperature must be provided to ensure that all of the materials reach the brazing temperature.

Cooling rate: In order to obviate the part deformation and crack formation due to thermal stresses brazed joints should be cooled in the furnace.

The temperature profile used throughout the study for brazing C/SiC composite and titanium alloy is shown in Figure 3.3. The brazing furnace was heated at 5 °C/min until 600 °C temperature was maintained. Initially, at 600 °C, a holding time of 60 min was applied. Further, the temperature was raised to the intended brazing temperature with a heating rate of 3 °C/min. Brazing process was performed at varying temperatures for different brazing filler alloys which were within the range of 850-930 °C for a constant time. Moreover, brazing was also conducted at different holding times between 1 and 30 min at a constant brazing temperature. The joints were processed under the vacuum level of 4.5×10^{-8} Torr, and cooling of samples after processing was done slowly in the furnace. Applied brazing temperature and brazing time conditions used in the study are given in the Table 3.5.

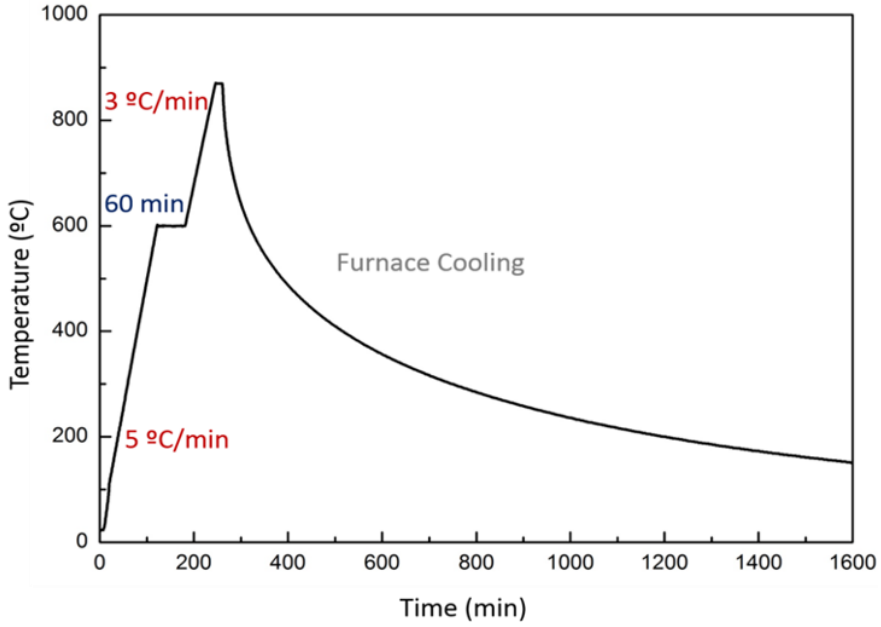

Figure 3.3 The temperature profile for brazing experiments.

Table 3.5 Brazing conditions varying according to brazing alloy used in the study.

	Brazing Temperature (°C)	**Brazing Time (min)**
Cusil	850, 875, 900	10
Cusil-ABA	850, 875, 900	5, 10, 15
Ticusil	900, 905, 915, 925, 930	1, 5, 15, 30

3.3.3 Material Preparation Steps for Characterization After Brazing

To characterize the joints' microstructures and to perform mechanical tests, brazed joints were cut through their cross-sections and subsequently metallographically prepared by grinding and polishing prior to inspection (Figure 3.4). To prevent fracture of the specimens during sectioning, brazed joints were mounted using epoxy resin before the sectioning step. Grinding and polishing were used as surface

preparation stages for microstructural characterization, with SiC grinding papers of 400-800-1200 grit size and diamond suspensions containing 6 and 1 μm particles, respectively.

Figure 3.4 a) C/SiC composite-Ti6Al4V alloy joint sectioned into two types of specimen sizes, b) Epoxy resin mounted brazed joints, c) Sectioning direction of the brazed joints.

3.4 Particle Incorporation to the Brazing Filler Alloy

In order to tailor the properties of the filler alloy two different silicon carbide (SiC) powders with different particle sizes (nano-sized and micron-sized) were incorporated into Ticusil brazing filler alloy as an additive material. SEM micrographs of the nano-sized and micron-sized additive SiC powders are given in Figure 3.5 For the nanoparticle addition, nano-SiC powders (NG04CO1505 supplied by Nanografi Nanotechnology, Turkey) having purity higher 99.5% and particle size in the range of 50-70 nm with an average particle size of 53 nm were used. High purity (>99.9 %) SiC micro-powders (supplied by Sigma Aldrich, USA) having an average particle size of around 40 μm with particle size changing between 35 and 60 μm were used as the second type of additive.

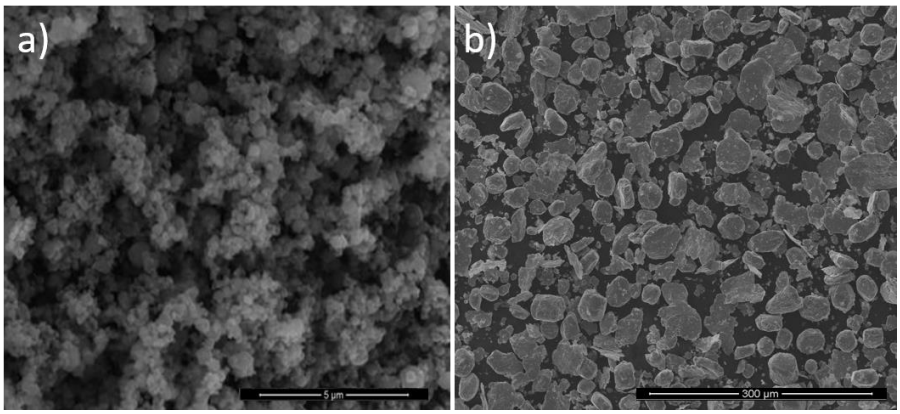

Figure 3.5 Additive materials used in the study a) nano-SiC powders, b) SiC micro-powders.

3.5 Coating Application on C/SiC Ceramic Composite Base Material

C/SiC composite surfaces were coated with titanium film in order to investigate the effect of titanium layer on microstructural evolution and mechanical properties of C/SiC composite-Ti6Al4V alloy joints. Magnetron sputtering technique was used for coating experiments. Before coating process, C/SiC composite surfaces were cleaned in ethanol and plasma cleaning was applied using argon ions for 15 min. Magnetron Sputter Ion Plating equipment (NVSP-400, Nanovak, Turkey) was used during the coating experiments. Classification of the samples studied based on the brazing filler type, coating material, coating thickness and applied brazing temperature/time is given in Table 3.6.

Table 3.6 Classification of the samples studied based on brazing filler, coating type and coating thickness.

Brazing Filler	Coating	Coating Thickness	Brazing Temperature /Time
Cusil	Titanium	0.1 µm	875 °C / 10 min
Cusil-ABA	Titanium	0.1 µm	875 °C / 10 min

3.6 Wetting Experiments

The wetting behavior of the molten brazing alloy on the C/SiC surface is a critical issue in the performance of the brazed joints where proper chemical and physical interaction between the ceramic matrix composite surface and the brazing filler alloy should be ensured. Therefore, contact angle measurement was performed to study the wetting behavior of the brazing filler alloy and to examine the presence of chemical reactions at the interface between the liquid brazing filler alloy and the C/SiC composite surface. Wetting experiments were conducted in an atmosphere-controlled horizontal tube furnace specially developed and in-house modified for this purpose. The experimental set-up used in this study is depicted in Figure 3.6.

The designed set-up consists of a sealed Mullite tube, a K-type thermocouple, two PMMA windows and a high-resolution CCD camera. Brazing filler alloy, which was initially in powder form, was converted into the paste form by mixing with ethanol. Prepared paste was shaped into a thin disc by a uni-axial press applying 30 MPa of pressure. The compact disc-shaped brazing filler alloy approximately 5 mm in diameter and 1 mm in thickness was separated into two halves through the thickness direction. The same surface preparation procedure used before brazing experiments was applied to the surface of the C/SiC composite before wetting experiments. The C/SiC composite specimen with the size of 15 ×10 × 10 mm was placed in the alumina crucible, and one half of the pressed brazing alloy was put on its surface as shown in Figure 3.7.

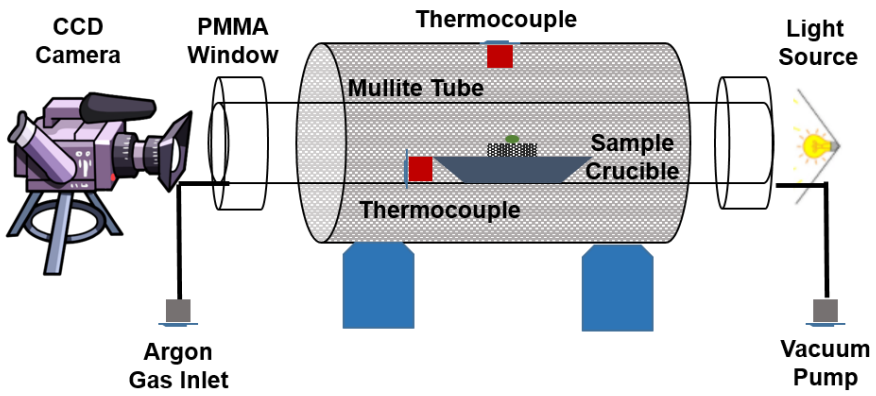

Figure 3.6 Schematic illustration of the in-house modified furnace used for wetting experiments.

In case of the 2D C/C-SiC composites, the thickness of the composite specimen was approximately 5 mm, which was insufficient to fill the alumina crucible. Therefore, a dummy piece of 3D C/SiC composite was used as a heat-resistant support material not to introduce different materials that might contaminate the furnace. Figure 3.8 displays the placement of 2D C/C-SiC composites with a size of 5 × 5 × 5 mm on top of the dummy 3D C/SiC composite surface.

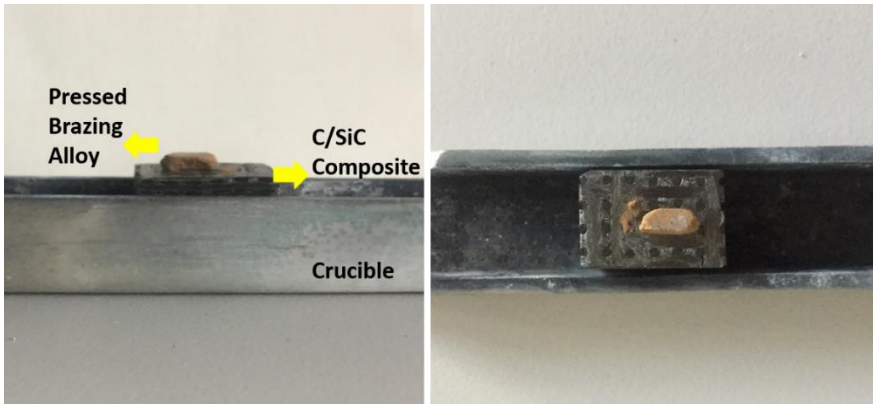

Figure 3.7 Placement of the compacted disc-shaped brazing filler alloy on the 3D C/SiC composite surface before the wetting experiment.

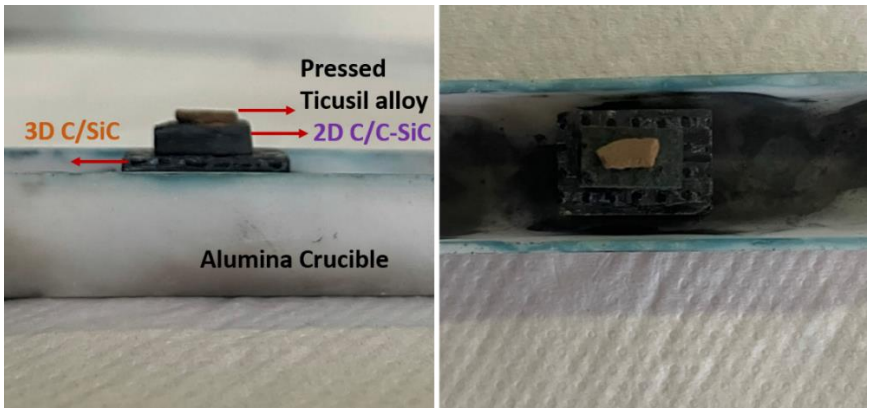

Figure 3.8 Placement of the compacted disc-shaped brazing filler alloy on the 2D C/C-SiC composite surface before the wetting experiment.

Prepared samples were transferred into the hot zone of the atmosphere-controlled horizontal tube furnace carefully. The materials were heated to experiment temperature at a continuous rate of 5 °C/min in wetting analysis tests, and then cooled slowly in the furnace after holding them at the experiment temperature for 1 h. In order to measure the contact angle, morphological changes of the molten filler alloy droplet were recorded with the aid of the CCD camera. The contact angles were determined on the taken images using image analysis software (ImageJ) after the wetting experiments. Parameters used as variables in the wetting experiments are given in Table 3.7.

Table 3.7 Parameters used as variables in wetting experiments

Substrate	Coating	Brazing Filler	Additive Material	Wetting Experiment Temperature /Time
C/SiC composite	-	Ticusil	-	915 °C / 15 min
SiC	-	Ticusil	-	915 °C / 15 min
C/SiC composite	-	Cusil	-	780 °C / 50 min
SiC	-	Cusil	-	780 °C / 50 min
C/SiC composite	+	Cusil	-	780 °C / 15 min
C/SiC composite	-	Cusil	1.25 wt% Ti	780 °C / 15 min
C/SiC composite	+	Cusil	1.25 wt% Ti	780 °C / 15 min
C/SiC composite	-	Ticusil	1% wt M-SiC*	915 °C / 15 min
C/SiC composite	-	Ticusil	2% wt M-SiC	915 °C / 15 min
C/SiC composite	-	Ticusil	5% wt M-SiC	915 °C / 15 min
C/SiC composite	-	Ticusil	10% wt M-SiC	915 °C / 15 min
C/SiC composite	-	Ticusil	20% wt M-SiC	915 °C / 15 min
C/SiC composite	-	Ticusil	1% wt nano-SiC	915 °C / 15 min
C/SiC composite	-	Ticusil	2% wt nano-SiC	915 °C / 15 min
C/SiC composite	-	Ticusil	5% wt nano-SiC	915 °C / 15 min
C/C-SiC composite	-	Ticusil	-	915 °C / 15 min
CNT impregnated C/C-SiC composite	-	Ticusil	-	915 °C / 15 min

*M-SiC denotes micron-sized SiC particles incorporated into the brazing filler alloy as additive

3.7 Characterization Studies

3.7.1 Microstructural Characterization

FEI Nova Nano SEM 430 type scanning electron microscope (SEM) was used to characterize the brazed joints as well as the samples of the wetting experiments microstructurally. SEM observations were carried out at a 20 kV accelerating voltage. Average reaction layer thickness values of the brazed joints were calculated applying the line measurement method of the software embedded in the SEM system during microstructural characterization. Using ten measurements taken from each SEM image, the average reaction layer thickness was determined for varying cases.

3.7.2 Phase Analysis by X-ray Diffraction (XRD)

The phase content of the brazed joints was determined using X-ray diffraction (XRD) analysis on a Rigaku D/MAX2200/PC equipment. Cu Kα radiation with a wavelength of 1.54056 Å was used as the source. Scans were performed at a rate of 2°/min in the 2θ angle range of 10-80°.

3.7.3 Shear Strength Test

Room temperature lap-shear tests with a screw-driven type testing machine were used to determine the mechanical properties of the joints under compression loading. The lap-shear tests were conducted using an in-house designed fixture (Figure 3.9(b)). The dimensions of the C/SiC composite side of the lap shear test specimens were 15 ×10 × 5 mm while those of the Ti6Al4V alloy side were 10 × 5 × 5 mm. A cross-head speed of 0.5 mm/min was used during testing. Equation (3.1) was used to compute the lap-shear strength (τ);

$$\tau = P / A \qquad (3.1)$$

where P is the force applied to the Ti6Al4V alloy side (Figure 3.9(a)), and A is the contact area between the two base materials of the brazed joints. Three distinct tests were used to calculate the average test results for each processing condition.

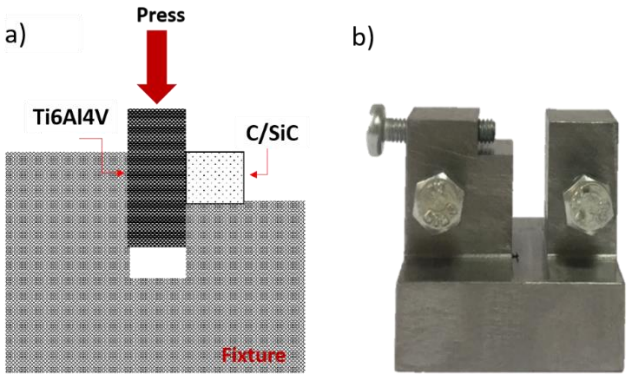

Figure 3.9 a) The schematics of the lap-shear test of the brazed joints and b) In-house designed fixture for the lap-shear test.

3.7.4 Microhardness Measurement

HMV-2 Shimadzu Scientific microhardness tester has been used to assess microhardness. A maximum load of 100 g was applied on the brazed joints for 10 s. Polished surfaces of the brazed joints were subjected to microhardness measurements. Microhardness tests were performed on both the C/SiC composite and the Ti6Al4V alloy base materials as well as around the interface. Each intended location was measured five times, and average of the results were reported.

3.7.5 Fractography Analysis

SEM was used to investigate the fracture surfaces of the mechanically tested joints to identify the mode of their fracture. Accelerating voltage of 20 kV was applied during the examinations.

3.7.6 Fluidity Analysis

The fluidity of the Ticusil brazing filler alloy on the composite surfaces has been investigated. The fluidity of the Ticusil brazing filler alloy has been calculated and compared using the height and spreading area of the solidified brazing filler alloy after wetting experiments. A schematic diagram for the identification of fluidity is given in Figure 3.10.

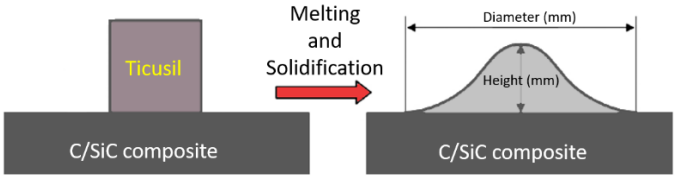

Figure 3.10 Schematic diagram of the fluidity calculation.

3.7.7 FEM Analysis

Finite element analysis (FEM) has been carried out to investigate the effect of different thermal properties of the ceramic composites on the mechanical strength of the brazed joints. In addition to the thermal properties of the composites obtained experimentally (thermal expansion coefficient, thermal conductivity, heat capacity), elastic modulus and density of the composites were also used for the finite element analysis.

3.7.8 Thermal Analysis

In order to investigate the thermal behavior differences of the 3D C/SiC composite, 2D C/C-SiC composite without CNT impregnation and 2D C/C-SiC composite with CNT impregnation, thermal diffusivity, specific heat, thermal conductivity and thermal expansion coefficient of each ceramic composite type were analyzed.

3.7.8.1 Thermal Diffusivity

The thermal diffusivity (α) of the carbon fiber reinforced ceramic composites was measured from room temperature to 1000 °C according to ASTM E 1461. A laser flash analyzer (DLF 1200, TA Instruments, USA) was used during the analysis. The samples utilized in the testing had a diameter of 12.7 mm and a height of 3 mm.

3.7.8.2 Specific Heat

A differential scanning calorimeter (DSC) was used to assess the specific heat (Cp) values of the ceramic composites in nitrogen atmosphere. Specimen dimensions were 5 × 5 × 1 mm. Specific heat measurement was conducted according to ASTM 1269 standard.

3.7.8.3 Thermal Conductivity

The thermal conductivity values of the ceramic composites were calculated using Equation (3.2);

$$\lambda = \rho \, . \, \alpha \, . \, Cp \qquad (3.2)$$

where ρ represents the density of the composite (g/cm^3). Thermal conductivities were measured parallel and perpendicular to the surface of the carbon fiber woven fabric in the composites.

3.7.8.4 Thermal Expansion Coefficient

Thermal expansion coefficient of the ceramic composites were determined according to ASTM E831-86 standard. NETZSCH DIL 402 PC type dilatometer was used for the tests with the sample size of 5 × 5 × 5 mm.

CHAPTER 4

RESULTS AND DISCUSSION

This chapter is divided into four sections. The interface evolution mechanism and mechanical performance of the ceramic matrix composite – metal brazed joints have been investigated using different brazing filler alloys in the first phase of the study to understand the effects of the active titanium (Ti) element on the brazing performance of the brazed joints. Furthermore, the influence of the brazing filler composition on the contact angle morphology and its change with time was also investigated. The second phase of the study has focused upon the effect of brazing temperature and time on the reaction layer formation at the interface region of C/SiC composite and Ti6Al4V alloy when Ticusil brazing alloy is used. Moreover, the effect of processing parameters (temperature and time) on the thickness/microstructure of the reaction layer has been investigated and discussed in detail. Additionally, spreading behavior of the Ticusil brazing alloy on C/SiC composite surfaces has been examined at various temperatures and holding time via wetting tests to enhance the joining performance of C/SiC composite to Ti6Al4V alloy. Furthermore, the influence of the thickness/microstructure of the interlayer and wetting behavior of the brazing alloy on the mechanical properties of the joints has been discussed comprehensively. Thirdly, influence of particle addition to the filler alloy on the interfacial reaction and resulting mechanical properties of the brazed joints has been investigated. The microstructural evolution and mechanical strength as well as the wetting behavior of the additive containing C/SiC composite/Ti6Al4V alloy joints were analyzed in detail. Finally, effects of various material characteristics and reinforcing structures of the ceramic matrix composite on the wetting behavior and related brazing performance of the C/SiC composite/ Ti6Al4V alloy joints have been discussed.

4.1 Effect of Active Brazing on Interface Evolution Mechanism and Mechanical Properties of C/SiC Composite/Ti6Al4V Alloy Joints

When compared to alternative joining methods, brazing of ceramic matrix composites and metallic materials has gained popularity in recent years due to its simplicity, lower cost, and potential as a mass production process [77-79]. One of the most problematic parts of brazing ceramic matrix composites to metallic components is the wetting of ceramic matrix composites. To remedy this issue, an active metal is introduced into the brazing filler to initiate the chemical reactions at the interface between the ceramic matrix composite and the filler material [68,81,82]. Thus, brazing filler materials for ceramic matrix composite/metals are produced by adding an active element (Ti, Hf, Cr, etc.) to a conventional filler alloys to assist the wetting of the ceramic matrix composite surface. [82,83].

In the present study, the brazing of C/SiC composites by using Cusil and Cusil-ABA brazing filler alloy are examined. Moreover, the interface evolution mechanism of the C/SiC composite/Ag–Cu based alloys/Ti6Al4V alloy joint is analyzed. The difference between Cusil and Cusil-ABA brazing filler alloy, Cusil-ABA contains a small amount of active Ti element in it. The amount of Ti in Cusil-ABA is 1.25 wt%. Both of the brazing filler alloys are in the sheet form and have 100 µm thickness. The aim of this study is to understand the effects of active brazing on the interface evolution mechanism and mechanical properties of C/SiC composite/Ti6Al4V alloy joints. Furthermore, the benefits of the lower brazing temperature and time have been categorized in the literature as regulated interfacial reactions, minimized substrate erosion, minimal loss of base material qualities, and minimal residual stresses [84-86]. Therefore, the effect of brazing parameters (such as temperature and time) on microstructural evolution and mechanical properties of C/SiC composite/Ti6Al4V alloy joints is investigated for both brazing filler alloys. Moreover, when the ceramic matrix composite surface is metalized, brazing of ceramic composite materials to metals becomes possible, and joint strength improves. To improve the wettability of

the substrates and the generation of the reaction product layer, the active Ti element was deposited on C/SiC composite surfaces via magnetron sputtering method.

4.1.1 Effect of Brazing Temperature on Microstructural Evolution and Mechanical Properties of C/SiC Composite/Ti6Al4V Alloy Joints

4.1.1.1 Cusil Brazing Filler Alloy

C/SiC composite and Ti6Al4V alloy specimens are brazed by using Cusil and Cusil-ABA brazing filler alloy at 850, 875 and 900 ºC, for 10 minutes. All of the joints formed with Cusil brazing filler alloy are subjected to fracture while cutting of the specimens in order to get cross-section. The fracture surfaces of the brazed joints were studied to determine the effect of brazing temperature on the spreading of brazing filler alloy over the C/SiC composite surface. (Figure 4.1). SEM micrographs reveal that the bonding and reaction formation between the C/SiC composite and the Ag-Cu filler alloy do not improve as the brazing temperature is raised.

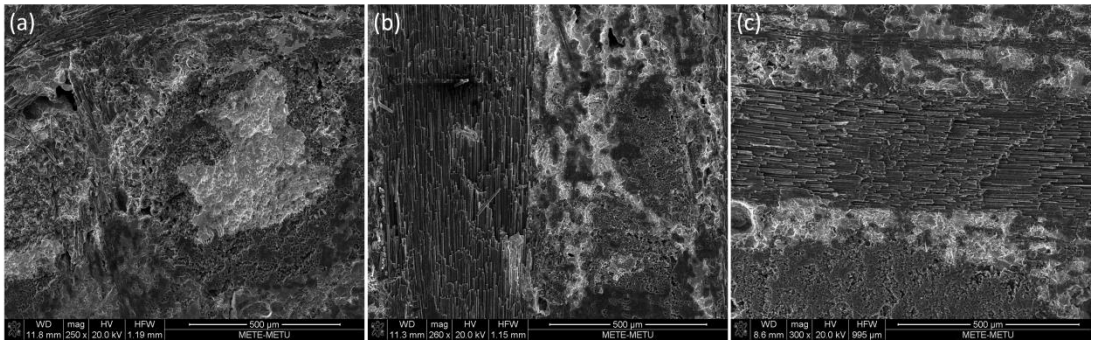

Figure 4.1 Microstructures of Ag-Cu brazing filler alloy over the C/SiC composite surface with brazing temperatures of a) 850, b) 875 and c) 900 ºC.

As it is seen from the Figure 4.1, C/SiC composite surface contains residual amount brazing filler alloy and these brazing filler containing regions are represented as light gray. According to the EDS analysis it can be stated that the molten Cusil braze alloy splits into two different liquids during brazing. One of these liquids is abundant in

Ag, whereas the other is abundant in Cu and contains a trace of Ti (Figure 4.2). Therefore, the silver rich region and the titanium-copper rich region are represented as white and gray respectively. These phases are dispersed in the interlayer upon cooling process. Although Cusil brazing filler alloy does not contain any titanium, because of existing Titanium content in Ti6Al4V alloy, the Ti6Al4V alloy base material itself provides the Ti element because of dissolution.

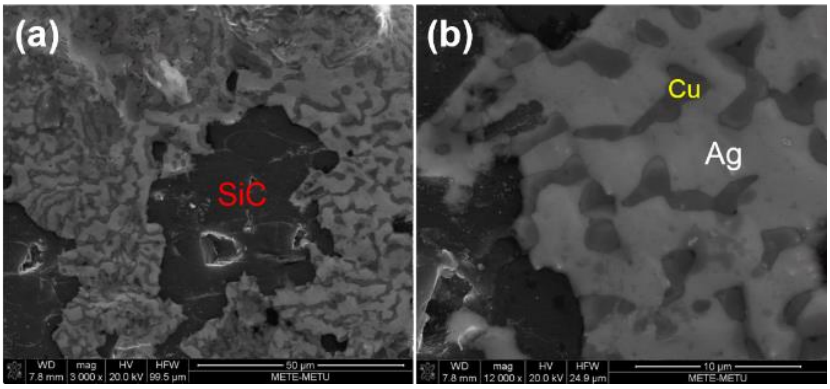

Figure 4.2 Microstructures of Cusil brazing filler alloy over the C/SiC surface.

For the Cusil brazing filler alloy, insufficient bonding is observed for all brazing temperatures due to lack of adhesion and wetting of the C/SiC composite. Therefore, it could be declared that dissolution of the Ti atoms from the metallic base materials are not available in sufficient quantity to ensure a uniform reaction layer for wetting and subsequent adhesion of the C/SiC composite.

Although Cusil brazing filler alloy does not wet the C/SiC composite, the alloy wets the Ti6Al4V metallic surface properly. Therefore, by the help of the atomic diffusion, interfacial bond without any defect and void is formed between two layers for all of the brazing temperatures. Fracture surfaces are examined to determine the effect of brazing temperature on the thickness of the diffusion reaction layer. (Figure 4.3). SEM micrographs present that fracture morphologies are same for all of the brazing temperatures and calculated average reaction layer thickness is approximately 25 μm.

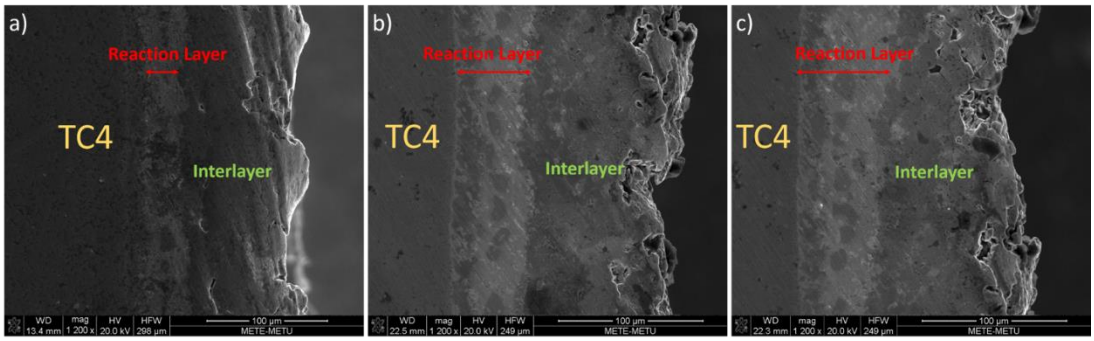

Figure 4.3 Fracture surfaces of Ti6Al4V metallic surface with brazing temperatures of a) 850, b) 875 and c) 900 ºC.

According to the EDS line analysis, diffusion reaction layers mainly contain Cu and Ti atoms and these Ti atoms are due to dissolution of the Ti element in the molten filler alloy. Cu atoms from the molten Cusil brazing filler tend to form intermetallic with Ti atoms from the metallic base material. Therefore, in order to monitor the occurrence of possible phases at the diffusion reaction layer, X-ray diffraction analysis are conducted to Titanium alloy/brazing filler interface. The X-ray diffraction presented in Figure 4.4 indicates that titanium-copper phases are formed in the interface between Ti6Al4V alloy and interlayer.

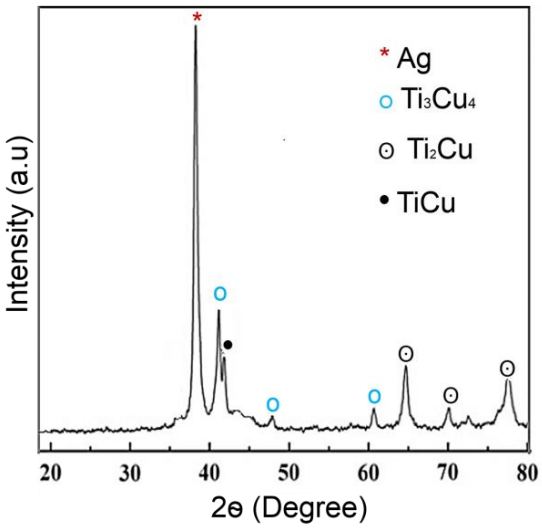

Figure 4.4 XRD analysis of Ti6Al4V/Cusil interlayer brazed at 875 ºC for 10 min.

4.1.1.2 Cusil-ABA Brazing Filler Alloy

In order to examine the effects of the active brazing alloy, brazing experiments were performed by using Cusil-ABA brazing filler alloy at 850, 875 and 900 ºC, for 10 minutes. According to the macrostructure and microstructure analysis (Figure 4.5), the joint interfaces are sound and well bonded. It can be stated that using Cusil-ABA brazing filler alloy instead of Cusil may cause to this improvement. For all of the brazing temperatures, although diffusion reaction layers exist between the interlayers and Ti6Al4V metallic parts, the reaction layer formation does not observe between the C/SiC composites and interlayers.

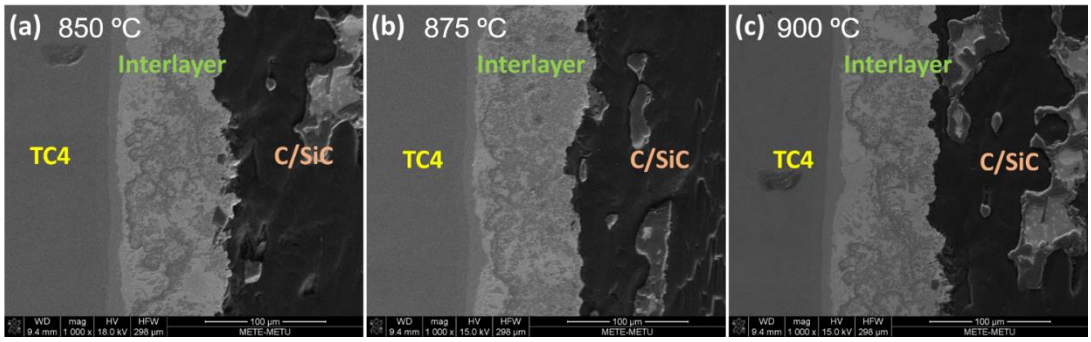

Figure 4.5 SEM micrographs of the interface between C/SiC composite and Ti6Al4V alloy joints brazed at a) 850 °C, b) 875 °C, and c) 900 °C

SEM micrographs of the interface between Ti6Al4V alloy and brazing filler alloy and the interface between C/SiC composite and filler alloy brazed by Cusil-ABA at 875 ºC for 10 min are presented in Figure 4.6(a) and (b), respectively.

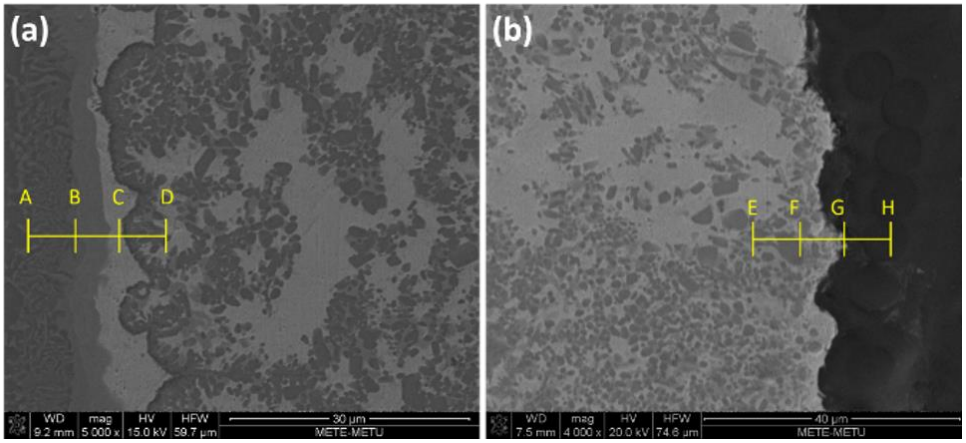

Figure 4.6. SEM micrographs of C/SiC Composite/Cusil-ABA/Ti6Al4V Alloy brazed at 875 °C, for 10 min a) the interface between Ti6Al4V alloy and the interlayer, b) the interface between C/SiC composite and the interlayer.

Table 4.1 The chemical composition of the C/SiC Composite/Cusil-ABA/Ti6Al4V Alloy brazed at 875 °C, for 10 min by EDS line analysis.

Element	***C***	***Si***	***Cu***	***Ag***	***Ti***	***Al***	***Possible Phases***
A	-	0.85	57.45	2.43	36.24	1.95	Ti_3Cu_4
B	-	1.35	36.84	2.33	48.62	8.21	Ti_2Cu, TiCu
C	4.32	-	20.7	81.8	1.53	-	Ag rich phase
D	0.96	0.73	55.72	4.33	38.26	-	Ti_3Cu_4
E	9.82	8.47	38.28	42.42	1.01	-	Cusil-ABA
F	8.32	8.35	51.8	2.78	28.75	-	Ti_3Cu_4
G	45.82	49.2	3.16	2.15	-	-	SiC matrix
H	89.02	5.72	2.14	3.12	-	-	Carbon fiber

Table 4.1 presents the chemical compositions of the brazed joint at 875 ◦C for 10 min. According to EDS analysis, possible phases for A and B points are Ti_2Cu, TiCu, and Ti_3Cu_4. According to the C, D and E points, silver rich region and the titanium-copper rich region disperse in the interlayer. Points G and H contain only Si and C elements; therefore, these microstructures represent the SiC matrix and carbon fiber. It is expected that the Ti element in the brazing alloy is predicted to react with the C/SiC composite surface during the brazing process, resulting in reaction products [56,87]. However, EDS analysis indicates that Ti_3SiC_2 and Ti_5Si_3 phases do not exist in the interlayer.

Table 4.2 Mechanical properties of brazed joints.

Brazing Parameters (Temperature/Time)	**Shear Strength (MPa)**
850 °C, 10 min	7.2
875 °C, 10 min	14.7
900 °C, 10 min	4.3

The effect of brazing temperature on the mechanical performance of brazed joints is demonstrated in Table 4.2. As it is presented, the joint strength increases at first and subsequently declines as the brazing temperature rises. By using Cusil-ABA brazing filler alloy, the joint brazed at 875 ºC for 10 min has the highest shear strength with 9.5 MPa. For all of the brazing temperatures, shear strength values are much lower comparing with the literature values [88]. As a result, for all brazing temperatures, the amount of atomic diffusion is restricted, and the reaction between brazing filler material and base materials is insufficient. The amount of titanium in the Cusil-ABA brazing filler alloy as an active element is insufficient to form the reaction product layers hence formation of strong interfacial bond between C/SiC composite and interlayer is absent. Moreover, it can be stated that for all of the joints fracture occurs at the C/SiC composite side due to the lack of interfacial bond.

The brazing temperature can be classified as the highest point in the brazing process, and it is higher than the liquidus of the brazing filler alloy. Reaction formations between the base materials and the brazing filler alloy are expected at this temperature for successful joining. The diffusion of the atoms is a thermally driven process and the kinetic energy of the atoms is controlled by the brazing temperature. Therefore, brazing temperature level directly affects the diffusivity of the atoms existing in the interlayer [89,90]. As a result, the brazing temperature has an impact on the kinetics of reactions at the C/SiC composite joint contact, as well as the phase distribution of the reaction layer. However, the amount of Ti in the brazing filler alloy composition that can diffuse to the C/SiC composite surface may be a factor [91].

Table 4.3 Shear strength values of the brazed joints.

Brazing Parameters (Temperature/Time)	**Shear Strength (MPa)**
5 min, 875 °C	3.5
10 min, 875 °C	14.7
15 min, 875 °C	4.8

At a brazing temperature of 875 °C, the influence of brazing duration on the shear strength of brazed joints is examined. As it is presented in Table 4.3, the joint brazed at 875 ºC for 10 min has the highest joint strength with 9.5 MPa, which is considerably less than the shear strength values mentioned in the literature [78]. Figure 4.16 displays the SEM micrographs of the interface between C/SiC composite and filler alloy brazed by Cusil ABA at 875 ºC for 5 min. According to the SEM micrographs and the average chemical composition of the C/SiC Composite/Cusil-ABA interface by EDS line analysis (Table 4.4), it can be stated that the lack of reaction layer development at the C/SiC composite interlayer is owing to insufficient atom reaction at those values.

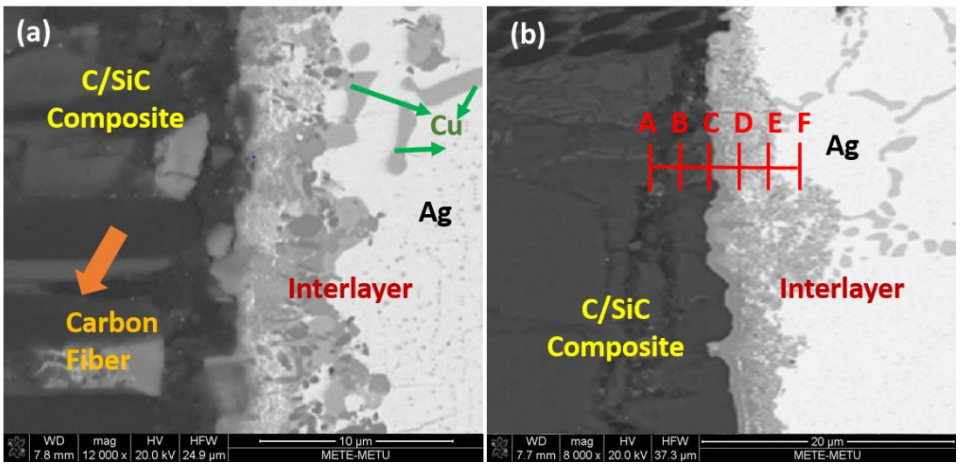

Figure 4.7 SEM micrographs of C/SiC Composite/Cusil-ABA/Ti6Al4V Alloy brazed at 875 °C, for 5 min a) and b) the interface between C/SiC composite and the interlayer.

Table 4.4 The chemical composition of the C/SiC Composite/Cusil-ABA/Ti6Al4V Alloy brazed at 875 °C, for 5 min by EDS line analysis.

Element	***C***	***Si***	***Cu***	***Ag***	***Ti***	***Al***	***Possible Phases***
A	24.64	69.40	3.84	2.12	-	-	SiC matrix
B	49.12	44.21	2.52	4.15	-	-	SiC matrix
C	36.92	54.72	5.89	10.8	0.22	-	No Ti_3SiC_2 and/or Ti_5Si_3
D	9.82	8.47	38.28	42.42	1.01	-	Cusil-ABA
E	7.12	9.43	40.42	41.51	1.62	-	Cusil-ABA
F	4.32	5.46	25.13	71.87	1.53	-	Cusil-ABA

In order to assess the mechanical performance of the brazed joints, microhardness test has been applied. Microhardness measurements are taken 1 mm interval for both

base materials. According to the analysis results, the residual brazing filler alloy at the Ti6Al4V alloy interface presents 173 Vickers hardness (Hv), which is less than the Ti6Al4V alloy hardness value of 261 Hv. It is seen that Ti6Al4V alloy/Cusil-ABA interface presents lower hardness than the metallic base material due to the existing of intermetallic compound mixture (Ti_3Cu_4, TiCu, Ti_2Cu) and flexible solid solution of silver phase. Furthermore, the hardness of C/SiC composite interface is 380 Hv while C/SiC composite has hardness value of 1300 Hv. For the C/SiC composite hardness values depend on carbon reinforcement and SiC matrix area. Carbon fiber containing regions have lower hardness values than the SiC matrix regions. The residual Cusil-ABA brazing filler alloy has a hardness of 138 Hv.

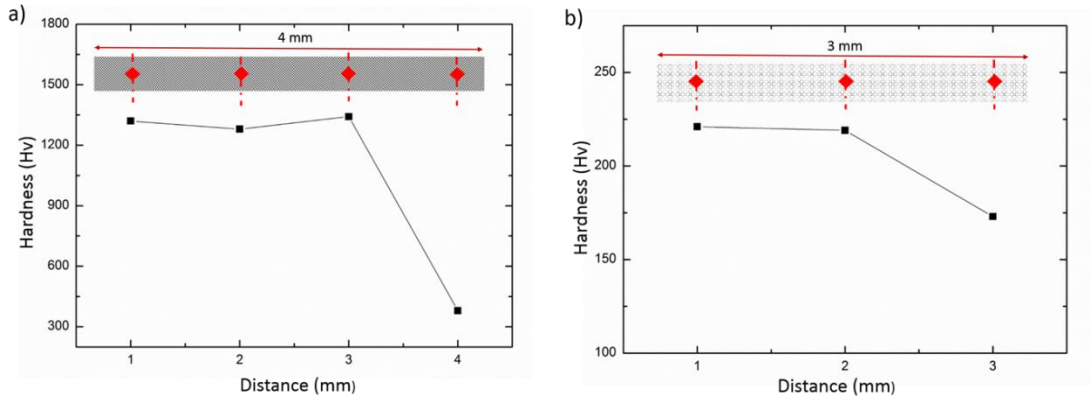

Figure 4.8 Microhardness analysis of C/SiC Composite/Cusil-ABA/Ti6Al4V alloy joint.

The interface evolution model of the C/SiC composite/Cusil-ABA/ Ti6Al4V brazed joint can be depicted schematically as shown in Figure 4.9. There are four phases to the entire brazing procedure:

a) Cusil-ABA brazing sheet melting: When furnace temperature approaches to melting point of the filler alloy, the alloy begins to melt and becomes liquid.

b) Diffusion of atoms: Some Ti and Cu atoms diffuse to both base material interfaces when brazing filler alloy is transformed into liquid.

Furthermore, some Ti atoms from the metallic base material tend to move to the brazing filler alloy. Some Si atoms from the SiC matrix are also expected to move towards to C/SiC composite/Cusil-ABA interface, however, Si atoms are not observed at the interface.

c) Forming reaction layers: According to EDS and XRD analysis, Ti_2Cu, TiCu and Ti_3Cu_4 phases are formed at the Cusil-ABA/Ti6Al4V alloy interface. Ti in the brazing alloy and the base metal, on the other hand, is inadequate to react with the ceramic matrix composite surface and generate reaction products.

d) Growing and solidification of the reaction layers: Thickness of the reaction layers formed at the Cusil-ABA/Ti6Al4V interface increase with increasing holding time and brazing temperature.

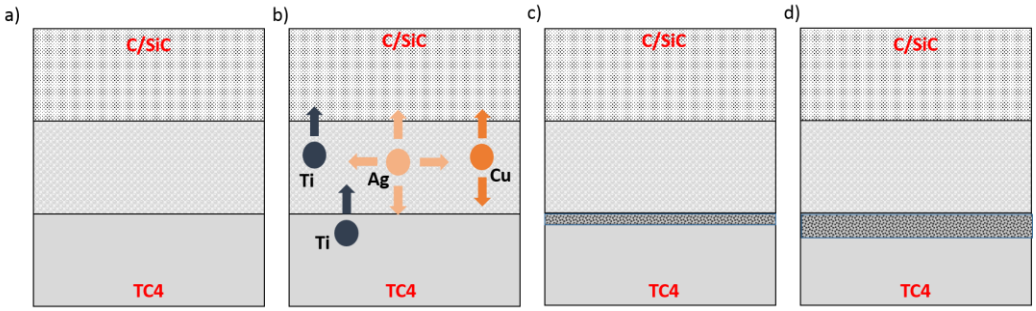

Figure 4.9 The interface evolution model for the C/SiC composite/Cusil-ABA/ Ti6Al4V alloy joint.

4.1.2 Effect of Titanium Layer Coating on Microstructural Evolution and Mechanical Properties of C/SiC Composite/ Ti6Al4V Alloy Joints

In this part of the study, active Ti element is coated on C/SiC composite surfaces by magnetron sputtering in order to enhance the wettability of the substrates and formation of the reaction product layer. Another purpose of this coating is to increase active Ti element amount of the brazing filler alloy. In order to examine the effects

of coated titanium layer on interface evolution and related mechanical performance of C/SiC composite/Ti6Al4V alloy joints, experimental studies have been carried with Cusil and Cusil-ABA brazing filler alloys at optimized brazing conditions. The test matrix including the type of brazing filler material and the type of coating is presented in Table 4.5.

Table 4.5 The test matrix depending on the type of brazing filler and the type of coating.

Brazing Filler	**Coating**	**Brazing Temperature /Time**
Cusil-ABA	Titanium (0.1 µm)	875 °C / 10 min
Cusil-ABA	-	875 °C / 10 min
Cusil	Titanium (0.1 µm)	875 °C / 10 min
Cusil	-	875 °C / 10 min

As shown in Figure 4.10, the right side presents C/SiC composite and the left side shows Ti6Al4V, between the base materials there exists an interlayer. The interfaces between the joints are well-bonded and free of flaws.

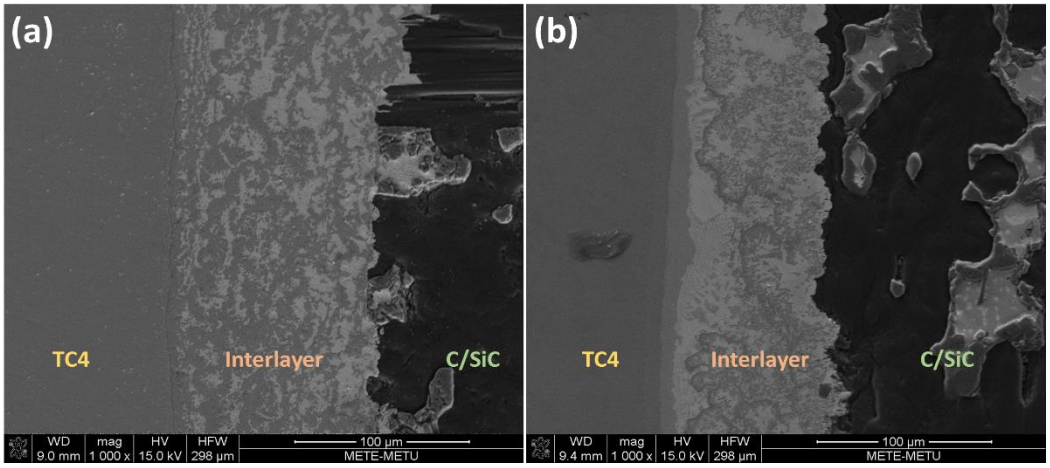

Figure 4.10 Microstructure of interface between C/SiC composite and Ti6Al4V alloy joints of (a) without Ti coating and (b) with Ti coating.

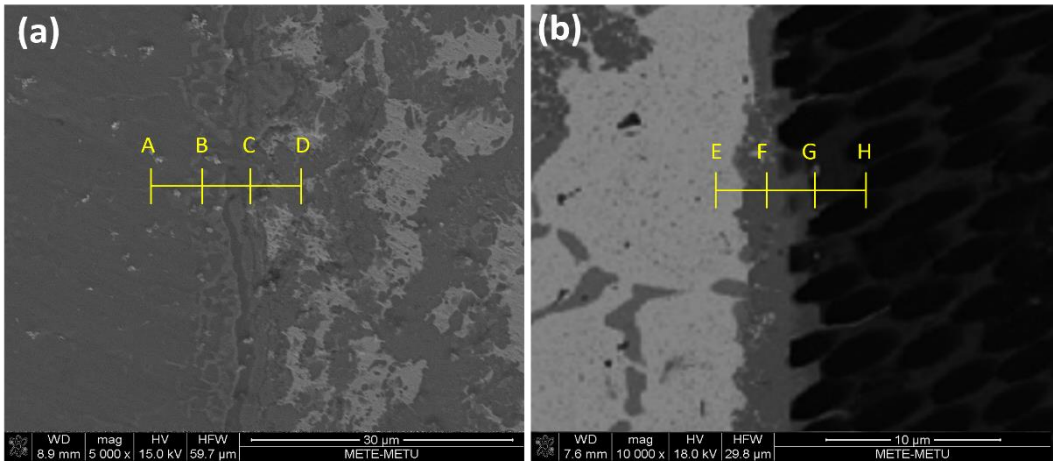

Figure 4.11 SEM micrographs of the interfaces between a)Ti6Al4V alloy and filler alloy and b) Ti layer coated C/SiC composite and filler alloy brazed by Cusil ABA at 875 ºC for 10 min.

SEM micrographs of the interface between metallic base material and Cusil-ABA alloy and the interface between Ti layer coated C/SiC composite and filler alloy brazed by Cusil ABA at 875 ºC for 10 min are presented in Figure 11(a) and (b),

respectively. As it is presented in the Figure 11(b), the reaction layer exists between the interlayer and the ceramic matrix composite base material.

Table 4.6 The chemical composition of A1 brazed joint by EDS line analysis.

Element	***C***	***Si***	***Cu***	***Ag***	***Ti***	***Al***	***Possible Phases***
A	-	-	0.54	1.08	88.64	6.31	TC4
B	0.63	0.22	56.30	1.23	38.44	2.02	Ti_3Cu_4
C	0.22	2.12	31.32	1.75	45.87	13.69	Ti_2Cu, TiCu
D	0.15	1.98	51.15	5.33	35.46	4.32	Ti_3Cu_4
E	3.32	-	21.67	79.89	3.53	-	Cusil-ABA
F	3.12	38.1	2.54	1.26	54.08	0.52	Ti_5Si_3
G	17.44	11.1	2.32	0.23	68.80	0.12	Ti_3SiC_2
H	96.15	3.85	-	-	-	-	Carbon fiber

According to EDS line analysis of points F and G (Table 4.6) and XRD analysis (Figure 4.12), possible phases for the reaction layer are Ti_3SiC_2 and Ti_5Si_3 compounds. Obtained Ti_3SiC_2 and Ti_5Si_3 reaction layer phases reveal that the coated Ti layer on the C/SiC composite surface enhances the wettability of the C/SiC composite surface that forms the reaction phases [92].

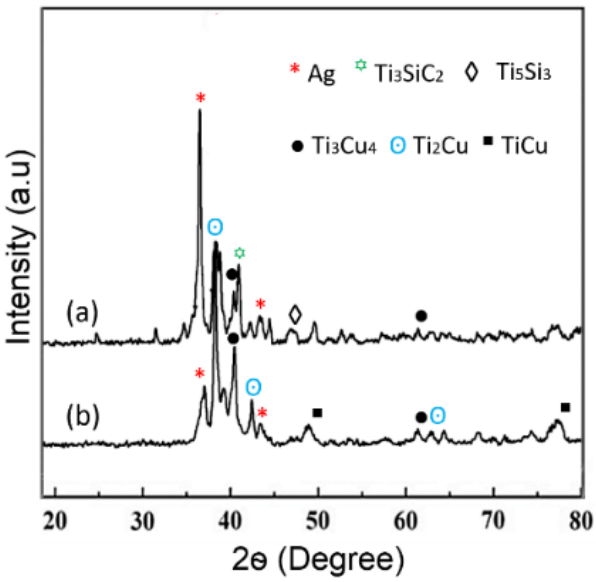

Figure 4.12 XRD analysis of (a) interface between Ti layer coated C/SiC composite and interlayer, (b) interface between Ti6Al4V alloy and interlayer.

When the brazing temperature reaches to liquidus of the brazing filler alloy, molten Cusil-ABA braze filler alloy tends to split into two liquids. There are two types of liquids: silver-rich and copper and titanium-rich. As a result, the Ag phase (presented in white color in SEM micrographs) and the Ti-Cu phase (presented in grey color in SEM micrographs) disperse in the interlayer throughout the cooling process. As illustrated in Figure 4.11(b), the Ti element existing in the brazing alloy and/or the coating reacts with the C/SiC composite surface during the brazing process, as a result, carbon fibers are extruded at the contact between the C/SiC composite and the interlayer. This appearance improves the mechanical performance of the joint, and it also suggests that Ti reacts more violently with SiC matrix than carbon fibers. According to the elemental analysis, as presented in Table 4.5, dark grey marks along the interface between the C/SiC composite and the interlayer are caused by the Ti_5Si_3 phase of the reaction products for the SiC matrix of the C/SiC composite. The other result could be the Ti_3SiC_2 compound, which is dispersed on the SiC matrix surface. In case of the Ti6Al4V alloy base material, Ti atoms diffuse into the molten braze alloy from metallic base material, whereas Cu atoms in the brazing filler alloy also

diffuse into the Ti6Al4V alloy. Figure 4.11(a) displays that diffusion reaction layer exists between interlayer and the Ti6Al4V alloy. Layers are mainly composed of Ti and Cu elements with Ti_3Cu_4/TiCu/Ti_2Cu/ phases according to EDS (Table 4.5) and XRD analysis (Figure 4.12) results.

As mentioned before, Cusil-ABA brazing filler alloy is defined as active brazing alloy containing small amount of Ti. Cusil, on the other hand, is a eutectic composition of Ag and Cu that lacks any active element for bond formation on the C/SiC composite surface. In order to check whether Ti layer coating on C/SiC surface improves bond formation of the Cusil or not, experimental studies have been carried with Cusil brazing filler alloy at optimized brazing conditions. Microstructural evolution of Ti layer coated C/SiC composite interface brazed by Cusil brazing filler alloy is compared with Ti layer coated C/SiC composite interface brazed by Cusil-ABA in order to monitor the differences. Figure 10(a) and (b) present SEM micrographs of the interfaces between Ti6Al4V alloy/interlayer and Ti layer coated C/SiC composite/interlayer, respectively.

Different form the brazing experiments carried out by Cusil-ABA brazing filler alloy, Ti layer coated C/SiC composite/Cusil/Ti6Al4V alloy joint contains some crack and voids at the C/SiC composite interlayer. Besides, the interlayer is not homogeneous in terms of Cu and Ag phases as the previous brazing experiments. It can be stated that, 0.1 μm Ti layer coating is insufficient to create the reaction product layers at the C/SiC composite side and not available in sufficient quantity to ensure a uniform reaction layer for good adhesion and wetting of the C/SiC composite.

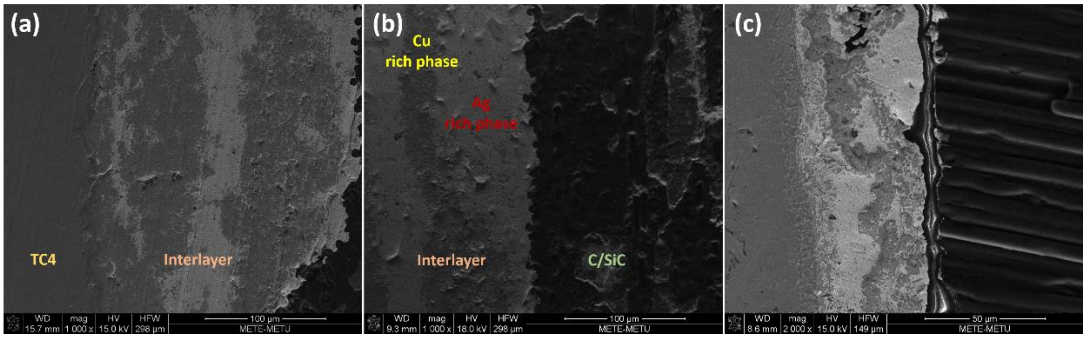

Figure 4.13 SEM micrographs of the interfaces between a) Ti6Al4V alloy and interlayer, b) interlayer and Ti layer coated C/SiC composite, c) the interlayer between C/SiC composite and Ti6Al4V alloy joints.

Table 4.7 Mechanical properties of brazed joints

Sample Name	**Brazing Temperature/ Time**	**Shear Strength (MPa)**
Ti layer coated C/SiC composite/Cusil ABA/Ti6Al4V alloy	875 °C / 10 min	23.8
C/SiC composite/Cusil ABA/Ti6Al4V alloy	875 °C / 10 min	14.7
Ti layer coated C/SiC composite/Cusil/Ti6Al4V alloy	875 °C / 10 min	3.2
C/SiC composite/Cusil/Ti6Al4V alloy	875 °C / 10 min	3.6

Ti layer coating effects on the shear strength of the brazed joints is shared in Table 4.7. It can be stated that by using Cusil ABA brazing filler alloy, the joint brazed at 875 ºC for 10 min with Ti layer coating presents the maximum shear strength of 23.8 MPa. Ti present in the Cusil-ABA brazing filler alloy is in insufficient amount to create the reaction product layers hence the formation of the strong interfacial bond between C/SiC composite and the interlayer. The coated Ti layer on the C/SiC composite surface enhances the wettability of the C/SiC composite surface that forms the reaction phases that result in a strong interfacial connection between C/SiC

composite and the interlayer. For Cusil brazing filler alloy, insufficient bonding shows that Ti layer coating cannot provide enough reactive elements for bond formation on the C/SiC composite side. Therefore, as a result of the lack of a reaction layer, the brazing filler material behaves as an adhesive bonding, causing failure of the joints at low shear forces.

4.1.3 Wetting Behavior of Brazing Filler Alloys

During the wetting of the ceramic matrix composite surface by the molten brazing filler alloy, dissolution or phase formation may occur due to the reactions taking place at the interface. According to the Reaction Product Control Model, contact angle has two stages; initial contact angle, θ_0, and observed contact angle on the reaction layer, θ_F, [48]. Details of the Reaction Product Control Model are given in Section 2.6.2 of Chapter 2 Literature Research. In this section, observed contact angle on the reaction layer, θ_F, is referred to as contact angle during the discussion of the experiments.

4.1.3.1 Wetting Mechanism of SiC Ceramic and Cusil Brazing Filler Alloy

Wetting behavior of Cusil brazing filler alloy on monolithic SiC ceramic surfaces has been studied at varying temperature and time conditions. The change in the morphology of the Cusil brazing filler during the wetting experiment and the variation of the contact angle measured as a function of time at 780 °C are shown in Figure 4.14 and 4.15, respectively. Figure 4.14 demonstrates that the morphology of the brazing filler alloy does not change considerably at temperatures up to 750 °C; nevertheless, as the temperature reaches to 770 °C, the brazing filler alloy begins to expand. At 780 °C, the Cusil brazing filler alloy begins to melt, and it takes 30 s for the melting to complete. The measured initial contact angle is ~110° at 780 °C. Initially, it reduces slowly to ~100° in the range of 0–100 s, and then it remains constant. During the experiment, spreading was not observed and the diameter of the

molten brazing filler alloy remained constant after 300 s. The contact angle being higher than 90° and remaining at a constant value indicates that Cusil brazing filler alloy presents non-wetting condition.

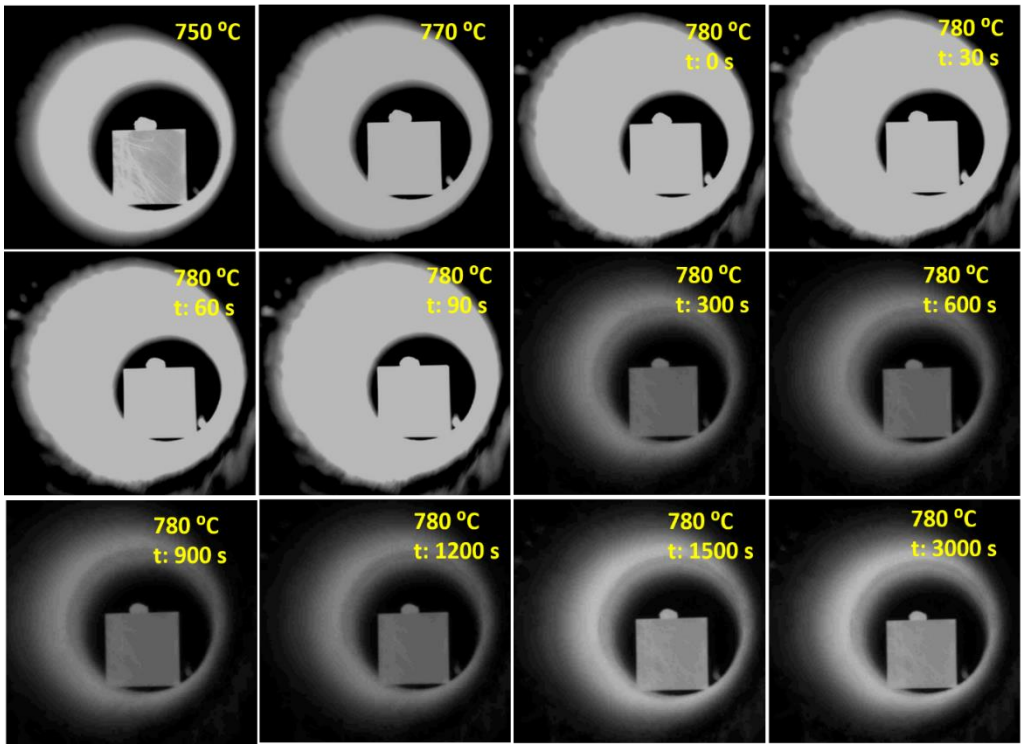

Figure 4.14 Morphological changes of Cusil brazing filler alloy on monolithic SiC ceramic surface under different temperature and time conditions.

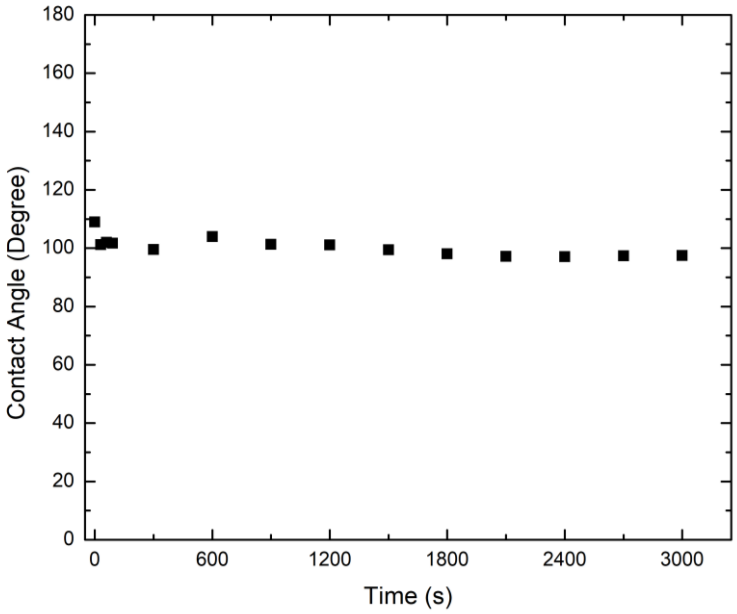

Figure 4.15 Contact angle variation of Cusil brazing filler alloy with respect to time at 780 °C on monolithic SiC ceramic.

4.1.3.2 Wetting Mechanism of C/SiC Composite and Cusil Brazing Filler Alloy

The wetting behavior of Cusil brazing filler alloy on C/SiC composite surface has been investigated with respect to temperature and time to reveal the effect of active Ti element on wetting. It is known that compared to the Cusil-ABA brazing filler alloy, Cusil is mainly composed of Cu and Ag having a melting point of 780 °C. Variation of the contact angle measured with respect to time at 780 °C is presented in Figure 4.17. The morphology of Cusil brazing filler on C/SiC composite during heating up to the temperature of 780 °C and the subsequent change in the morphology of the filler alloy when the composite material is held at the constant temperature of 780 °C is given in Figure 4.16.

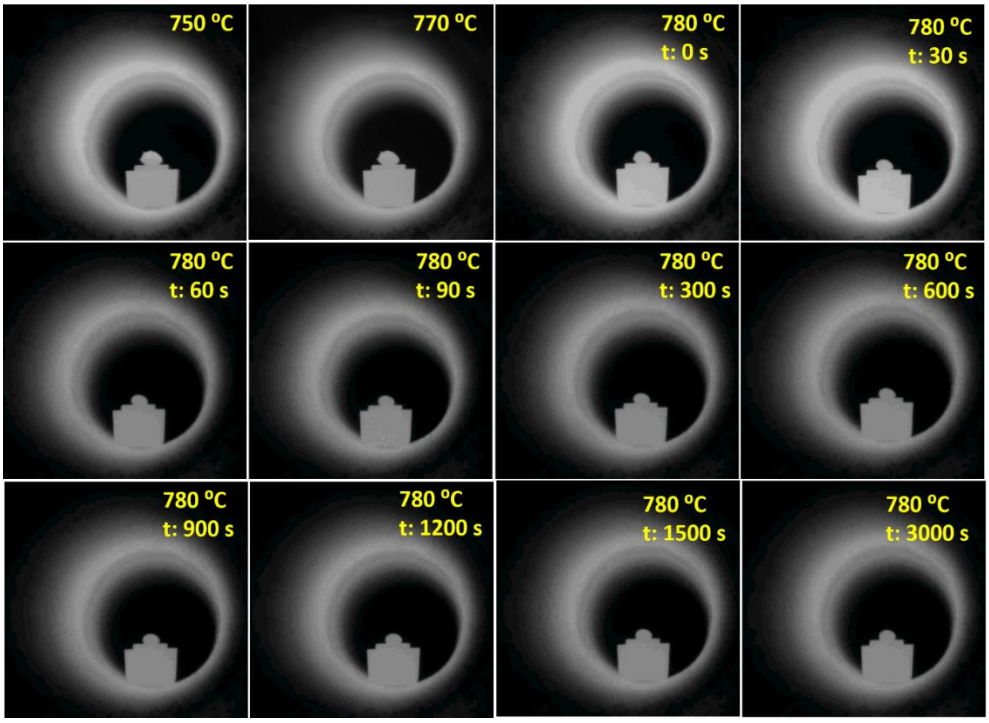

Figure 4.16 Morphological changes of Cusil brazing filler alloy on C/SiC composite surface under different temperature and time conditions.

Figure 4.17 presents the fluctuation in the contact angle of Cusil brazing filler alloy as a function of time at 780 °C for both C/SiC composite and monolithic SiC ceramic. The results were used to understand how the heterogeneity of the C/SiC composite together with the presence of the carbon fibers in the structure affect the wetting behavior. Observed contact angles of 120° and 100° for C/SiC composite and SiC ceramic, respectively, point out to the fact that both of them are being insufficiently wet by Cusil filler alloy, as shown in Figure 4.17. The non-spreading morphology of the droplets is consistent over time and does not change. Because existing carbon fibers in the structure further hinder the spreading of the molten Cusil filler alloy on the surface, C/SiC composite has a larger contact angle than monolithic SiC ceramic.

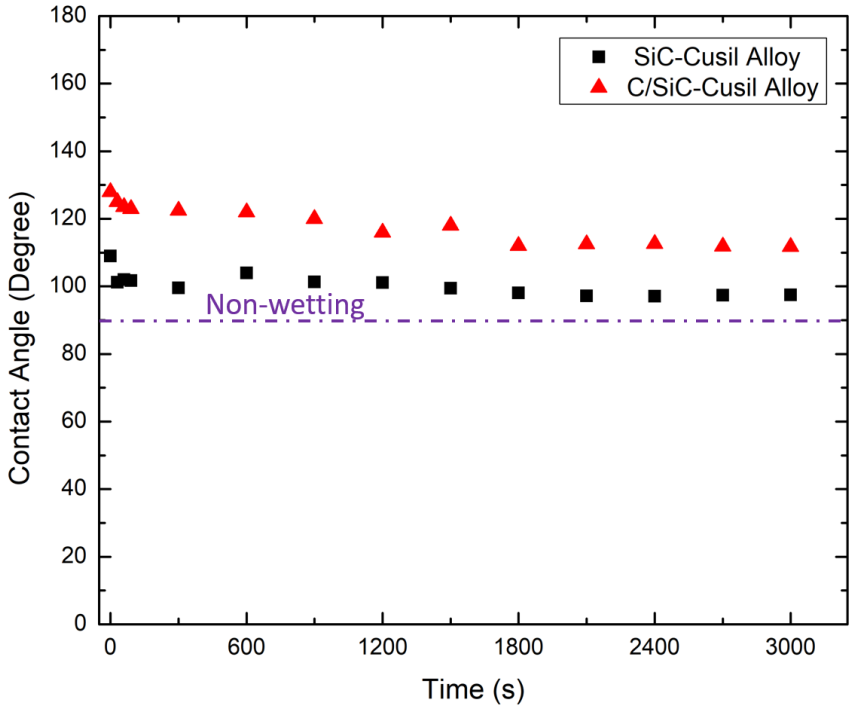

Figure 4.17 Contact angle variation of Cusil brazing filler alloy with respect to time at 780 °C on both C/SiC composite and monolithic SiC ceramic.

Because of their ionic/covalent bonding patterns, ceramics have low wettability when compared to metallic parts. In the present case, the wettability of the C/SiC composite is further negatively affected by chemical and structural heterogeneity, as well as by the presence of carbon fibers on the surface. The use of active brazing fillers should be recommended as a solution to improve the wettability of ceramic matrix composites. In active brazing, the brazing filler alloy incorporates surface-active elements such as Ti which improve adhesion and bonding properties of the material.

4.1.3.3 Wetting Mechanism of Ti Layer Coated C/SiC Composite and Cusil Brazing Filler Alloy

The influence of an active Ti layer on the wetting behavior of the Cusil has been examined. Figure 4.18 presents the morphological variations of the Cusil brazing filler alloy on the Ti layer coated C/SiC composite surface under various temperature and time conditions. The Cusil brazing alloy starts to melt at 770 °C, and observed contact angle is approximately 90° at the 780 °C. The contact angle value decreases to 60° when the experiment time reaches to 90 s. Finally, it reaches a steady-state contact angle of 55° indicating partial wetting behavior.

The effect of Ti layer coating on the variation of measured contact angle at 780 °C as a function of time is demonstrated in Figure 4.19. While there is non-wetting behavior of Cusil brazing filler alloy on the uncoated C/SiC surface, the Ti layer coating significantly improves wetting behavior. It can be stated that the Ti atoms existing in the Ti coating layer interact with the molten brazing alloy and form thin reaction products improving the wetting behavior of the brazing filler alloy [93].

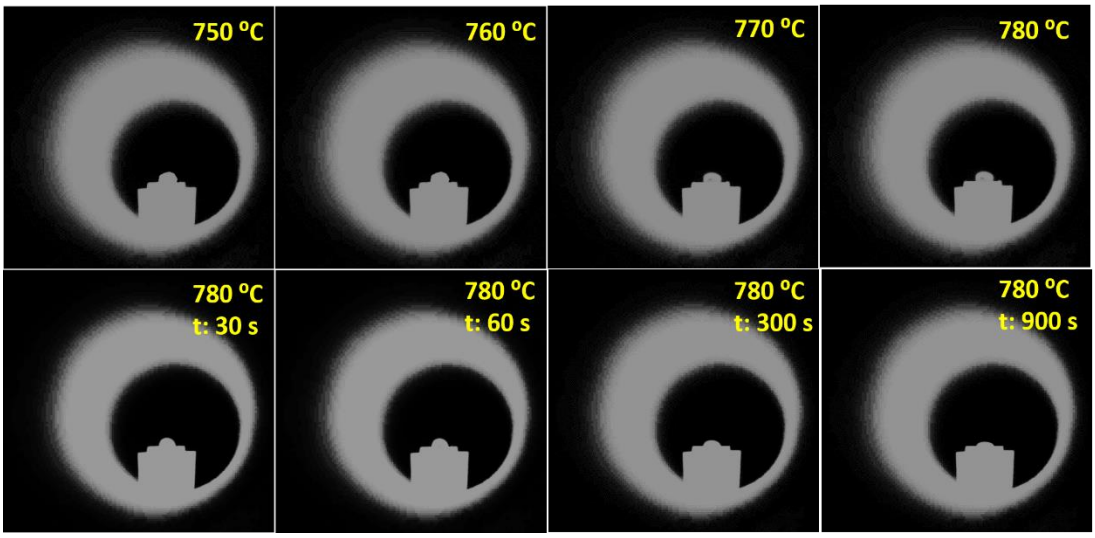

Figure 4.18 Morphological changes of Cusil brazing filler alloy on the Ti layer coated C/SiC composite surface under different temperature and time conditions.

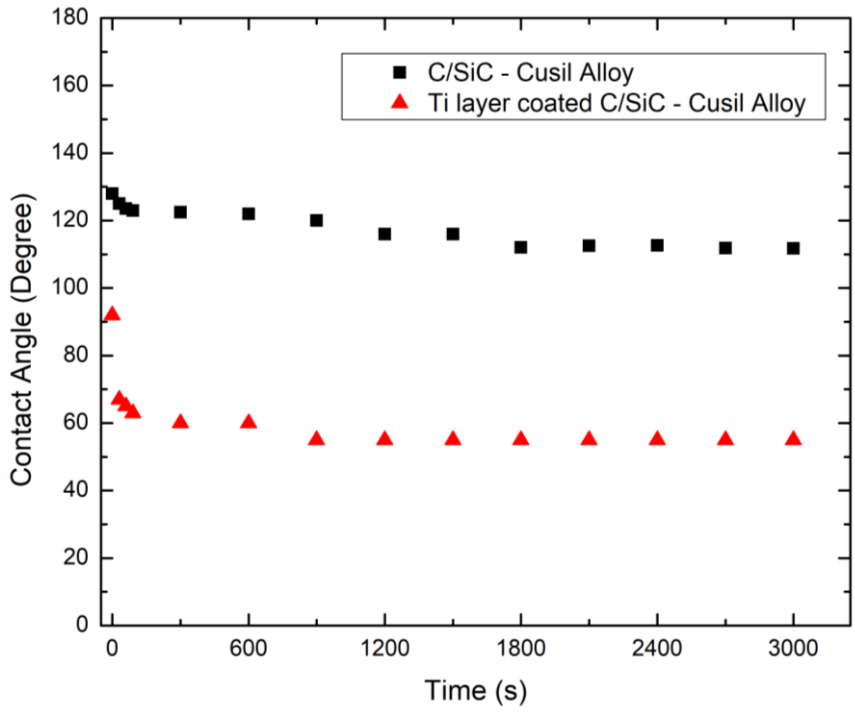

Figure 4.19 Effect of Ti layer coating on the contact angle variation of Cusil brazing filler alloy with respect to time at 780 °C.

4.1.3.4 Wetting Mechanism of C/SiC Composite and 1.25 wt% Ti Powder Containing Cusil Brazing Filler Alloy

Wetting behavior of Ti powder added Cusil brazing filler alloy has been investigated under different temperature and time conditions. Because it has a sheet form, originally Ti containing Cusil-ABA filler alloy is not suitable for use in wetting tests. As a result, the experiment was conducted by adding 1.25% Ti by weight into the Cusil alloy in the form of a paste. The morphology changes of 1.25 wt% Ti powder containing Cusil brazing filler with respect to temperature and time are presented in Figure 4.20. As it is seen in Figure 4.20, as the temperature exceeds 780 °C, the brazing alloy begins to melt. At 780 °C in the first 300 s, the contact angle decreases dramatically from 80° to 55°, where it reaches a steady state contact angle of 52° suggesting appropriate wetting behavior (Figure 4.21).

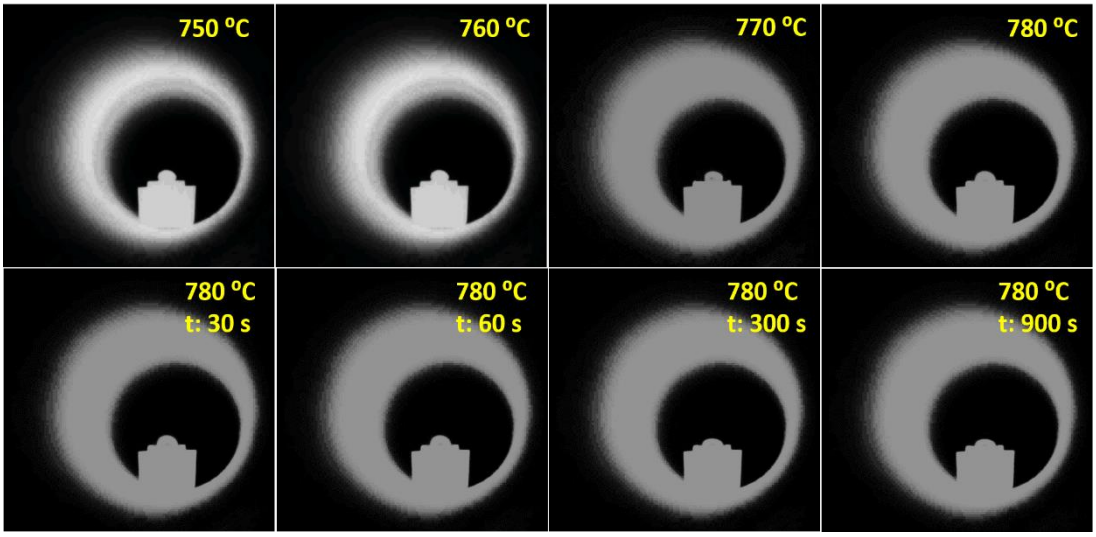

Figure 4.20 Morphological changes of 1.25 wt% Ti powder containing Cusil brazing filler alloy on C/SiC composite surface under different temperature and time conditions.

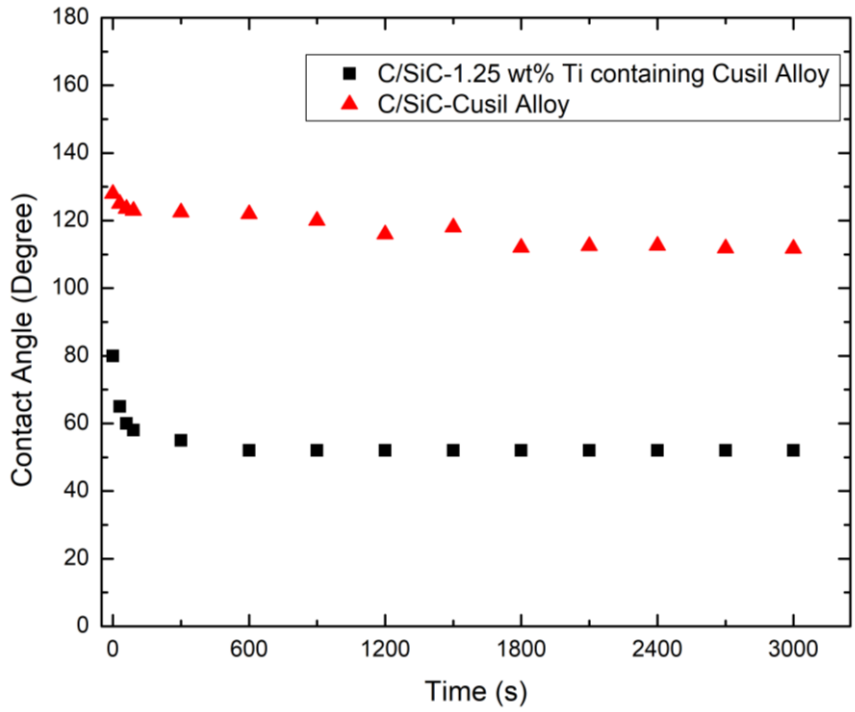

Figure 4.21 Contact angle variation of Cusil and 1.25 wt% Ti containing Cusil brazing filler alloys with respect to time at 780 °C.

Effect of 1.25 wt% active Ti element addition on the contact angle variation at 780 °C has been investigated as a function of time. According to Figure 4.21 it can be stated that the steep decrease in the contact angle continues up to 300 s for 1.25 wt% Ti added Cusil brazing filler alloy, while it terminates in 60 s for the Cusil brazing filler alloy (Figure 4.21). Although the contact angle of Cusil on C/SiC composite is 110°, and hence it cannot wet the ceramic composite surface, wetting angle obtained by adding 1.25 wt% Ti renders the filler material alloy wettable.

The chemical interaction of active Ti element with the ceramic matrix composite surface accounts for the decrease in the contact angle observed with the addition of a small amount of activate Ti element. At the contact between the C/SiC composite surface and the molten filler material, dissolution of the active Ti element in the molten filler alloy takes place. Therefore, a reaction layer composed of reaction products is formed. The surface tension of the C/SiC composite surface is

significantly reduced as a result of the improved chemical structure allowing the brazing filler material to wet the C/SiC composite surface sufficiently [94][53][95].

4.1.3.5 Wetting Mechanism of Ti Layer Coated C/SiC Composite and 1.25% Ti Powder Containing Cusil Brazing Filler Alloy

The effect of Ti layer coating on the ceramic matrix composite surface and 1.25 wt% Ti addition to Cusil brazing filler alloy on the wetting behavior has been investigated, simultaneously. The morphological changes of the 1.25 wt% Ti added brazing filler alloy on the Ti layer coated C/SiC composite under different temperature and time conditions are displayed in Figure 4.22. At 780 °C observed initial contact angle is 75°, and this level decreases up to 45° within the time interval of approximately 300 s. The contact angle did not alter significantly in the following periods, and it was reported as 45° at the end of the wetting experiment.

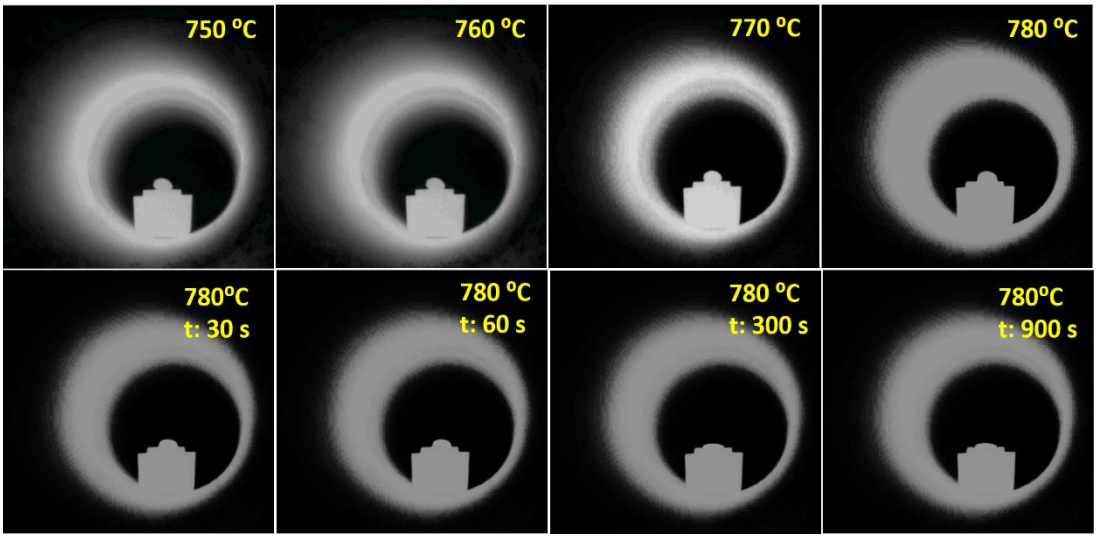

Figure 4.22 Morphological changes of 1.25 wt% Ti powder containing Cusil brazing filler alloy on the Ti layer coated C/SiC composite surface under different temperature and time conditions.

Figure 4.23 shows the variation in observed contact angle for active Ti element added Cusil brazing filler on Ti layer coated and uncoated C/SiC composite surface at 780 °C with respect to time. As it is seen in the figure, the starting contact angles are nearly identical and present a comparable decreasing tendency over time. Under identical conditions, the uncoated C/SiC composite surface has a contact angle of 52°, whereas the Ti layer coated composite surface has a contact angle of 45°. It can be stated that for 1.25 wt% Ti containing Cusil brazing filler alloy, the use of Ti layer coating applied on the ceramic composite surface improves the wetting behavior, even though the improvement does not seem so significant.

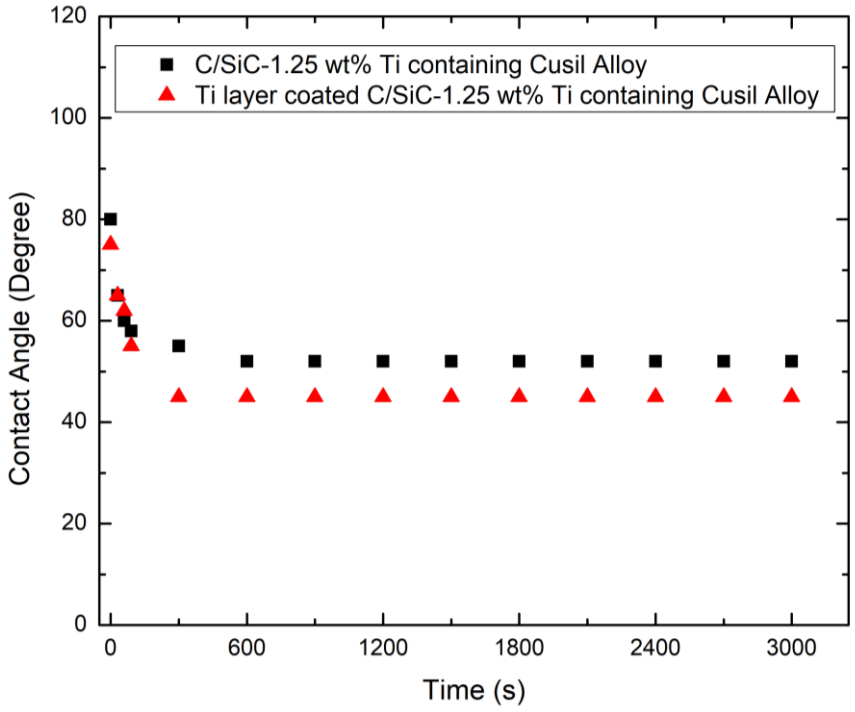

Figure 4.23 Effect of Ti layer coating on the ceramic composite surface and addition of Ti element to the brazing filler alloy on the contact angle variation of Cusil with respect to time at 780 °C.

4.1.3.6 Wetting Mechanism of SiC Ceramic and Ticusil Brazing Filler Alloy

Under different temperature and time settings, the wetting behavior of the 4.5 wt% Ti containing Ticusil brazing filler alloy on the monolithic SiC ceramic has been examined. The morphology of Ticusil brazing filler on the SiC ceramic during the wetting experiment is shown in Figure 4.24. As it is presented in Figure 4.24, the morphology of the brazing filler alloy does not change significantly up to 870 °C; however, when the temperature reaches to 880 °C, the brazing filler alloy exhibits a curved morphology at the margins. At ~903 °C, the contact angle starts to decrease.

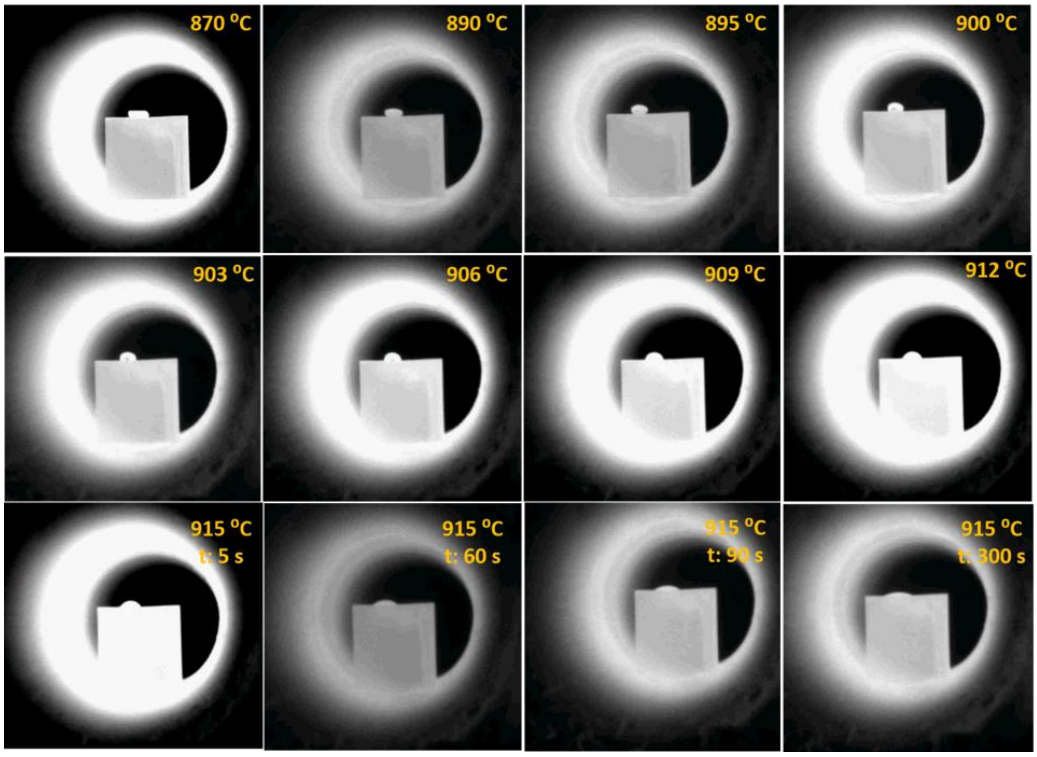

Figure 4.24 Morphological changes of Ticusil brazing filler alloy on monolithic SiC ceramic surface under different temperature and time conditions.

Figure 4.25 presents the variation of the contact angle as a function of time at 915 °C. The measured initial contact angle is ~45° at 915 °C. The contact angle declines from ~45° to ~10° when the sample is held up to 300 s at 915 °C. As it is seen from Figure 4.25 the contact angle does not change considerably when the samples are kept at 915 °C for 900 s. When compared to the obtained value of 100° for Cusil brazing filler alloy on the SiC ceramic surface, a contact angle of 10° indicates good wetting of SiC ceramic by Ticusil filler alloy.

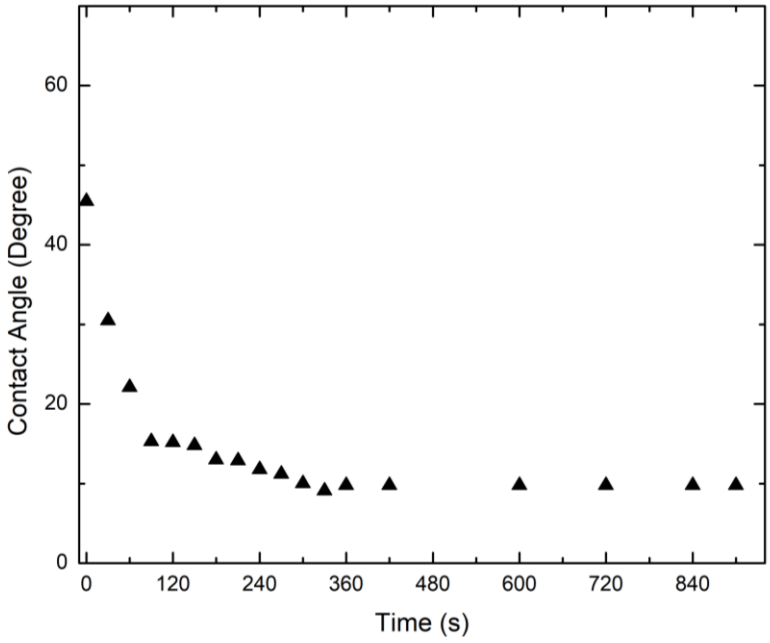

Figure 4.25 Contact angle variation of Ticusil brazing filler alloy monolithic SiC ceramic with respect to time at 915 °C.

4.1.3.7 Wetting Mechanism of C/SiC Composite and Ticusil Brazing Filler Alloy

The wetting behavior of the C/SiC composite controls the efficiency of the brazing process and interfacial reactions. The wetting behavior of the brazing filler alloy on the C/SiC composite surface has been investigated with respect to temperature and

time to reveal optimized brazing conditions. It is known that the brazing filler alloy used in the present study has a liquidus temperature of 900 °C. The change of the measured contact angle with temperature and time is shown in Figure 4.26. The figure displays the change of the morphology of brazing filler on C/SiC composite during heating to brazing temperature of 915 °C and subsequent change in the contact angle when the sample is held for 900 s at a constant temperature of 915 °C. At temperatures up to 780 °C, there is no significant change in the brazing filler alloy morphology; however, when the temperature reaches to 780 °C, the brazing filler alloy starts to expand and have a curved morphology at the edges. According to Figure 4.26, the brazing filler alloy is completely melted and begins to spread at ~903 °C, and the spreading morphology remains unchanged between 903 and 912 °C. The contact angle is nearly constant because time is required for active Ti atoms to dissolve in the liquid metal and move to the interface between C/SiC composite and brazing filler by diffusion. Following this stage, the contact angle starts to decrease.

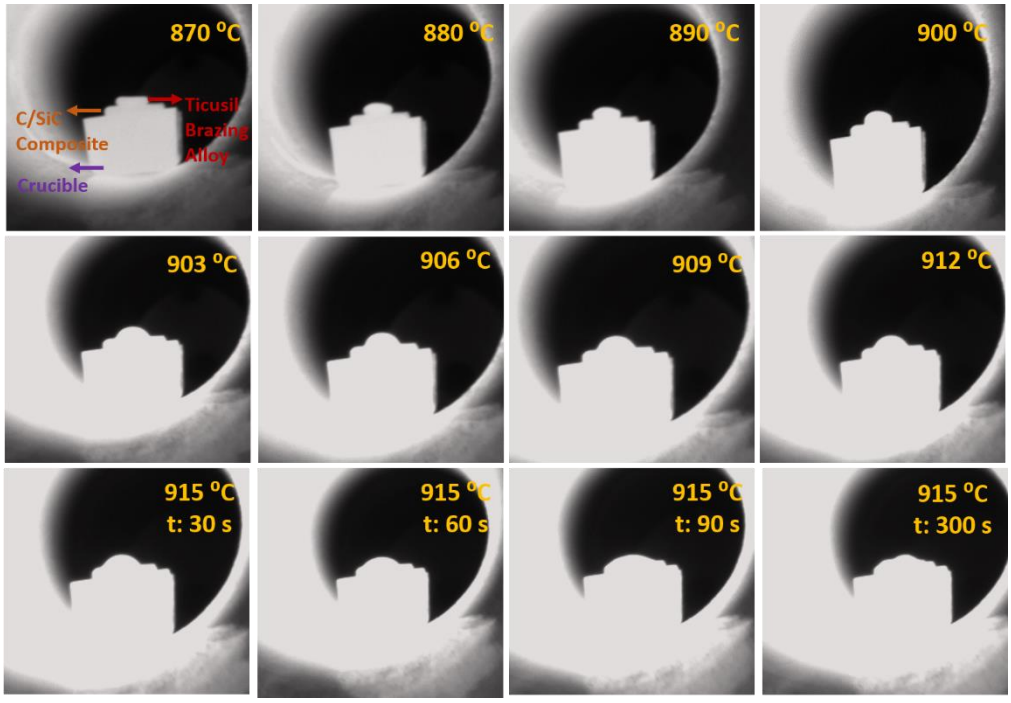

Figure 4.26 Morphological changes of brazing filler alloy on C/SiC composite surface under different temperature and time conditions.

The measured initial contact angle, which is shown as instant zero in Figure 4.27, is ~50° at 915 °C. The contact angle displays two different changes at two different time intervals. Initially, it reduces dramatically up to 100 s and decreases slowly in the range of 100–300 s. Finally, it reaches a steady-state contact angle of ~15°, which corresponds to excellent wetting. In the present study, better wetting condition is obtained with very low contact angle compared to similar studies present in the literature. For example, achieved minimum contact angle values were reported as 27° and 50° for C/C composite and SiC/SiC composite materials, respectively, when the brazing alloy identical to that of the current study was used [96]. Therefore, Ticusil alloy seems to be a more suitable brazing alloy for C/SiC composites during brazing.

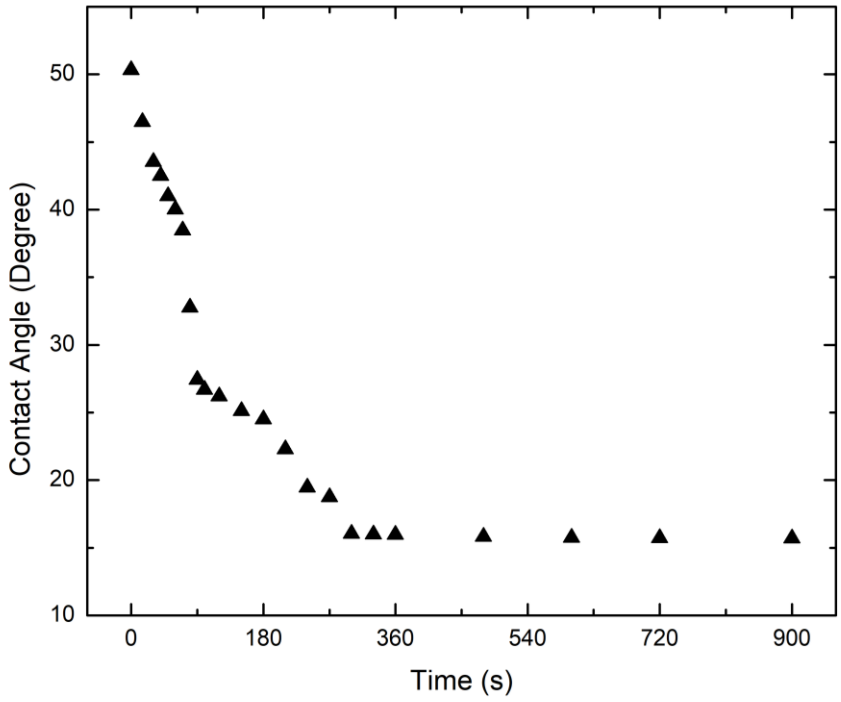

Figure 4.27 Change in the measured contact angle as a function of time at 915 °C.

The spreading behavior of the brazing filler alloy on the C/SiC composite surface, which is evaluated by the diameter change of the molten brazing filler alloy, is rapid at the beginning of melting and then becomes slower as the wetting experiment proceeds. It can be noted that the wetting reaches an equilibrium state when the diameter of the molten brazing filler alloy remains constant. Significant change in the contact angle was not observed when the holding time was increased to 900 s at 915 °C. Similarly, the diameter of brazing alloys on the ceramic surfaces and their contact angles were observed to remain constant in several studies conducted on brazing [53,97]. For instance, Mao et al. [97] investigated the wetting behavior of molten Cu50Ti alloy on monolithic BN and observed that normalized diameter remained unchanged when the wetting reached to equilibrium. Another study [53] which was conducted on the wetting of monolithic alumina ceramic by the Cusil-ABA brazing filler alloy revealed similar results. In that study, equilibrium contact angle of ~10° was reached at the time of 1000 s, and it remained constant afterwards. Figure 4.28 demonstrates the fluctuation in the contact angle of Ticusil brazing filler alloy as a function of time at 915 °C for both C/SiC composite and monolithic SiC ceramic. The results were used to understand how the heterogeneity of the C/SiC composite together with the presence of the carbon fibers in the structure affect the wetting behavior. Because existing carbon fibers in the structure further hinder the spreading of the molten Ticusil filler alloy on the surface, C/SiC composite has a slightly higher contact angle than monolithic SiC ceramic.

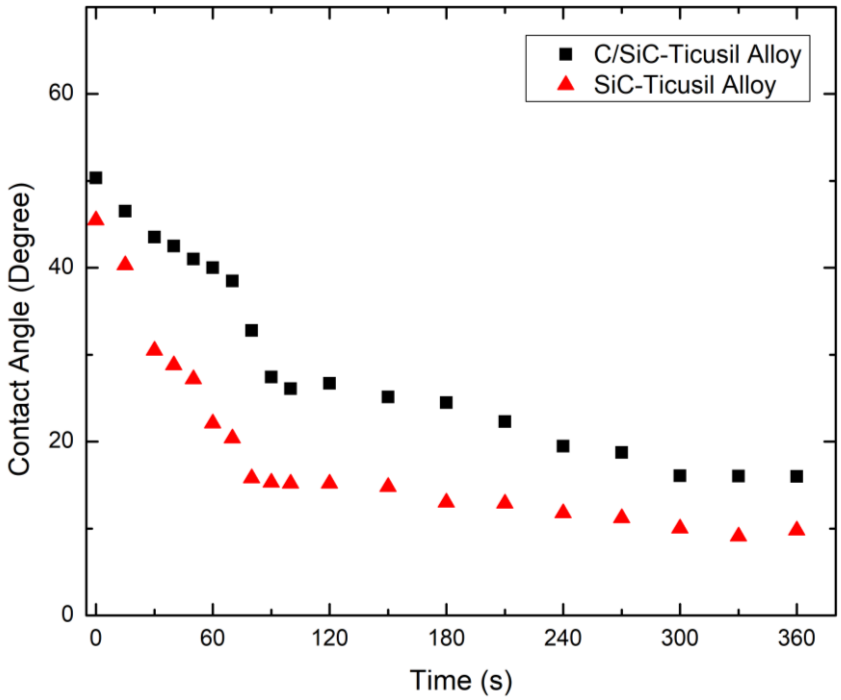

Figure 4.28 Contact angle variation of Ticusil brazing filler alloy with respect to time at 915 °C on both C/SiC composite and monolithic SiC ceramic.

The influence of the presence of active Ti element in the coating layer of C/SiC composite and/or in the brazing filler material on the contact angle variation is summarized in Figure 4.29. Cusil brazing filler alloy, without any active element, shows non-wetting behavior on both monolithic SiC and C/SiC composite. Whether the brazing filler alloy contains active Ti element or not, Ti layer coating on the ceramic matrix composite surface resulted in a considerable decrease in the contact angle. According to the recorded contact angle values, both methods can be used to improve the wetting behavior. Additionally, because the Ti containing Cusil showed the lowest contact angle of 45° on Ti layer coated C/SiC composite, it can be concluded that increasing the active element (Ti) concentration improves the wetting behavior. Furthermore, it can be stated that highest amount of Ti containing Ticusil filler alloy considerably improves the wetting behavior of both monolithic SiC ceramic and C/SiC composite material with contact angles of 10° and 15°, respectively.

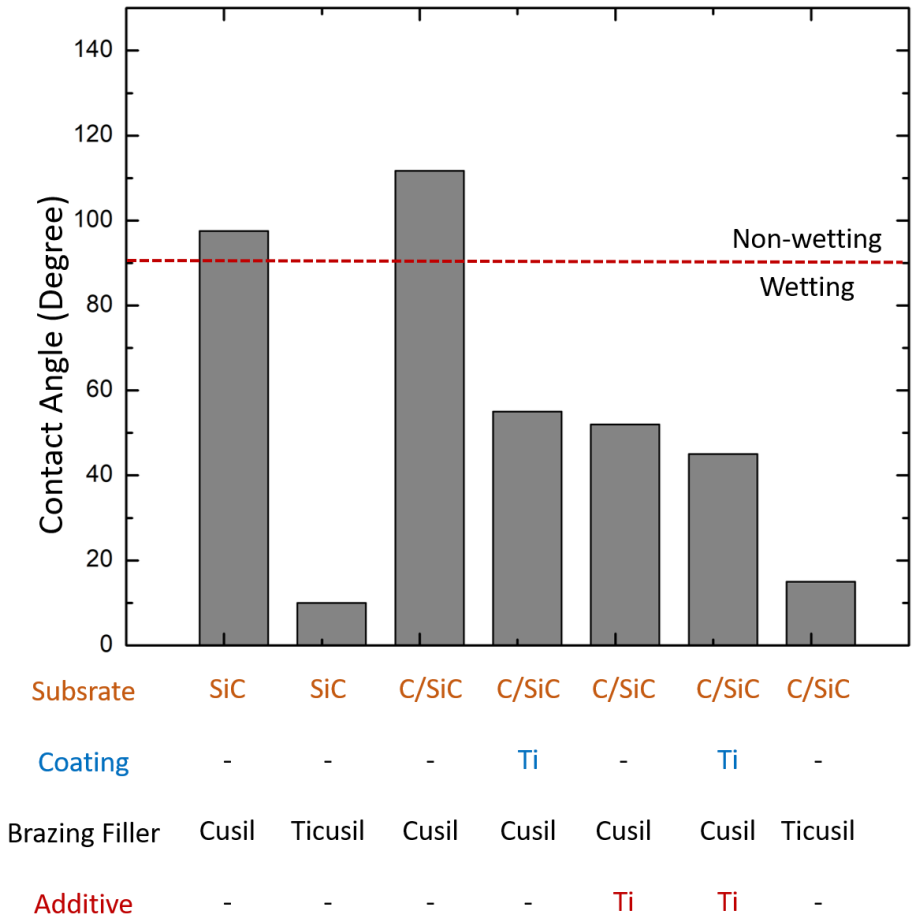

Figure 4.29 The effect of the presence of active Ti element in the coating layer and/or in the brazing filler material on the contact angle.

4.2 Effect of Brazing Temperature and Time on Wetting Behavior and Reaction Layer Formation of C/SiC Composite-Titanium Alloy Joints

As it is stated before brazing filler materials used for brazing must have good wetting on the base material surfaces to obtain perfect joining during brazing [60,98]. In active brazing systems, the interfacial reactions between the brazing filler alloy and the ceramic matrix composite lead to reaction layer formation, which affects the

resulting wettability, brazing performance and determines the mechanical properties of brazed parts [99]. Therefore, type and quantity of phases formed in reaction layer as well as the thickness of the layer are important factors controlling the mechanical properties. In order to have a homogenous and continuous reaction layer formation in the brazed parts, the brazing alloy should wet to surfaces of brazed parts adequately. The reaction existing between the corresponding ceramic matrix composite-metal interfaces promotes the wetting of the liquid brazing filler alloy [85,100]. Reaction not only enhances the wettability behavior of the ceramic matrix composite but also directly affects the mechanical performance of the brazed joint. Therefore, the wettability of C/SiC composite by Ag-Cu-Ti based brazing filler alloys and reaction layer formation during the wetting of the C/SiC composite surface should be further investigated to reveal the brazing mechanism clearly and for correlation of the mechanical performance with the phase distribution and thickness of the reaction layer, which is affected primarily from the brazing parameters.

Studies which are present in the literature do not adequately comprise the effect of brazing parameters on the reaction layer formation of the joints obtained by brazing C/SiC composites to Ti6Al4V alloys [101-104]. Therefore, to fill the research gap in the literature about the joining of C/SiC composite and Ti6Al4V, current study has focused upon the effect of brazing temperature and time on the reaction layer formation at the interface region of C/SiC composite and Ti6Al4V alloy when Ticusil brazing alloy is used. Moreover, the effect of processing parameters (temperature and time) on the thickness/microstructure of the reaction layer has been investigated and discussed in detail by comparing the experimental reaction layer thickness values with those obtained from theoretical diffusion models. Additionally, spreading behavior of the Ticusil brazing alloy on C/SiC composite surfaces has been examined at various temperatures and holding time via wetting tests to enhance joining performance of C/SiC composite to Ti6Al4V alloy. Finally, the influence of the thickness/microstructure of the interlayer and wetting behavior of the brazing

alloy on the mechanical performance of the joints have been discussed comprehensively [105].

4.2.1.1 Effect of Brazing Temperature and Time on Microstructural Evolution of C/SiC Composite/Ti6Al4V Alloy Joints

The schematic drawing of the brazed joint is given in Figure 4.30(a). All of the brazed joint contains five different regions. As shown in Figure 4.30, the left side presents C/SiC composite, and the right side shows Ti6Al4V alloy; between the C/SiC composite and Ti6Al4V alloy, there is an interlayer composed of the brazing filler alloy. The formation of a reaction layer next to C/SiC composite side and a diffusion-reaction layer next to the Ti6Al4V alloy side are observed, where the bonding is successful at brazed joints. C/SiC composites and Ti6Al4V alloys were brazed using Ticusil brazing filler alloy at 900, 905, 915, 925, and 930 ºC for 15 minutes to observe the effects of brazing temperature on microstructural evolution of the brazed joints. As shown in Figure 4.30(b-d), cracks and voids do not exist in the brazed joint microstructure; therefore, it can be stated that a continuous and uniform interlayer has been obtained by the applied brazing process.

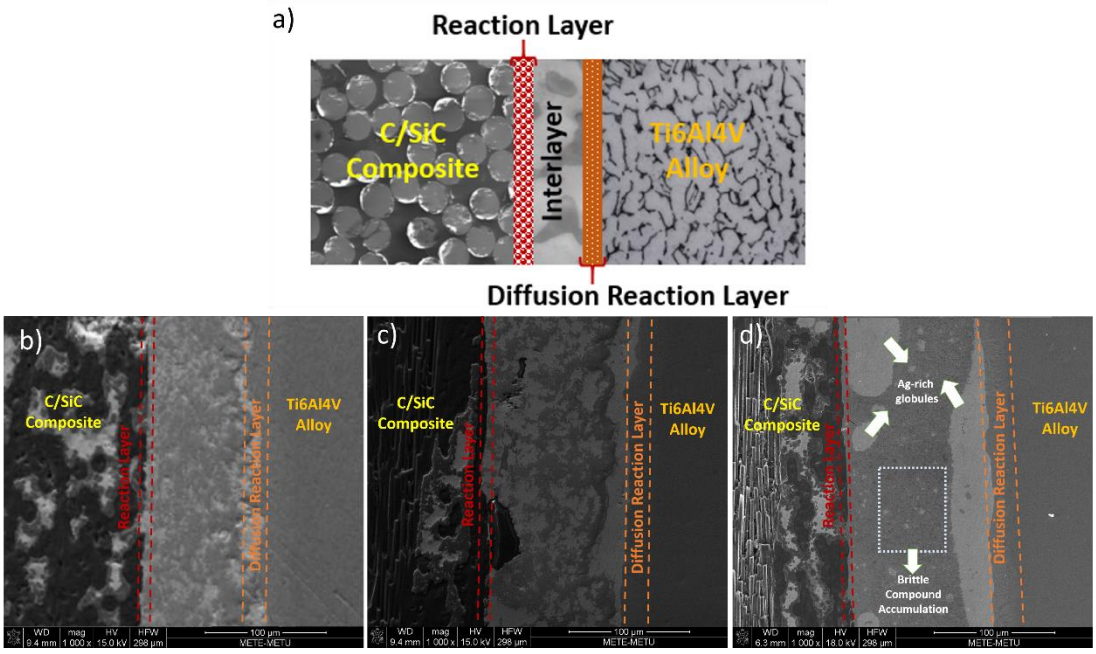

Figure 4.30 a) The schematic drawing of the C/SiC composite-Ti6Al4V alloy brazed joint. The microstructure of the interface between C/SiC composite and Ti6Al4V alloy joints brazed by Ticusil brazing filler alloy at b) 900 °C, c) 915 °C, and d) 930 °C.

As can be seen from Figure 4.31, the reaction layers were observed between the C/SiC composite and the interlayer for all brazing temperatures. However, there are microstructural differences between the reaction layers formed at different brazing temperatures. The reaction layer formed at 900 °C is not continuous and has the lowest thickness, whereas as the temperature raised to 915 °C, the reaction layer became continuous along the C/SiC composite surface. Different from other brazing temperatures, Ag-rich globules are observed at the interlayer of the joint brazed at 930 °C (Figure 4.30(d) and Figure 4.32(a)). For the joints brazed at 925 and 930 °C, accumulation of the brittle Ti-Si rich compounds is also observed between C/SiC composite and interlayer, as shown in Figure 4.31(d) and Figure 4.31(e). These Ti-Si rich phases accumulated in the interlayer have a sharp-edged morphology, as shown in Figure 4.31(b). In contrast to high brazing temperature conditions, for the

joints brazed at 905 and 915 °C, instead of Ti-Si rich phases, Ti-Cu rich phases exist in the interlayer (Figure 4.31(b) and (c)). Moreover, comparing the reaction layers obtained at different temperature conditions, it can be stated that the thickness of the reaction layer presents increasing trend with increasing brazing temperature, and it reaches to ~2.6 μm at the brazing temperature of 930 °C. The mobility of the atoms reacted and, accordingly, the amount of atoms diffusing through the already produced reaction layer is proportional to the brazing temperature [106]. An increase in the brazing temperature helps form a thicker reaction layer under constant brazing time conditions, as presented in Figure 4.31.

The change in the reaction layer thickness between C/SiC composite and Ticusil filler alloy at constant brazing temperature of 915 ºC under different brazing time conditions are presented in Figure 4.33. As it is presented in Figure 4.33, as the holding time is short (1 min), the reaction layer does not form at the C/SiC composite/Ticusil interface. The reaction layer cannot be observed because of limited amount of atomic diffusion leading to inadequate reaction between the filler and the C/SiC composite [107]. Reaction layer formation at the C/SiC composite/ Ticusil interlayer interface has been observed for the brazing durations of 5 min - 30 min (Figure 4.33(b-d)). It can be stated that with increasing brazing time, the average reaction layer thickness at the C/SiC composite/ Ticusil interlayer interface increases remarkably.

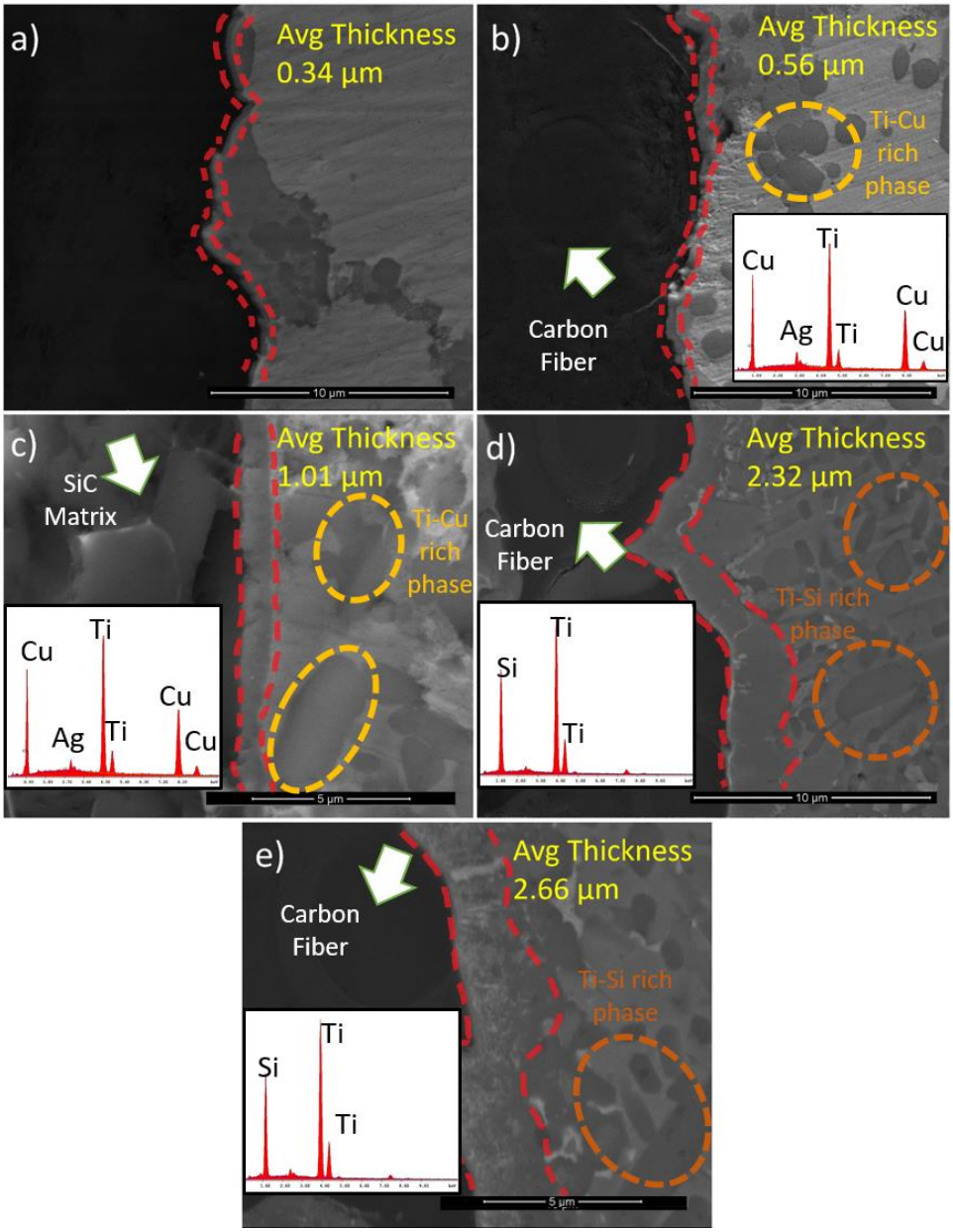

Figure 4.31 Average thickness values of the reaction layer at the C/SiC composite/Ticusil interlayer at constant brazing time of 15 min with brazing temperatures of a) 900 °C, b) 905 °C, c) 915 °C, d) 925 °C and e) 930 °C.

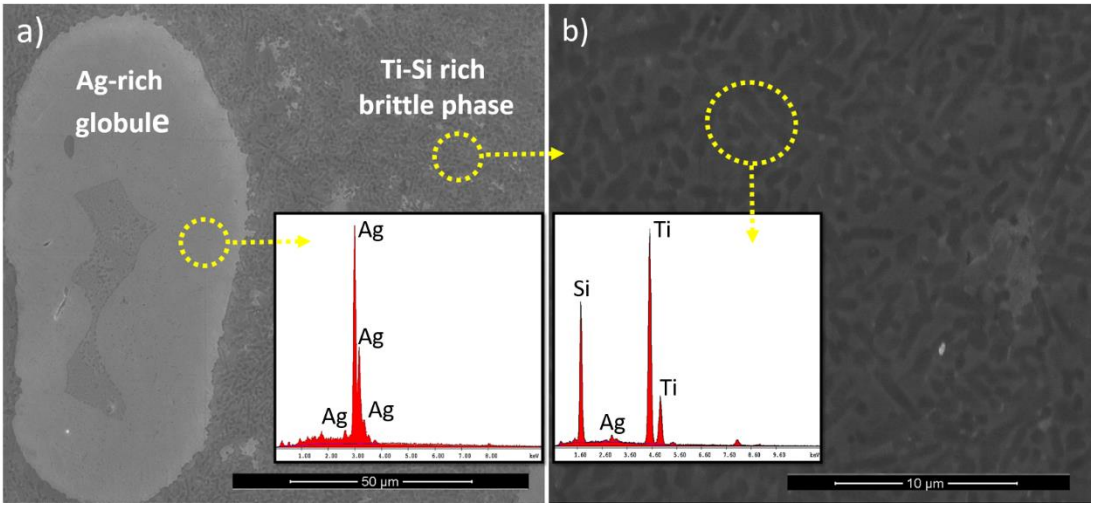

Figure 4.32 C/SiC composite/Ticusil interlayer at 930 °C for 15 min a) Ag-rich globules, b) Ti-Si rich brittle phases.

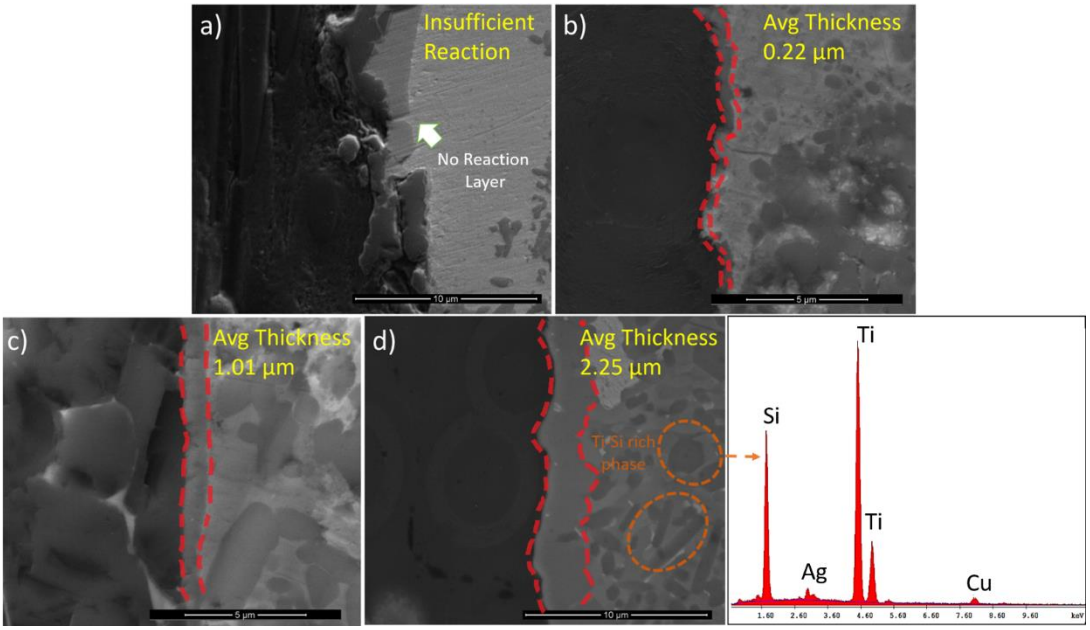

Figure 4.33 Average thickness values of the reaction layer at the C/SiC composite/Ticusil interlayer at constant brazing temperature of 915 °C with brazing time of a) 1 min, b) 5 min, c) 15 min, and d) 30 min.

Composition analysis of the formed reaction layer between C/SiC composite and Ticusil using EDS line analysis is conducted on sample processed at 915 °C for 15 min. According to EDS analysis, point A, shown in Figure 4.34(a) contains only Si and C elements; therefore, the microstructure corresponding to point A represents the SiC matrix. Based on point B EDS analysis, the reaction layer mainly contains Ti and Si atoms. Elemental analysis results were coupled by the applied XRD analysis in order to monitor the formation of the possible phases. EDS analysis results are shared in Figure 4.34(b) and the XRD analysis results presented in Figure 4.35 and 4.36 indicate that Ti_5Si_3 and Ti_3SiC_2 are the possible phases present in the reaction layer. The EDS analysis of points C and D show that the regions are mainly composed of Ti and Cu atoms. Hence, it can be stated that possible phases for points C and D are Ti_2Cu and TiCu.

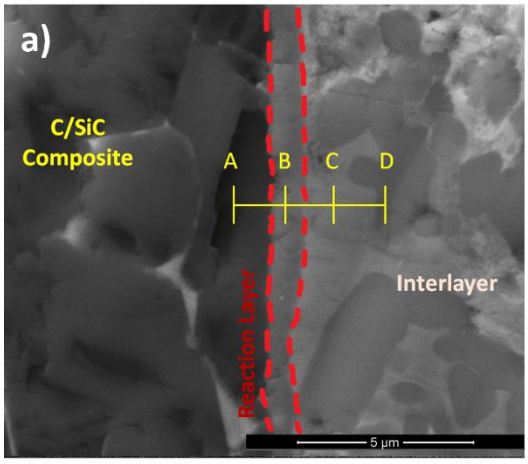

b)

	C	*Si*	*Cu*	*Ag*	*Ti*	*Al*	*V*	*Possible Phases*
A	24.6	69.4	3.8	2.2	-	-	-	SiC matrix
B	17.4	11.1	2.3	0.3	68.8	0.1	-	Ti_3SiC_2 or Ti_5Si_3
C	0.2	2.1	25.9	1.8	61.3	3.7	5.0	Ti_2Cu
D	1.2	1.9	35.5	5.3	51.2	4.3	0.6	Ti_2Cu, TiCu

Figure 4.34 Elemental distribution along the C/SiC composite/Ticusil interlayer interface according to a) SEM micrograph, b) EDS line analysis presenting average chemical composition.

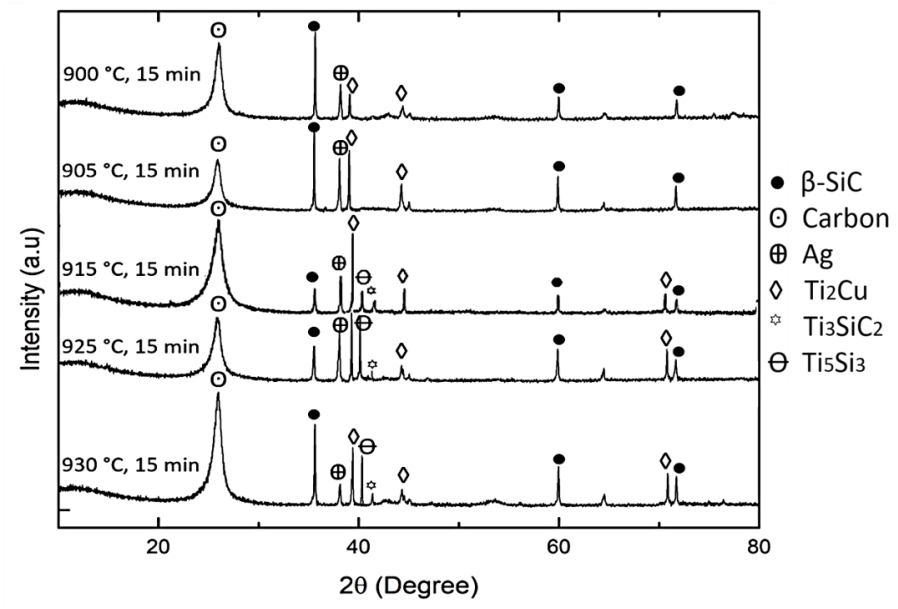

Figure 4.35 XRD results of the C/SiC composite/Ticusil interlayer interfaces with respect to varying brazing temperatures at constant brazing time of 15 min.

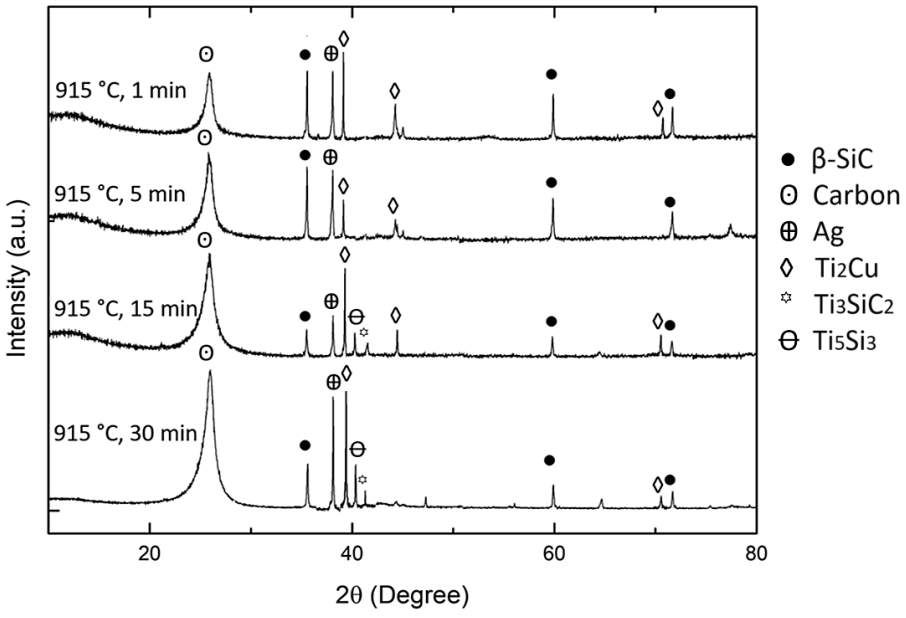

Figure 4.36 XRD results of the C/SiC composite/Ticusil interlayer interfaces with respect to varying brazing time at constant brazing temperature of 915 °C.

Occurrence of the possible phases existing in the reaction layer and the interlayer can be estimated as follows: Firstly, during the brazing process molten Ti-Cu phase gets into contact with the SiC matrix, and the Ti atoms in the Ti-Cu rich liquid reacts with the SiC matrix-forming TiC and Si as a product with regard to chemical reaction (4.1) below [10].

$$Ti + SiC \rightarrow TiC + Si \qquad (4.1)$$

Secondly, Ti atoms react with formed Si and TiC, and Ti_3SiC_2 phase arises at the interface of the C/SiC composite and interlayer (chemical reaction (4.2)) [10,11]

$$Ti + Si + TiC \rightarrow Ti_3SiC_2 \qquad (4.2)$$

Finally, in addition to Si atoms reacting with Ti and TiC, Si atoms diffuse to the interlayer. The molten phase reacts with Si atoms and form Ti_5Si_3 phases according to chemical reaction (4.3). Although the interface formed at 915 °C for 15 min contains Ti_5Si_3 and Ti_3SiC_2 phases according to XRD analysis, the interlayer is mainly based on Ti and Cu atoms according to the EDS analysis. Therefore it can be stated that in addition to the interlayer, the reaction layer at the interface also contains the Ti_5Si_3 phases.

$$Si + Ti \rightarrow Ti_5Si_3 \qquad (4.3)$$

According to the SEM micrographs shown in Figure 4.31(d-e) and Figure 4.30(d), different than the 915 °C for 15 min brazing condition, at higher brazing temperature and time conditions, not only the reaction layers contain Ti_5Si_3 phase but also Ti_5Si_3 particles are dispersedly embedded in residual Ti_2Cu.

XRD analyses conducted on the interface between the ceramic matrix composite and the interlayer (Figure 4.35 and 4.36) present the effect of time and temperature of brazing on the phase formation in the reaction layer in detail. It can be seen from Figure 4.35 that only Ti_2Cu peaks were observed on the interface brazed at 900 ºC

and 905 ºC for the constant holding time of 15 min. Although the reaction layer formation can be seen clearly in the SEM micrographs (Figure 4.31(a) and (b)), diffraction peaks of Ti_5Si_3 and Ti_3SiC_2 phases are below the analysis limitation of the XRD technique, which can be attributed to the lower amount of reaction layer formation at the lower brazing temperatures. As it is clear from the diffractograms, the interfaces formed at brazing temperatures higher than 915 ºC are composed of Ti_2Cu, Ti_5Si_3, and Ti_3SiC_2 phases.

The XRD patterns of C/SiC composite interface brazed for different durations at a constant temperature of 915 ºC are presented in Figure 4.36. As it is clear from the diffraction patterns, interfaces brazed for 1 min, and 5 min contain only carbon, β-SiC, silver, and Ti_2Cu peaks. In contrast, Ti_5Si_3 and Ti_3SiC_2 phases are detected in samples brazed for longer durations. According to SEM analysis, while the reaction layer formation does not exist due to insufficient reaction at 1 min of brazing time (Figure 4.33(a)), the reaction layer formation is too low to detect the possible phases using XRD analysis at 5 min of brazing time (Figure 4.36). Therefore, it can be stated that the microstructural evolution observed by the SEM micrographs is in agreement with the XRD analysis results of the C/SiC composite/Ticusil interlayer interface.

The change in the reaction layer thickness presented in the SEM images (Figure 4.31 and Figure 4.33) reveals that the reaction layer growth follows a parabolic trend because the interfacial reaction of the C/SiC composite and the Ti6Al4V alloy mainly depends on the diffusion between the ceramic matrix composite and the metallic alloy. The thickness of the reaction layer can be determined using Equations (4.4) and (4.5) [103].

$$X = Kt^{0.5} \qquad (4.4)$$

$$K = k_0 \exp(-Q/RT) \qquad (4.5)$$

where;

X (m) is the reaction layer thickness,

K (m^2/s) is the reaction rate constant,

Q (kJ/mol) is the activation energy,

k_0 (m^2/s) is the pre-exponential factor,

R (J/K mol) is gas constant equal to 8.314,

t (s) is the time,

T (K) is the temperature.

Using the linear fitting results given in Figure 4.37, k_0 and Q can be calculated as 2.13 x 10^{28} m^2/s and 813.989 kJ/mol, respectively.

The effect of holding time and brazing temperature on the reaction layer thickness can be revealed by Equation (4.6):

$$X = 2.13 \times 10^{28} \exp(-813.989 \times 10^{3}) / 8.314\ T) \times t^{0.5} \quad (4.6)$$

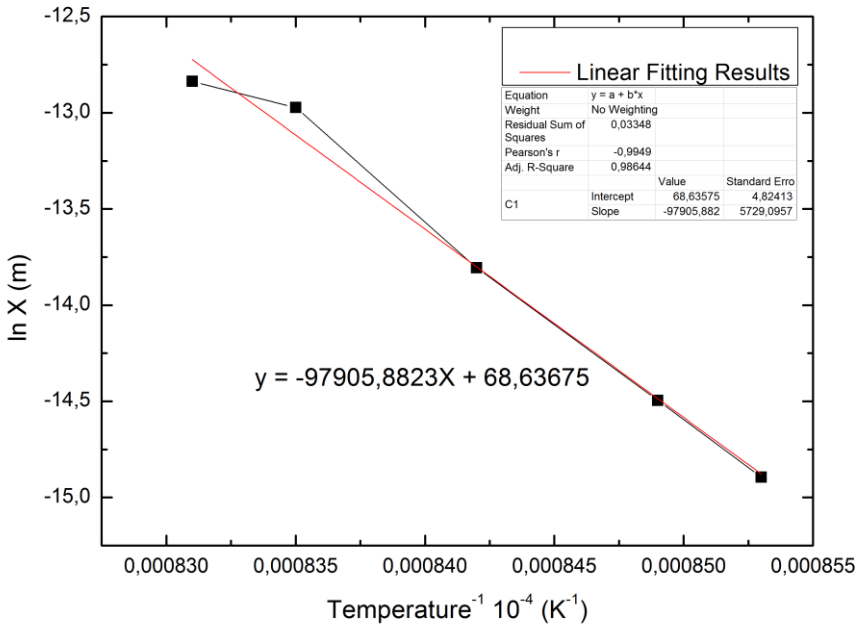

Figure 4.37 Linear fitting results for brazing time of 15 min.

In order to check the accuracy of the determined relationship, the reaction layer thickness values observed experimentally at different brazing times for constant temperature were compared with theoretical thickness values obtained using Equation (4.6). In Figure 4.38, the reaction layer thickness values were determined using Equation (4.6) and measured experimentally using the SEM images. As shown in Figure 4.38, the calculated values are close to the experimentally observed reaction layer thickness mean values. Therefore, it can be stated that the derived relationship can be used to estimate the reaction layer thickness at different brazing temperatures and time conditions. The decrease in the reaction layer growth rate with the increase in brazing time (Figure 4.38) points out the fact that the formed reaction layer at the interface constitutes a barrier for the further reaction between Ti and C/SiC composite [108-111]. Furthermore, the reaction rate constant is considerably influenced by temperature, as shown in Figure 4.39, which shows the change in the reaction rate constant as a function of temperature.

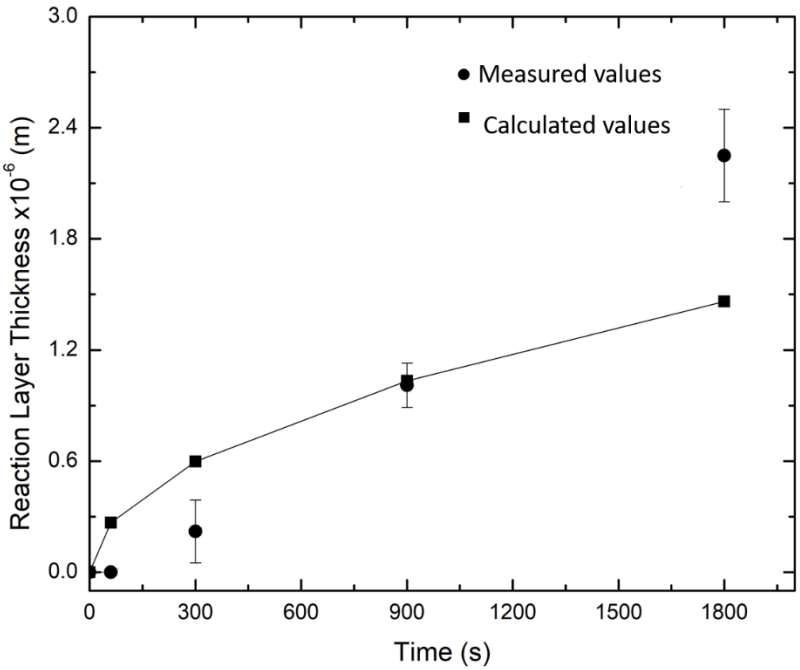

Figure 4.38 The comparison of the theoretical and experimental data of the reaction layer thickness obtained at a constant temperature of 915 ºC.

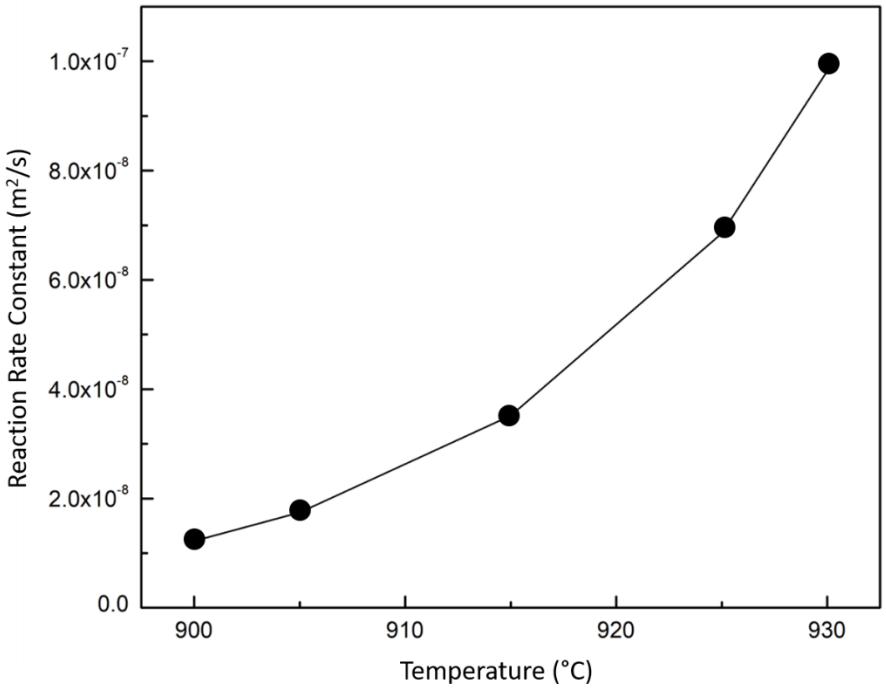

Figure 4.39 Reaction rate constant versus temperature diagram.

4.2.1.2 Effect of Brazing Temperature and Time on Mechanical Properties of C/SiC Composite/Ti6Al4V Alloy Joints

Shear tests were conducted on the joints brazed at various temperatures and holding times. According to Figure 4.40 and 4.41, with increasing brazing temperature and holding time, the shear strength values of the brazed joints clearly increase at first, then decline. However, brazing duration and temperature have a direct relationship with reaction layer thickness. The joint brazed at 915 ºC for 15 min presents the highest shear strength of 33.2 MPa.

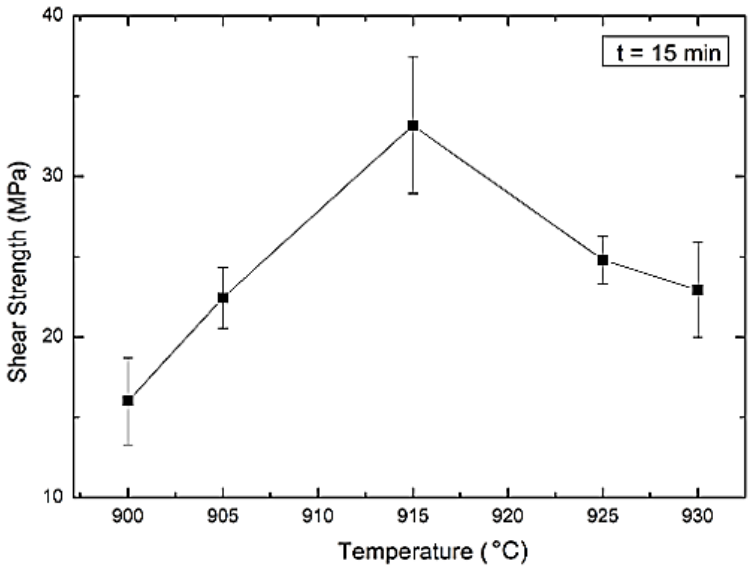

Figure 4.40 Shear test results of the brazed joints with respect to brazing temperature at constant brazing time.

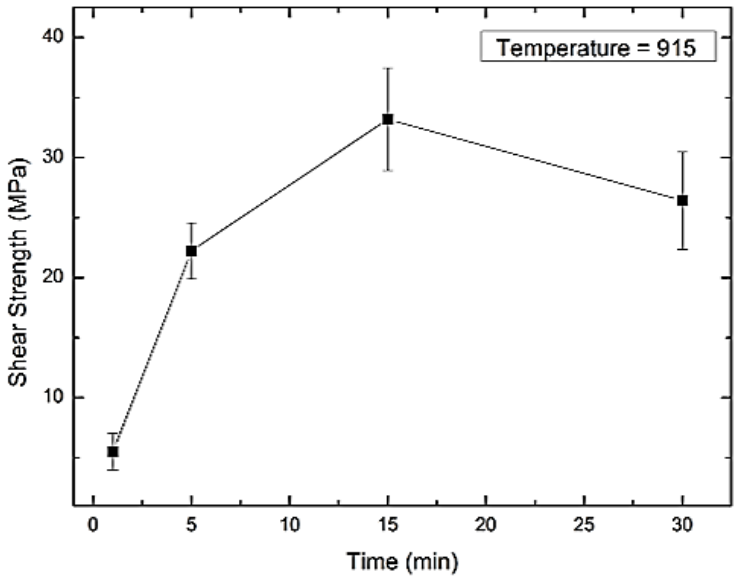

Figure 4.41 Shear test results of the brazed joints with respect to brazing time at constant brazing temperature.

Using obtained results, the relationship between the brazing temperatures, brazing time, shear strength and the reaction layer thickness was examined. Reaction layer thickness which is controlled primarily by the brazing parameters, importantly has impact on the mechanical strength of the joint. Comparing the shear strength values given in Figure 4.40 and 4.41 and the reaction layer thickness values presented in Figure 4.31 and Figure 4.33, it can be stated that the strength of brazed joints has an increasing initially and then a decreasing trend with increasing reaction layer thickness. If the reaction layer is absent or too thin, the bond between the ceramic matrix composite and the interlayer is insufficient, resulting in low shear strength values. Moreover, owing to the fact that the reaction layer phases have brittle nature due to the presence of brittle intermetallic Ti_5Si_3 phases, shear strength starts to decrease with increasing reaction layer thickness. Therefore, it can be stated that the reaction layer thickness should be optimized to have optimum shear strength [108,112].

Moreover, the decline in mechanical strength can be associated with the quantity of brittle phases existing in the interlayer. As presented in the SEM (Figure. 4.31, 32, and 33) analysis results, by increasing temperature and time level, the amount of sharp-edged Ti_5Si_3 phases embedded in residual Ti_2Cu increases. Furthermore, at higher brazing temperature, i.e. 930 °C, the spreading of Ag-rich globules at the interface (Figure 4.31(d)) leads to a non-uniform and weak interface resulting in a decrease in the mechanical strength. Similarly, the existence of the brittle Ti_5Si_3 phase in the interlayer evidenced by the micrographs in both Figure 4.31(e) and Figure 4.31(b) and by the XRD patterns in both Figure 4.35 and 4.36 indicates that it has considerable impact on the mechanical strengths of the brazed joints at higher brazing times.

Fracture surfaces of both Ti6Al4V alloy and C/SiC composite part are shown in Figure 4.42. Figure 42(i-iv) displays the macro images of fracture surfaces both Ti6Al4V and C/SiC composite parts brazed at 930 and 915 °C for 15 min.

Macrostructural examination revealed that even Ti6Al4V alloy surface was composed of residues of C/SiC composite and Ticusil. As it is seen from the figures, the carbon fibers are pulled out, and pit formation is observed at the C/SiC composite fracture surfaces. Silver-gray regions on the fracture surfaces indicate that the brazing filler alloy penetrates into the existing pores of C/SiC composite during brazing [113,114].

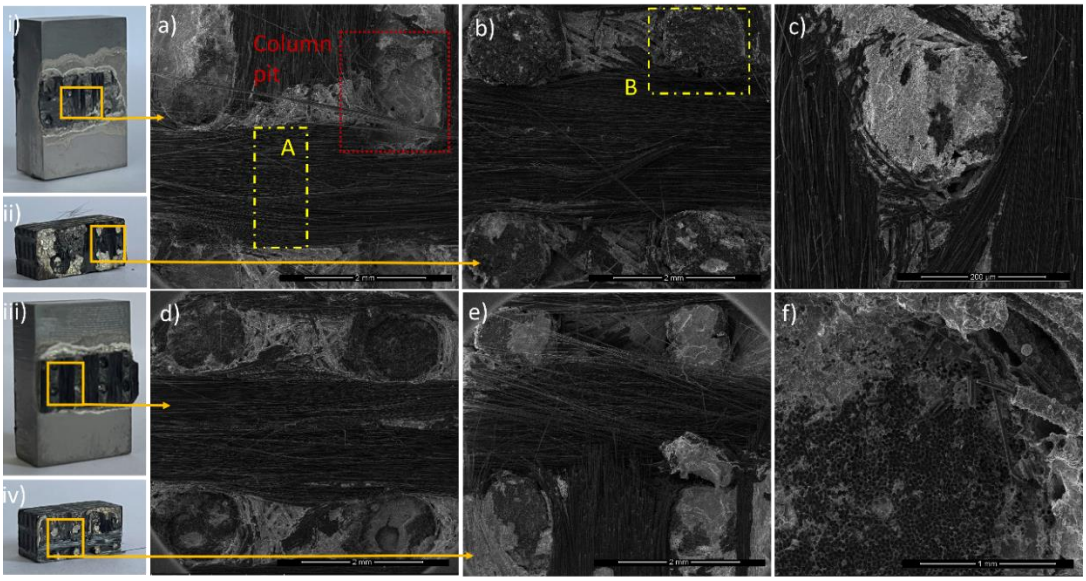

Figure 4.42 The fracture surface of the brazed joints at macro level i) Ti6Al4V alloy (930 °C, 15 min, ii) C/SiC composite (930 °C, 15 min), iii) Ti6Al4V alloy (915 °C, 15 min), iv) C/SiC composite (915 °C, 15 min); the fracture surfaces in micro level a) Ti6Al4V alloy (930 °C, 15 min), b) C/SiC composite (930 °C, 15 min), c) residual Ticusil alloy on the C/SiC composite surface (930 °C, 15 min), d) Ti6Al4V alloy (915 °C, 15 min), e) C/SiC composite (915 °C, 15 min), f) residual Ticusil alloy on the C/SiC composite surface (915 °C, 15 min).

According to micrographs given in Figures 4.42(a-f), the fracture surface of the brazed joints contains two main regions, namely, carbon fibers and the residual brazing filler, which is infiltrated through the carbon fiber bundles during brazing.

Due to the 3D fiber orientation in C/SiC composite, the carbon fiber fracture is observed in two ways, including the fracture in carbon fibers parallel to the brazing filler alloy and the fracture in carbon fibers perpendicular to the brazing filler alloy. While the carbon fibers parallel to the brazing filler alloy (shown as A in Figure 42(a)) are easy to peel off from the C/SiC composite, it is difficult to separate the carbon fibers from the composite, which are perpendicular to the brazing filler alloy (shown as B in Figure 4.42(b)). Moreover, the separation of the perpendicular carbon fibers from the composite gives rise to the formation of the columnar pits on the fracture surface. The presence of these columnar pits on the fracture surfaces denotes the occurrence of the fracture within the ceramic composite rather than at the composite/filler alloy interface resulting in the highest shear strength of the joint which has 915 °C of brazing temperature and 15 min of brazing time.

4.2.1.3 Wetting Behavior and Interfacial Interactions of Brazing Filler Alloy on C/SiC Composite

In addition to examination of wetting behavior of the Ticusil brazing filler alloy, microstructural changes and interfacial reactions between C/SiC composite and brazing filler alloy are also investigated and wetting mechanism is proposed. As demonstrated by the SEM micrographs given in Figure 4.43, brazing filler alloy successfully wets the C/SiC composite surface at 915 °C. As observed in brazing experiments, cracks and voids do not exist in the C/SiC composite interlayer. In addition to that, as it is seen in Figure 4.43(d), molten brazing filler alloy seems to have penetrated into the C/SiC composite surface. It fills the porosity of the ceramic matrix composite surface, which has a porous structure depending on the fiber orientation direction. As shown in Figure 4.43(c), the reaction layer is observed between the C/SiC composite and the brazing filler interlayer. Comparing the reaction layers formed during the brazing experiments and wetting experiments, it can be stated that the thickness of the reaction layers is similar at a temperature of

915 °C. Moreover, similar interfacial reaction mechanisms were observed on the C/SiC composite surfaces for both brazing and wetting experiments.

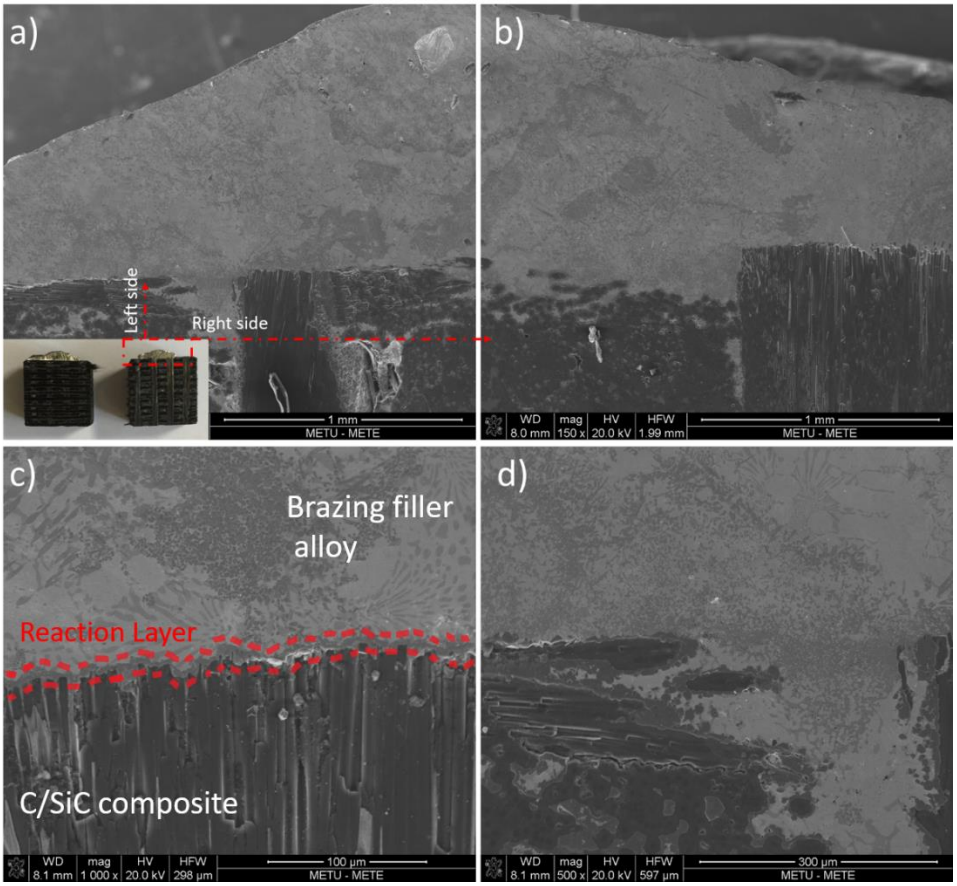

Figure 4.43 Cross-sectional view of the brazing filler alloy/C/SiC composite surface samples after wetting experiments at 915 °C for 15 minutes a) left side of the sample b) right side of the sample c) reaction layer formation at the interface of the C/SiC composite and brazing filler interlayer and d) penetration of the molten brazing filler alloy into the pores of the C/SiC composite.

The wetting mechanism of the brazing filler alloy on the C/SiC composite surface can be depicted as follows (Figure 4.44). Firstly, the molten brazing filler alloy starts to penetrate to the porous C/SiC composite surface as the temperature rises the brazing filler alloy melting point. Secondly, as in the case of the brazing experiments, the existing Ag phase in the brazing alloy increases the activity of Ti remarkably;

therefore, the possibility of interfacial reactions between C/SiC composite and Ti atoms increases. With the help of the reactions between Ti and SiC, the thin reaction layer forms on the C/SiC composite surface. Consequently, the reaction layer formed at the C/SiC composite surface improves the wetting behavior by decreasing the surface tension [115,118].

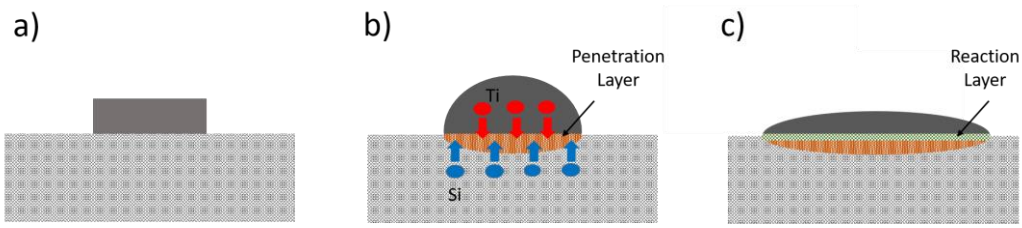

Figure 4.44 Wetting mechanism of the brazing filler alloy on the C/SiC composite surface.

4.3 Effect of Additive Particle Size and Content on the Brazing Performance and Wetting Behavior

For the brazing of two dissimilar materials like ceramic composites and metallic alloys, there are two essential issues that need to be improved during the process. The first is the high thermal expansion difference between ceramic matrix composites and metallic materials, which is significant, and the second one is the difficulty in wetting of ceramic matrix composite surfaces compared to metallic materials [60]. Several experiments have been conducted to alleviate the disadvantage of high thermal stresses induced by coefficient of thermal expansion (CTE) mismatch. These studies primarily focused on introducing soft metals between the joint materials or adding reinforcing particles with low CTE into the brazing filler alloys [119]. In the literature, to decrease the residual stresses at the interface and to improve the mechanical properties of the joints, particles such as SiC, TiC, B_4C, W and fibers such as carbon fibers have been added into the brazing filler materials [119,123]. Moreover, studies have also been performed for the in situ

synthesized reinforcement phases in order to obtain small and uniformly dispersed reinforcement phases [124,126].

Xiong et al. (2013) studied C/SiC composite and Ti alloy brazing with three different additive ceramic powders (SiC, TiC, and W with a particle size of 2.6 μm, 8 μm and 200 mesh, respectively). According to the results of this study, the residual stresses in the heterogeneous joint was relieved by all types of additional reinforcing particles, which increased joint strength [120]. Liu et al. (2019) used carbon fiber as a reinforcement material in the Ticusil brazing filler alloy to braze C/C composite and Ti6Al4V joints. They revealed that carbon fiber, in an optimum amount, mainly decreased the residual stresses and reduced the brittle reaction layer's thickness close to the C/C composite. However, excess carbon fiber incorporation caused a negative effect on mechanical performance of the joints due to insufficient reaction between C/C composite and brazing material [127]. Dai et al. (2016) successfully brazed monolithic SiC ceramics by reinforcing the brazing filler alloy with B_4C particles. Mechanical strength of the joint has been increased by the formation of low CTE TiB whiskers and TiC particles in the interlayer with the help of additive B_4C particles [119]. In another study, Wang et al. (2018) used TiC particles with the particle sizes of 600-800 (~15-20 μm) and 1000 mesh (~10 μm) in TiZrCuNi brazing filler alloy for C/SiC composite/Ti6Al4V alloy joints. At the same particle content, different sizes of the TiC particles were investigated for two different brazing temperature conditions. The study presented that the smaller the reinforcement particle is, the greater the mechanical performance of the joints gets due to the uniform and compact dispersion of the newly formed phases [123]. While the study successfully explains the effect of reinforcement particles at two different temperatures with a constant amount of reinforcement material, it does not examine the impact of reinforcement particle size and amount simultaneously under constant temperature conditions.

In the following section the impact of additive materials on the wetting behavior of the Ticusil brazing filler alloy were analyzed in detail. Moreover, apart from the

wetting behavior of the brazing filler alloy on the C/SiC surface, effect of additive particle size and amount on the properties of C/SiC composite/Ti6Al4V alloy joints obtained by vacuum brazing technique have been investigated.

4.3.1 Effect of Additive Particle Size and Amount on Microstructural Evolution of C/SiC Composite/Ti6Al4V Alloy Joints

The SEM micrographs of the brazed joints containing additive particles with different size and content are given in Figure 4.45. All of the brazed joints contain three different regions. As indicated in Figure 4.45(a), the left side presents C/SiC composite, and the right side demonstrates the Ti6Al4V alloy, where there exists an interlayer composed of the brazing filler alloy between the C/SiC composite and Ti6Al4V alloy. C/SiC composites and Ti6Al4V alloys were brazed using non-additive and additive containing Ticusil brazing filler alloy at 915 ºC for 15 minutes to observe the effects of SiC additive particle size and content on the microstructural evolution of the brazed joints. Except for Figure 4.45(e) and (h), because there are no cracking or delamination in the brazed joint microstructure, it can be said that the applied brazing procedure was successful in producing a sound and continuous interlayer. Furthermore, SEM micrographs of the 20 wt% micron level SiC brazing filler containing interlayer could not be captured, because all of the samples fractured during the specimen preparation step. For the 20 wt% micron level additive, brazing procedure could not be completed effectively due to partial melting of the brazing filler alloy at 915 ºC for 15 minutes, as in the wetting test, and hence bond formation between the joining materials could not be achieved.

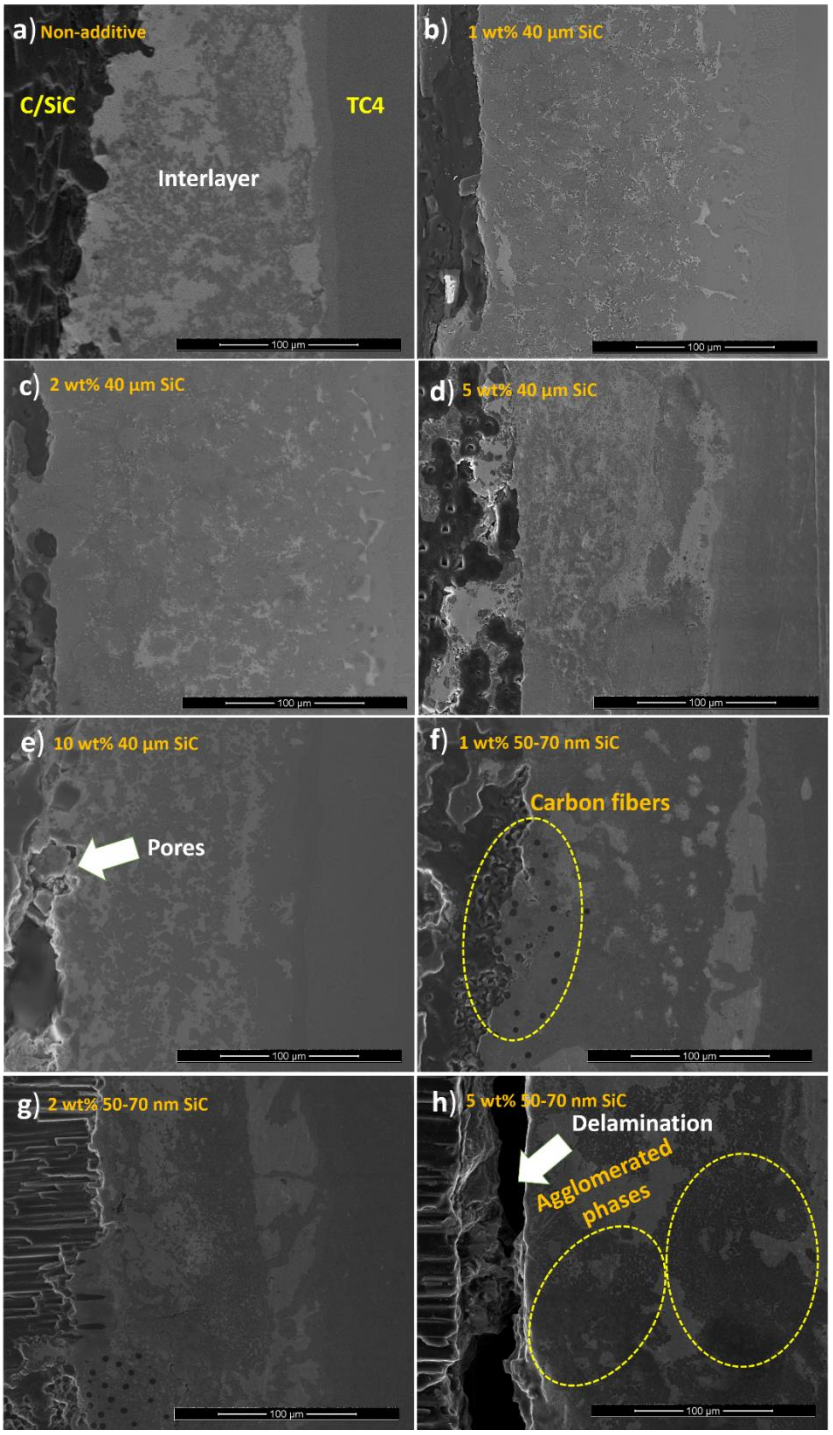

Figure 4.45 The microstructure of the interface between C/SiC composite and Ti6Al4V alloy joints brazed by Ticusil brazing filler alloy containing a) non-additive, b) 1 wt% micron level, c) 2 wt% micron level, d) 5 wt% micron level, e) 10 wt% micron level, f) 1 wt% nano level, g) 2 wt% nano level and h) 5 wt% nano level.

As it is presented in Figure 4.46, according to the SEM observation and elemental analysis, the Ti element in the brazing filler alloy reacts with the additional SiC particles [122]. Because of the reaction between SiC particles and Ti element, Ti-Si containing phases are dominant in the interlayer for both micron and nano additive cases. Unreacted SiC particles covered by a thin film of Ti-Si phases exist in the interlayer for 1 wt% micro level additive, unlike nano level additive cases. As it seen from Figure 4.46(b) and (c), when compared on the same magnification level Ti-Si phases present in the nano-sized additive containing interlayer have smaller particle size and more uniform distribution compared to micron-sized additive containing one.

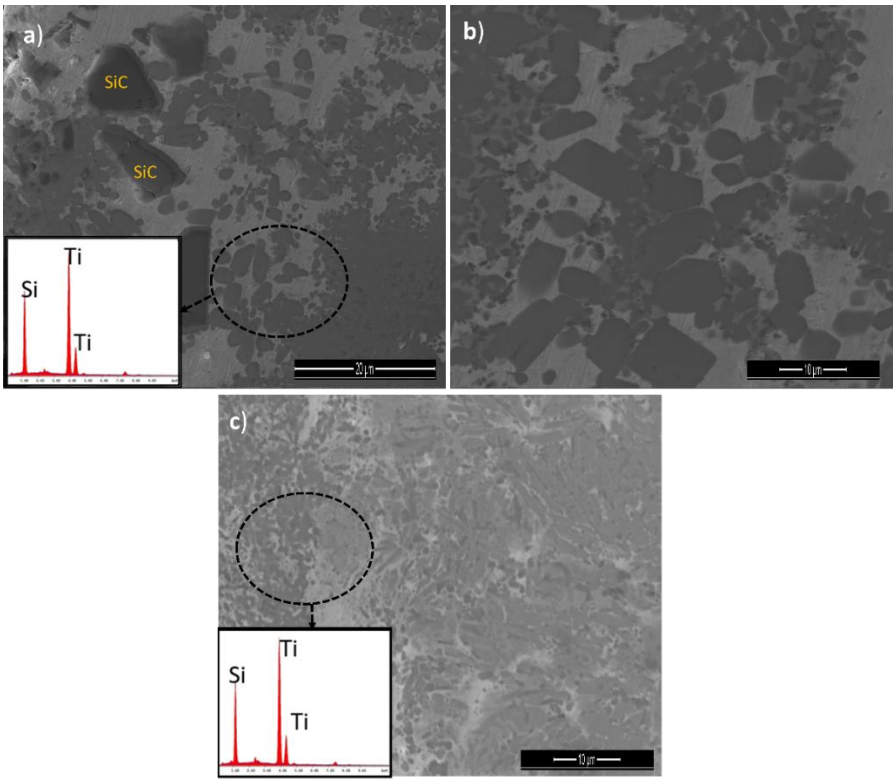

Figure 4.46 The microstructure of the interlayer between C/SiC composite and Ti6Al4V alloy joints brazed by Ticusil brazing filler alloy containing a) and b) 1 wt% micron level, c) 2 wt% nano level.

4.3.2 Effect of Additive Particle Size and Amount on the Wetting Behavior of Brazing Filler Alloy on C/SiC Composite

Performance of the brazed joints and the interfacial reactions at the interface are controlled by the wetting of the ceramic matrix composite surfaces in C/SiC composite/metal joints. Therefore, wetting experiments serve as a guide for the further improvement of the joining processes. Consequently, in order to investigate the effects of the SiC particle size and content on the wettability of the C/SiC composite, the wetting behavior of the SiC additive containing Ticusil brazing filler alloy on the C/SiC composite surface has been examined at constant temperature with variable SiC particle size and content. Ticusil brazing filler alloy has solidus and liquidus temperatures of 780 °C and 900 °C, respectively. During the experiments heating from 780 to 915°C with a heating rate of 5 °C/min and keeping the samples at the 915 °C for 900 s was applied to simulate the starting and finishing points of the brazing procedure. As a result, in this study the change in contact angle with regard to SiC additive size and content has been studied at constant temperature (915 °C) for varying durations.

Figure 4.47 depicts the change in the morphology of the brazing filler alloy containing different amounts of micron level SiC additive on C/SiC composite at 700 °C, where melting and hence wetting did not start, and at 915 °C where the samples were kept for 900 s for the wetting procedure to be completed. Figure 4.47 shows that the additive content for the micron level SiC powder has a great influence on the contact angle morphology. Apart from the 20 wt% micron level SiC case (Figure 4.47(f)), non-additive and additive containing brazing filler alloys have spreading and change in droplet morphology. The morphology of the 20 wt% micron level brazing filler does not alter and present any melting behavior.

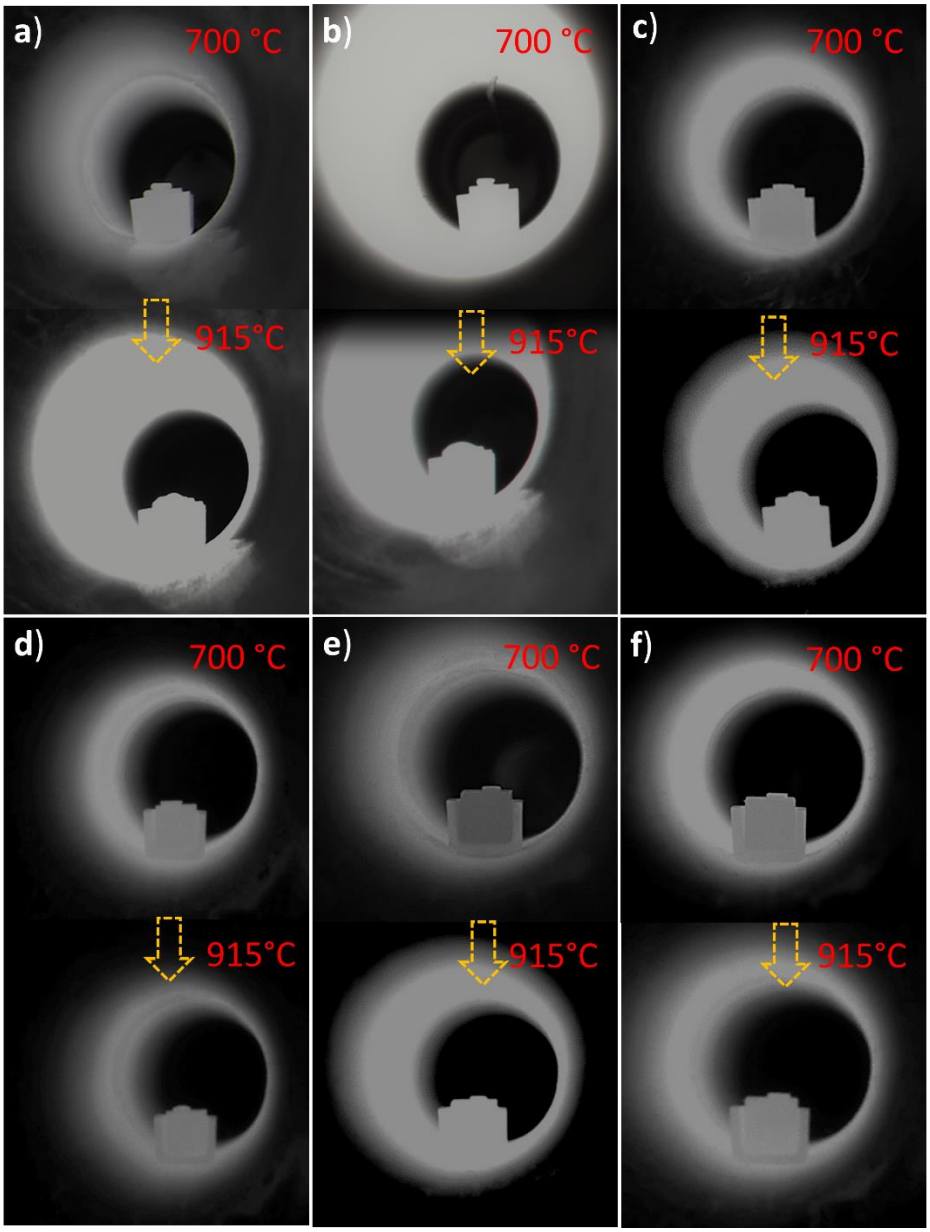

Figure 4.47 Morphological changes of brazing filler alloy on C/SiC composite surface containing different amounts of micron level SiC additive a) non-additive brazing filler alloy, b) 1 wt% micron level SiC, c) 2 wt% micron level SiC, d) 5 wt% micron level SiC, e) 10 wt% micron level SiC, f) 20 wt% micron level SiC.

The variation of the contact angle with time at the constant temperature of 915 °C is given in Figure 4.48 for different amounts of micron level SiC additive. In case of

non-additive containing filler alloy, the initial contact angle was measured as 50° when the temperature reached to 915 °C. For two separate time intervals, the contact angle presents two different variation trends. Despite a substantial reduction in the contact angle from 0 to 100 s, it changes slowly in the time interval of 100-300 s. At the end of the wetting experiment, the contact angle was measured as 15° indicating good wetting characteristic for the active brazing filler alloy, as also stated in the literature. According to Figure 4.48 it can be stated that with increasing micron level SiC additive content up to 2 wt%, the initial contact angle increases at 915 °C. On the other hand, the initial contact angles for 2 wt%, 5 wt% and 10 wt% micron level SiC addition are similar at approximately 130°. As in the case of non-additive containing brazing filler alloy, two distinct trends are observed in the contact angle variation for the micron level additive containing brazing filler alloys. With the exception of the 2 wt% and 5 wt% micron level additives, the drastic drop period extends as the filler amount increases. It can be stated that 2 wt% and 5 wt% micron level SiC additive containing brazing filler alloys present similar wetting behavior.

According to Figure 4.47 and 4.48, at the end of the wetting experiment, finally measured contact angle values increase with increasing amount of micron level SiC additive. However, there are two compositions which do not fit this trend. Firstly, for 2 wt% and 5 wt% additive cases, as for the contact angle variation trend, the final contact angle values are very close to each other at the value of approximately 60°. Secondly, data could not be collected precisely for the 20 wt% additive case, as the alloy did not melt completely at 915 °C (Figure 4.47(f)). Considering these with non-wetting behavior of the 10 wt% micron level SiC additive containing alloy having a contact angle of ~90°, it can be concluded that the wetting behavior of the brazing filler alloy is negatively affected at extreme amounts of micron level SiC additions.

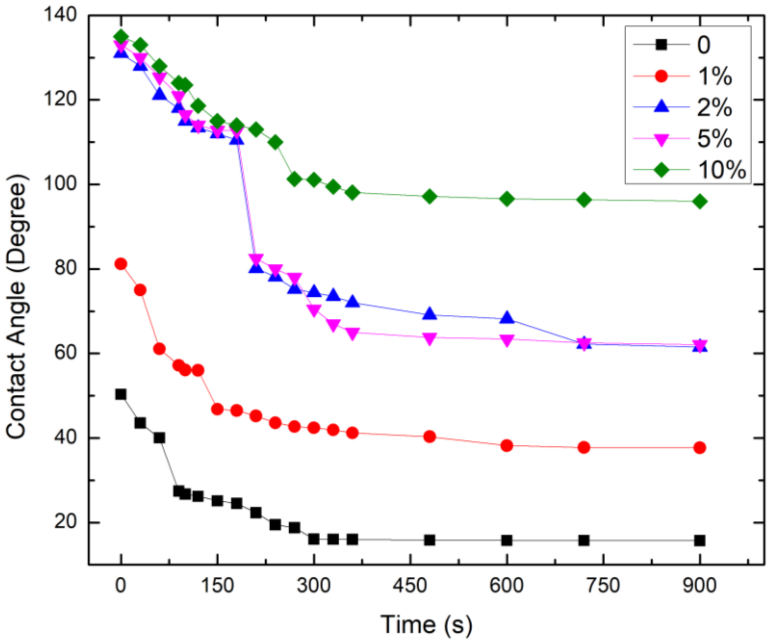

Figure 4.48 Change in measured contact angle as a function of time at 915 °C for brazing filler alloy with different micron level SiC additive amounts.

The effect of increasing nano level SiC additive content on the morphology and contact angle variation were also examined. The change in the morphology of the brazing filler alloy on C/SiC composite surface before and after the wetting experiment is shown in Figure 4.49. It can be seen in Figure 4.49 that for all of the nano level SiC additive contents (1 wt%, 2 wt% and 5 wt%), molten droplets have spreading morphologies with different contact angles. Although 1 and 2 wt% nano level SiC additive containing brazing filler alloys have good wetting behavior according to their spreading morphology, 5 wt% containing one has poor wetting.

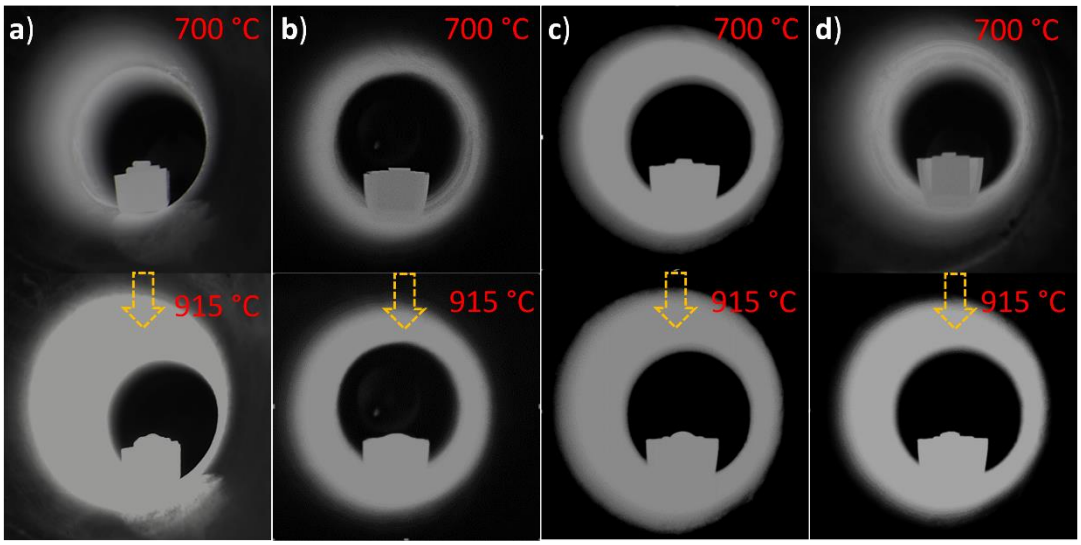

Figure 4.49 Morphological changes of brazing filler alloy on C/SiC composite surface containing different amounts of nano level SiC additive a) non-additive brazing filler alloy, b) 1 wt% nano level SiC, c) 2 wt% nano level SiC, d) 5 wt% nano level SiC.

Figure 4.50 presents the change in contact angles with time at a constant temperature of 915 °C for varying amounts of nano level SiC additive. Except for the 5 wt% nano SiC additive case, other two nano level SiC additive contents exhibit similar initial contact angles at 915 °C when compared to the non-additive containing brazing filler alloy. Moreover, at the end of the wetting experiments the contact angles were measured as 20°, 42° and 88° for 1, 2 and 5 wt% nano level SiC additive contents, respectively. There are two distinct patterns in contact angle variation observed in nano level additive containing brazing filler alloys, similar to the non-additive and micron level additive containing brazing filler alloys. Furthermore, as the amount of the nano level SiC additive increases, the time at which the drastic contact angle drop occurs shifts to longer times.

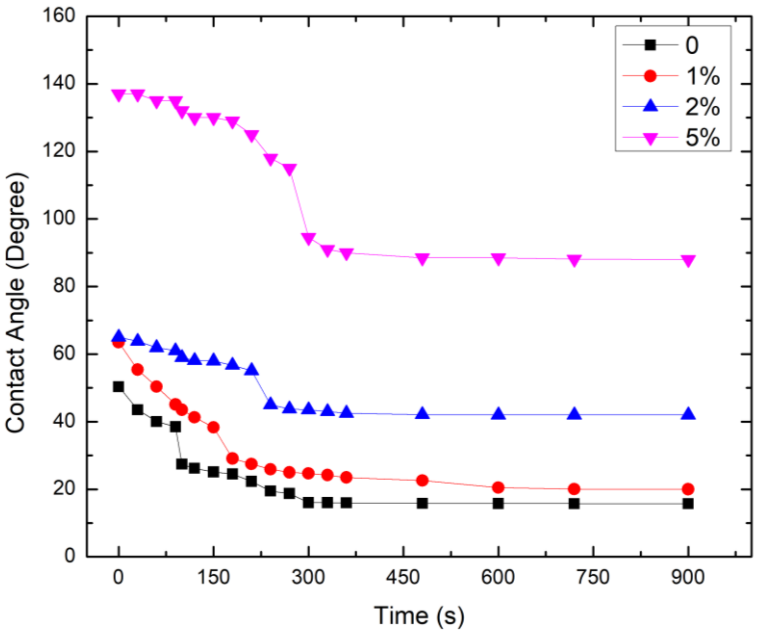

Figure 4.50 Change in measured contact angle as a function of time at 915 °C for brazing filler alloy with different nano level SiC additive amounts.

In Figure 4.51, the effect of SiC additive particle size and content on the contact angle of the brazing filler alloy is summarized along with the observed spreading morphologies. As presented in Figure 4.51, for both micron and nano level additives, the contact angle value decreases with increasing additive amount. However, the increase in the contact angle with the additive content is higher for micron sized SiC particles.

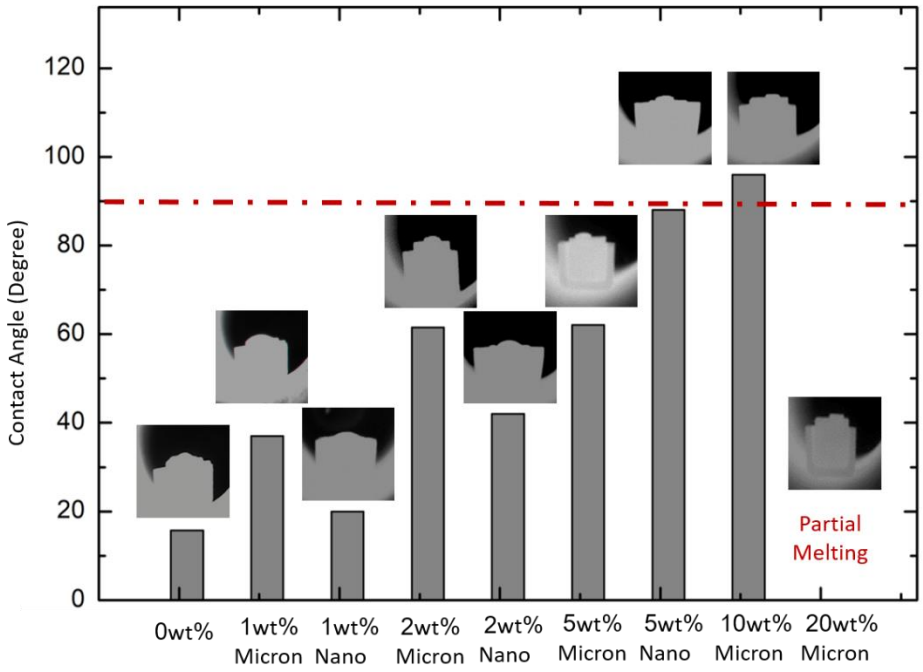

Figure 4.51 Effects of SiC additive particle size and content on the contact angle of the brazing filler alloy.

The change in the fluidity of the Ticusil brazing filler alloy with varying size and content of SiC additive has been studied via the spreading morphology of the solidified droplet on the C/SiC ceramic composite surface. The height and spreading area of the alloy solidified after the wetting experiments were used to calculate and compare the fluidity of the Ticusil brazing filler alloy.

According to Figure 4.52(a) and (b), it can be stated that SiC particle addition results in the decrease of the spreading diameter of the Ticusil brazing filler alloy. It is seen that the height of the solidified Ticusil brazing filler rises as the SiC content increases, while the spreading area of the brazing filler alloy diminishes. Fluidity is directly related to the interfacial reactions between the brazing filler alloy and ceramic matrix composite surface. Furthermore, as the fluidity of the brazing filler alloy decreases, the activity of Ti atoms in the interlayer also decreases resulting in lower contact angle and lower mechanical strength [128] .

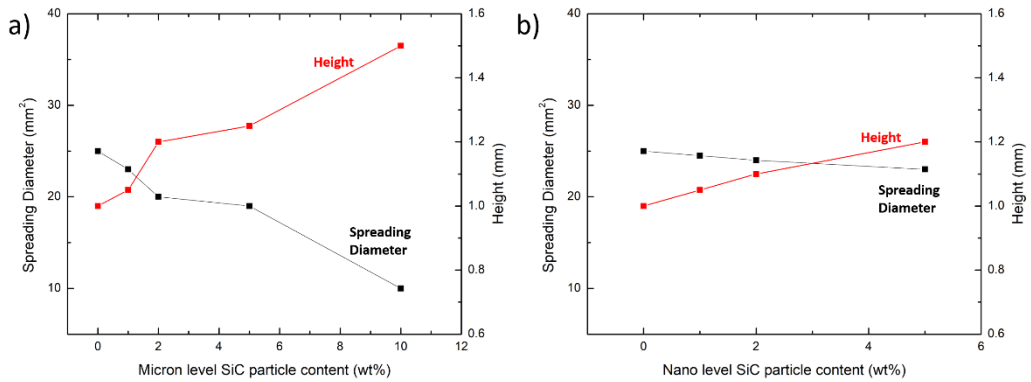

Figure 4.52 Fluidity of the Ticusil brazing filler alloy containing SiC additive with varying size and content.

The infiltration depth analysis of the Ticusil brazing filler alloy is conducted in order to observe the effect of SiC particle size and content on the infiltration behavior of the molten brazing filler alloy into the C/SiC composite. For this purpose experiments were carried out in the brazing furnace in order to include the effect of vacuum on infiltration as it is the case during the actual brazing process. As shown in Figure 4.53, micron level SiC additive has a greater impact on the infiltration depth of the molten brazing alloy compared to nano level SiC additive. For instance, for the 5 wt% SiC additive content, the decrease observed in the infiltration depth as compared to the non-additive containing alloy is 75% for the micron level SiC additive, while it is 20% for the nano level containing one. It can be concluded that larger additive size and higher additive content decreases the fluidity of the filler alloy remarkably suppressing its penetration ability to the ceramic composite rendering a potentially weaker interaction and bonding at the brazed joint.

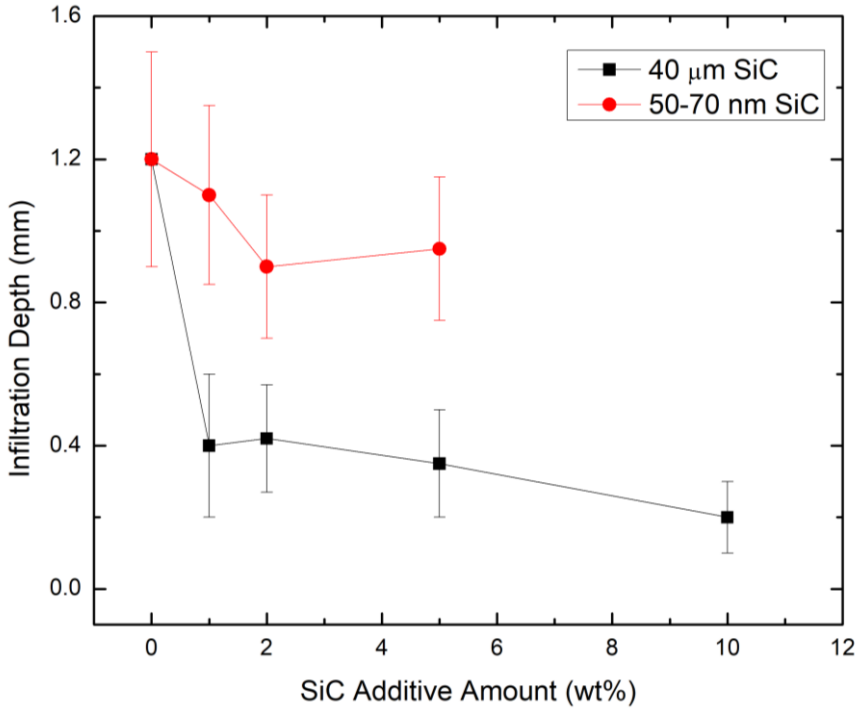

Figure 4.53 Infiltration depth values of the Ticusil brazing filler alloy in accordance with the different content and size of SiC additive.

The DSC curves for Ticusil brazing filler alloy and SiC additive containing Ticusil alloy, which have the highest mechanical strength, are shown in Figure 4.54. According to the figure it can be stated that all of them have similar solidus temperature and approximately same heat release values during melting (Figure 4.54). Because the non-additive and additive-containing Ticusil brazing filler alloys have equal solidus temperatures and heat release values, it may be concluded that the solidus temperature is unaffected by the additive SiC particles. Therefore, identical temperature was utilized for the wetting experiment and brazing process of all filler alloys.

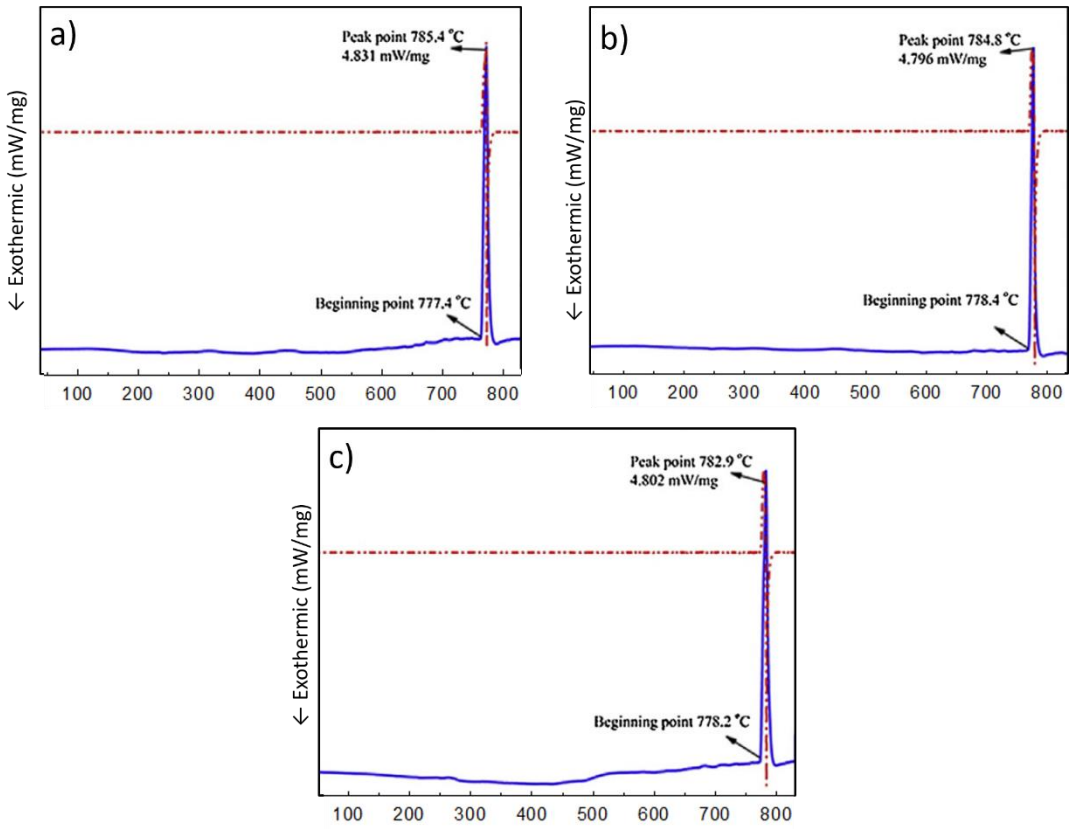

Figure 4.54 DSC curves for Ticusil brazing filler alloy containing a) non-additive b) 1 wt% micron level SiC and c) 2 wt% nano level SiC.

4.3.3 Effect of Additive Particle Size and Amount on the Mechanical Performance of C/SiC Composite/Ti6Al4V Alloy Joints

The link between the additive concentration, additive particle size and the mechanical performance of the C/SiC composite/Ti6Al4V alloy brazed joints was investigated by comparing shear strength test results. According to the shear strength values shown in Figure 4.55, the shear strength of brazed joints increases first, then decreases as the amount of both micron and nano-sized additives increases. The joint containing 2 wt% nano level SiC additive presents the highest shear strength of 44.8 MPa.

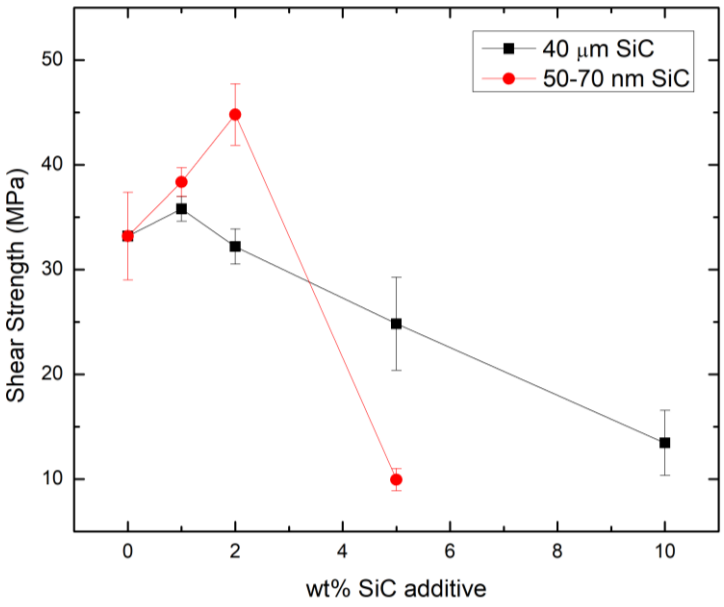

Figure 4.55 Mechanical properties of the brazed joints with respect to varying particle size and content of SiC additive.

For the 5 wt% nano level SiC additive case, shear strength decreases dramatically. It can be stated that nano-SiC particles are prone to agglomeration due to their small size and strong Van der Waals interactions between them [129,130]. Because of the agglomerations, the molten brazing filler alloy is mixed unevenly resulting in delamination at the interface (Figure 4.45(h)) and deterioration in the mechanical performance. Secondly, as presented in Figure 4.49(d)), a high nanoparticle content reduces the wettability of the brazing filler, which is critical for the development of strong bonds in brazing operations.

As it is shown in Figure 4.46, SiC present in the interlayer reacts with Ti element existing in the brazing filler alloy. For the high content of the additives, SiC particles not only lessen the fluidity of the brazing filler alloy but also reduce the Ti content which has to react with C/SiC and form the reaction layer for sufficient bond formation. Therefore, for the higher concentration of the additives wetting behavior and related mechanical performance are affected negatively. It can be stated that for

the micron level SiC addition, particle size of the formed reinforcement phases is larger than that of the nano level SiC addition. Compared to the micron level SiC addition, nano level SiC addition has finer and more uniform reinforcement phase distribution at the interlayer without reducing the activity of the Ti element in the brazing filler alloy [131]. Therefore, additive content and related wetting behavior should be tailored in order to provide optimal mechanical performance for both micron and nano level SiC additives. It can be stated that for both micron and nano level additive cases, the optimum contact angle for the highest joint performance is ~40°.

Reduction in the CTE value of the brazing alloy with the addition of SiC particles increases the shear strength of the joints. Although the interlayer for 1 wt% micron level SiC addition comprises both unreacted SiC phases and Ti_5Si_3 reaction products, the interlayer for 2 wt% nano level SiC addition exclusively contains generated Ti_5Si_3 phases, as shown in Figure 4.46(a) and (c). CTE value of the non-additive containing Ticusil brazing filler alloy is 18.5 x 10^{-6} C^{-1} [60]. Therefore, obtaining low CTE particles such as Ti_5Si_3 with the CTE value of 11 x 10-^{6} C^{-1} [132] and unreacted SiC phases with the CTE value of 4 x 10^{-6} C^{-1} [133] in the interlayer may reduce the thermal expansion mismatch between the C/SiC composite and brazing filler alloy. In this case residual stresses generated due to thermal expansion mismatch of the materials is lowered, and hence higher shear strength joints were obtained.

Fracture morphology of the brazed joints after the shear test are presented in Figure 4.56. Figure 4.56 displays the fracture surfaces of both Ti6Al4V and C/SiC composite sides detached from the brazed joints containing different additive particle size and content. SEM micrographs revealed that Ti6Al4V alloy surfaces detached from the joints having the highest shear strength values contain residues of C/SiC composite for both 2 wt% nano level (Figure 4.56(a)) and 1 wt% micron level (Figure 4.56(c)) SiC particle addition to Ticusil filler alloy. The carbon fibers are pulled out from the composite, and pit formation is seen at fracture surfaces.

Furthermore, the brazing filler alloy seems to have penetrated into the existing spaces and cracks of the C/SiC composite during brazing, as evidenced by silver-gray patches on the fracture surfaces. This penetration provides substantial mechanical strength improvement at the brazed joints. However, on the C/SiC surfaces detached from the joints containing the highest amount of nano or micron level SiC additive revealing the lowest shear strengths, there seems to be no pullout formation or brazing filler penetration (Figures 4.56(b) and 4.56(d)). In this case, there is inadequate interfacial interaction between the ceramic matrix composite and the molten brazing filler alloy resulting in weaker joints with lower mechanical strength [123].

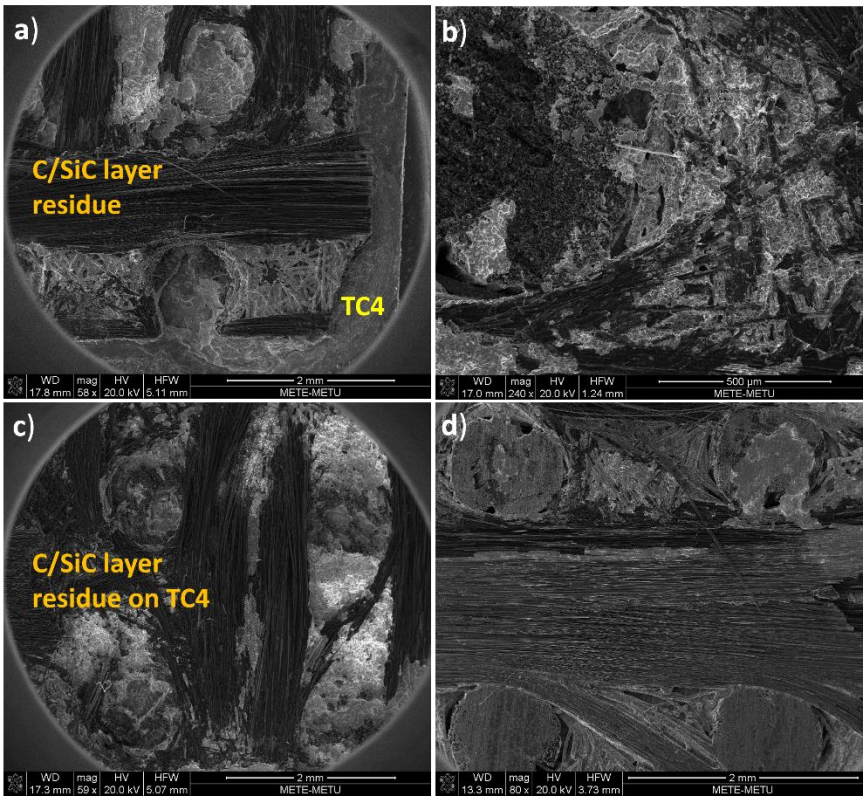

Figure 4.56 The fracture surface of the brazed joints a) C/SiC layer residual on Ti6Al4V alloy surface (2 wt% nano level), b) C/SiC composite surface (5 wt% nano level), c) C/SiC layer residual on Ti6Al4V alloy surface (1 wt% micron level), d) C/SiC composite surface (10 wt% micron level).

4.4 Effect of Material Properties and Reinforcement Structure of Ceramic Matrix Composites on Wetting Behavior and Brazing Performance of C/SiC Composite/Ti6Al4V Alloy Joints

In this study the main ceramic matrix composite base material used was C/SiC composite which has a three-dimensional (3D) reinforcement structure. As it is stated in the "Experimental Procedure" Chapter, the XZ plane of the C/SiC composite (Figure 3.1(b)) was utilized as the bonding surface in all of the experiments.

The production technique and reinforcing structure have a huge impact on the material properties and microstructures of C/SiC composites. Therefore, in order to investigate the effect of varying material properties and reinforcement structure of the C/SiC composites on the wetting behavior and related brazing performance of the composites, 2D C/C-SiC composites manufactured by liquid silicon infiltration method in an earlier study [7] were also used during this study. The efficacy of the densification, as well as the mechanical and thermal properties of the ceramic composites formed, are all affected by the primary variables in the LSI process. Mechanical and thermal properties of C/C-SiC composites are shown to be very sensitive to the microstructure and composition of the composite, according to literature [134,137]. The characteristics of the materials used in the composite manufacturing, pyrolysis conditions, and matrix reactivity all play a role in LSI efficiency [20]. Matrix additives with unique mechanical and thermal properties are also predicted to help the C/C-SiC composites densify and improve their qualities. Taking into account all of these factors that have a direct impact on the LSI process' efficiency, to improve the thermal properties of the C/C-SiC composites, carbon nanotubes (CNTs) were also impregnated during the ceramic matrix composite manufacturing step [6].

Figure 4.57 presents the gradient distribution of the CNTs achieved during the manufacturing of the C/C-SiC composites. As it is seen from the SEM micrographs given in Fig. 4.57(b) and (c), there is no discernible gradient distribution difference between the outer and inner regions of the C/C preform. Therefore, it can be

concluded that impregnation of the CNTs in to the C/C preforms was successfully applied.

The microstructures of CNT-impregnated composites are given in Fig 4.58. The gap between carbon fibers is filled with CNTs, and a homogeneously distributed percolating network of CNTs can be seen between the carbon fibers.

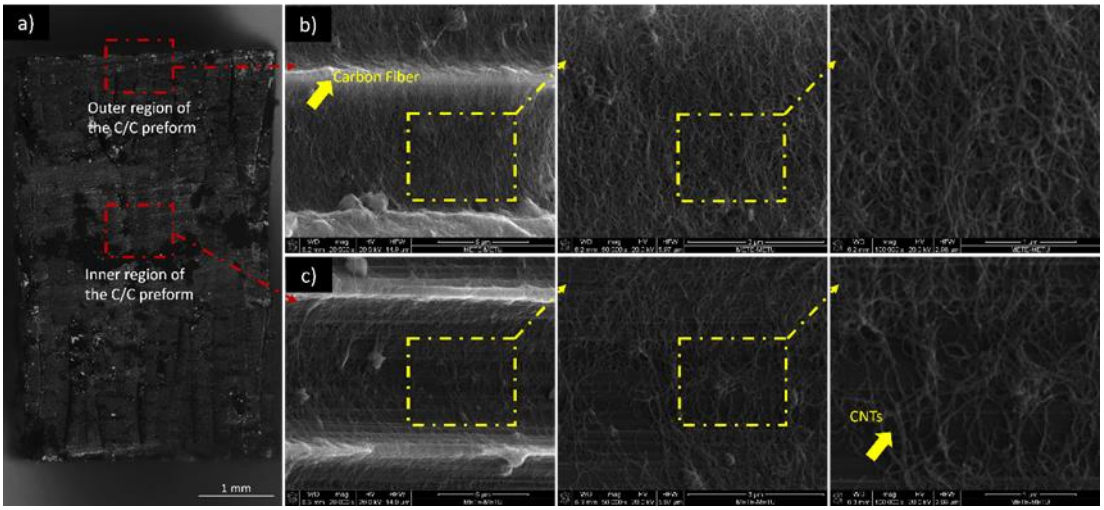

Figure 4.57 (a) View of the entire C/C preform in cross-section, with the CNTs distributed in a gradient manner (b) the outer part of the C/C preform and (c) the inner part of the C/C preform.

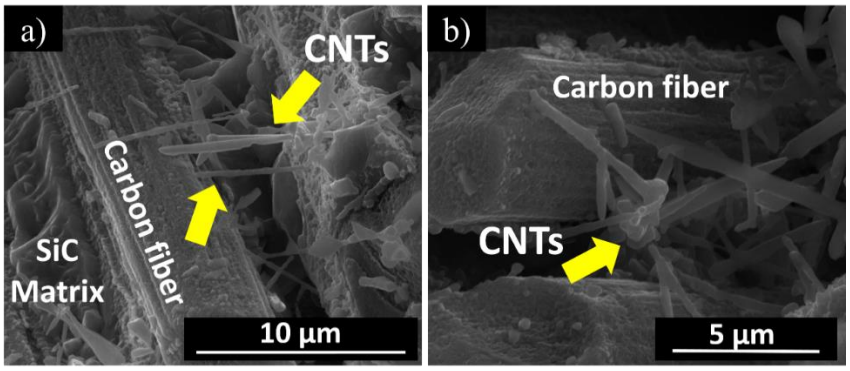

Figure 4.58 SEM microstructures of the CNT impregnated C/C-SiC composites.

Figures 4.59(a) and (b) depict the change in thermal diffusivity and heat capacity of the C/C-SiC composites with respect to temperature. According to the thermal analysis, with the impregnation of CNTs, the thermal diffusivity values in both directions increased while the heat capacity declined. As it is shown in Figure 4.60, CNT impregnation significantly enhanced the thermal conductivity values of the C/C-SiC composites being 31% in the parallel (∥) and 18% in the perpendicular (⊥) direction to the reinforcement fabric surface. Paths with higher thermal conductivity are provided by CNTs in the structure, which form an interconnected percolating network. Furthermore, when the CNTs and SiC matrix interfaces are coupled, the thermal resistance between the impregnated CNTs and the SiC matrix interfaces reduces. Aside from that, compared to the high inherent thermal conductivity of CNTs, the increase in thermal conductivity of CNT impregnated C/C-SiC composites is comparatively low. It can be stated that the increment in the thermal conductivity of the composite is due to the large interfacial surface area between the CNTs and the SiC matrix formed during silicon infiltration [138,141]. Moreover, according to Table 4.8, the thermal expansion coefficient of the C/SiC composites decreases in both directions with CNT impregnation.

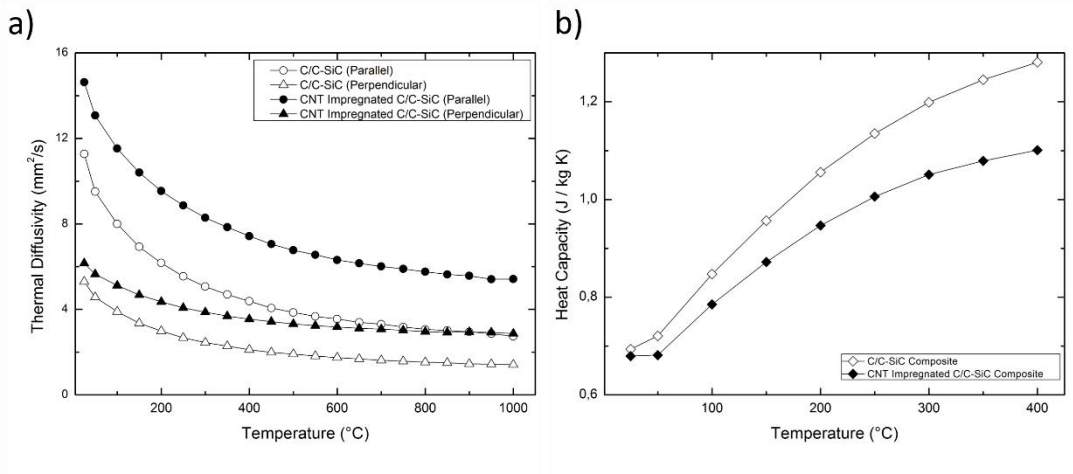

Figure 4.59 a) Thermal diffusivity and b) heat capacity values of the C/C-SiC composites.

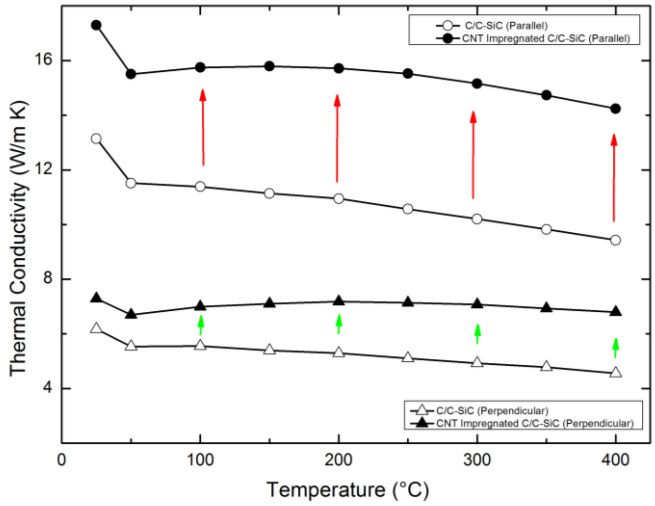

Figure 4.60 Thermal conductivity values of the C/C-SiC composites with and without CNT impregnation.

Table 4.9 shows the thermal characteristics of commercial 3D C/SiC composites used in this study. The comparison of the commercial 3D C/SiC composite and the 2D C/C-SiC composites produced by liquid silicon infiltration shows that thermal conductivity values of the 3D commercial C/SiC composite on the XZ plane are similar to the thermal conductivity values of the 2D C/C-SiC composites parallel to the C fiber woven fabric surface. However, a very large difference in the thermal conductivity value along the XY plane of the 3D C/SiC composite is observed. As it is seen from the Figure 4.59(b) and 4.61(b) for all types of composites and directions, the observed heat capacity values are close to each other. Using the thermal diffusivity values (Figure 4.59(a) and 4.61(a)), the thermal conductivity values of the composites (Figure 4.60) and 4.62), are calculated.

Table 4.8. Thermal properties of C/C-SiC composites with and without CNT impregnation.

Property / Material	Direction	CTE (10^{-6} K^{-1})	Thermal Diffusivity (mm^2/s)	Heat Capacity (J/g K)	Thermal Conductivity (W/m K)
2D C/C-SiC Composite CNT-impregnated	∥	2.30	14.631	0.679	17.313
	⊥	2.15	6.165	0.679	7.291
2D C/C-SiC Composite	∥	2.95	11.280	0.693	13.150
	⊥	2.98	5.297	0.693	6.170

Table 4 9. Thermal properties of the commercial C/SiC composite used in this study.

Property / Material	Direction	CTE	Thermal Diffusivity (mm^2/s)	Heat Capacity (J/g K)	Thermal Conductivity (W/m K)
3D C/SiC Composite	XZ	2.24	12	0.700	16
	XY	2.24	31	0.700	43

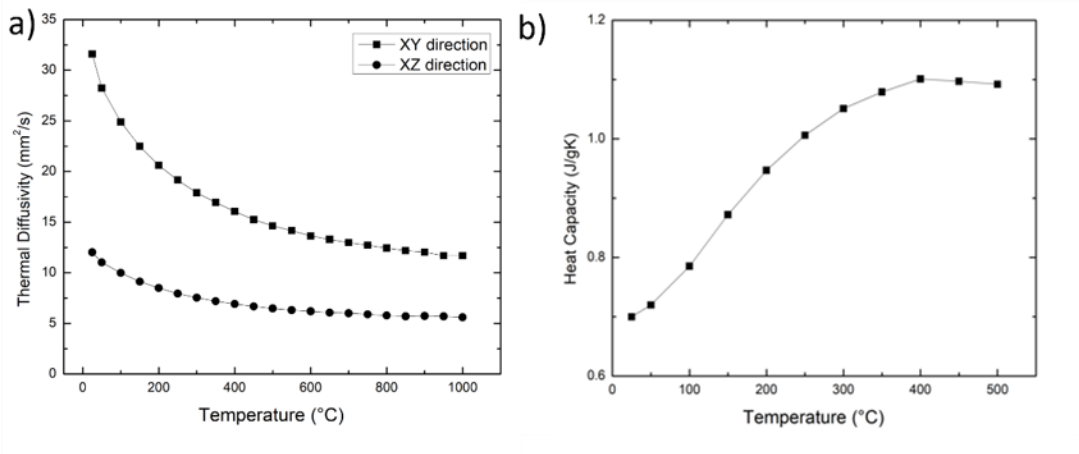

Figure 4.61 a) Thermal diffusivity and b) heat capacity values of the 3D C/SiC composite.

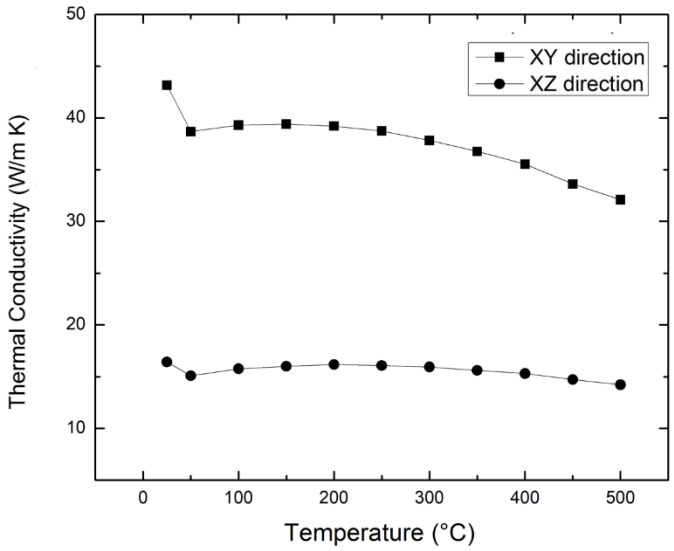

Figure 4.62 Thermal conductivity values of the 3D C/SiC composites.

4.4.1 Wetting Behavior

The wetting of the ceramic matrix composite surface in C/SiC composite/metallic alloy joints controls the interfacial responses and the performance of the brazed joints. As a result of this, wetting tests results provide valuable guidance to further improve joining activities. Therefore, the wetting behavior of the Ticusil brazing

filler alloy on the C/C-SiC composite surfaces has also been investigated at constant temperature in order to evaluate the effect of various material properties and reinforcing structure on the wetting behavior of the 2D C/C-SiC composite.

As it has been previously mentioned, Ticusil brazing filler alloy has solidus and liquidus temperatures of 780 and 900 °C, respectively. Heating procedure from 780 to 915°C with a heating rate of 5 °C/min and keeping the samples at the 915 °C for 900 s has been applied to simulate the starting and finishing points of the brazing procedure. Therefore, similar to previously discussed wetting experiments conducted at a constant temperature of 915 °C, the variations in contact angle with regard to reinforcement structure and material property differences of the 3D C/SiC and 2D C/C-SiC ceramic composites have been compared.

The variations of the contact angles with respect to time at 915 °C for 3D C/SiC, 2D C/C-SiC and CNT impregnated 2D C/C-SiC configurations are shown in Figure 4.63. According to Figure 4.63, the contact angles present similar variation trends with time for all of the cases. For the 2D C/C-SiC composite without CNT impregnation and 2D C/C-SiC composite with CNT impregnation, the contact angles are 32° and 9°, respectively, after 900 s. The contact angle of the 3D C/SiC composite, on the other hand, is 15°. It can be stated that good wetting has been achieved for all composite cases, since all wetting angles are less than 90°.

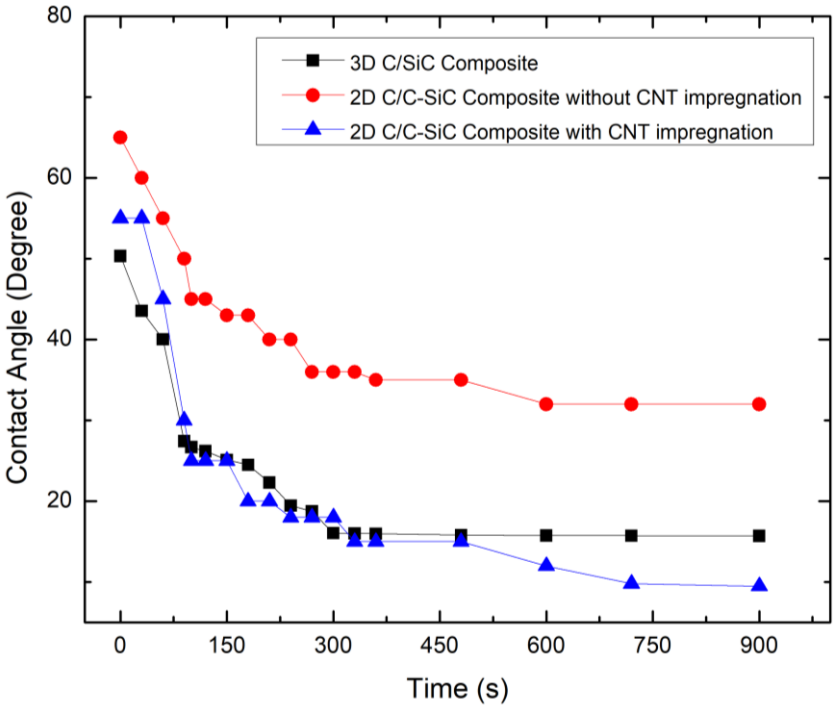

Figure 4.63 The variations of the contact angles with respect to time at the constant temperature of 915 °C for 3D C/SiC, 2D C/C-SiC and CNT impregnated 2D C/C-SiC configurations.

The change in morphology of the pressed Ticusil brazing filler alloy on three different composite surfaces before and after the wetting experiment is shown in Figure 4.64. It can be stated from Figure 4.64 that for all types of the composites molten droplets have a spreading morphology. While the contact angle of the 2D C/C-SiC composite without CNT impregnation is higher than that of the 3D C/SiC composite, the contact angle of the 2D C/C-SiC composite with CNT impregnation is slightly lower.

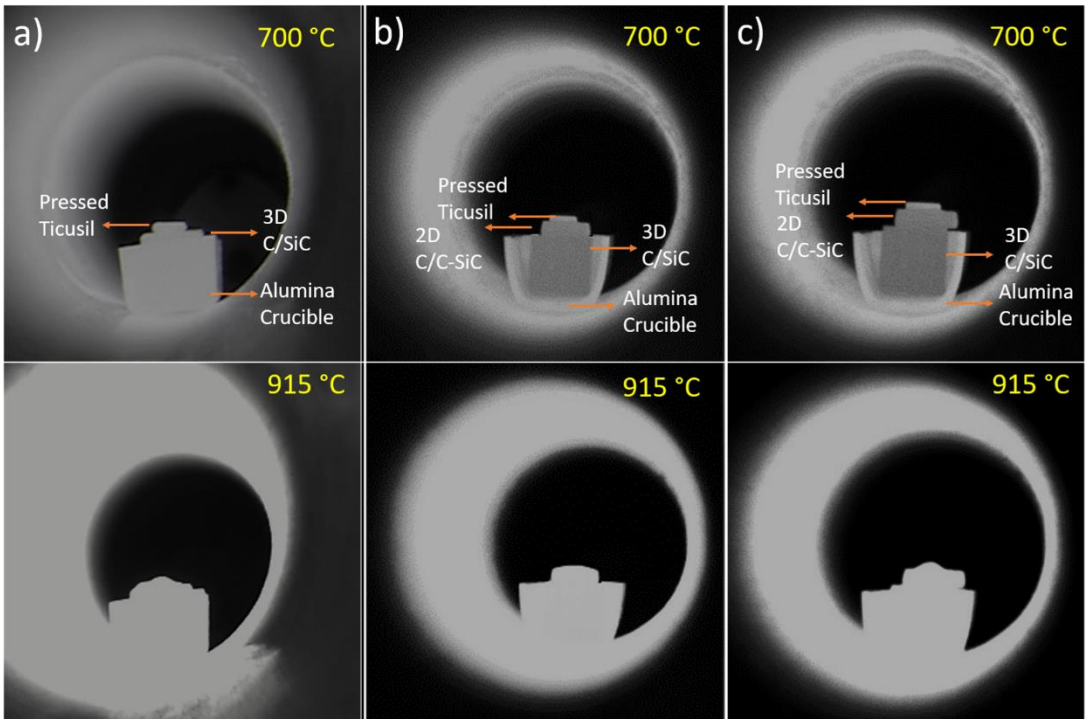

Figure 4.64 Morphological changes of Ticusil brazing filler alloy on different composite surfaces a) commercial 3D C/SiC composite, b) 2D C/C-SiC composite with CNT impregnation, c) 2D C/C-SiC composite without CNT impregnation.

The samples were cut after wetting tests to study the microstructural changes and interfacial interactions between the composites and the brazing filler alloy by examining their cross-sections using SEM. At 915 °C, the Ticusil brazing filler alloy seems to adequately wet all types of the composite surfaces, as shown in the SEM micrographs in Figure 4.65. Cracks and voids are not present in the interface.

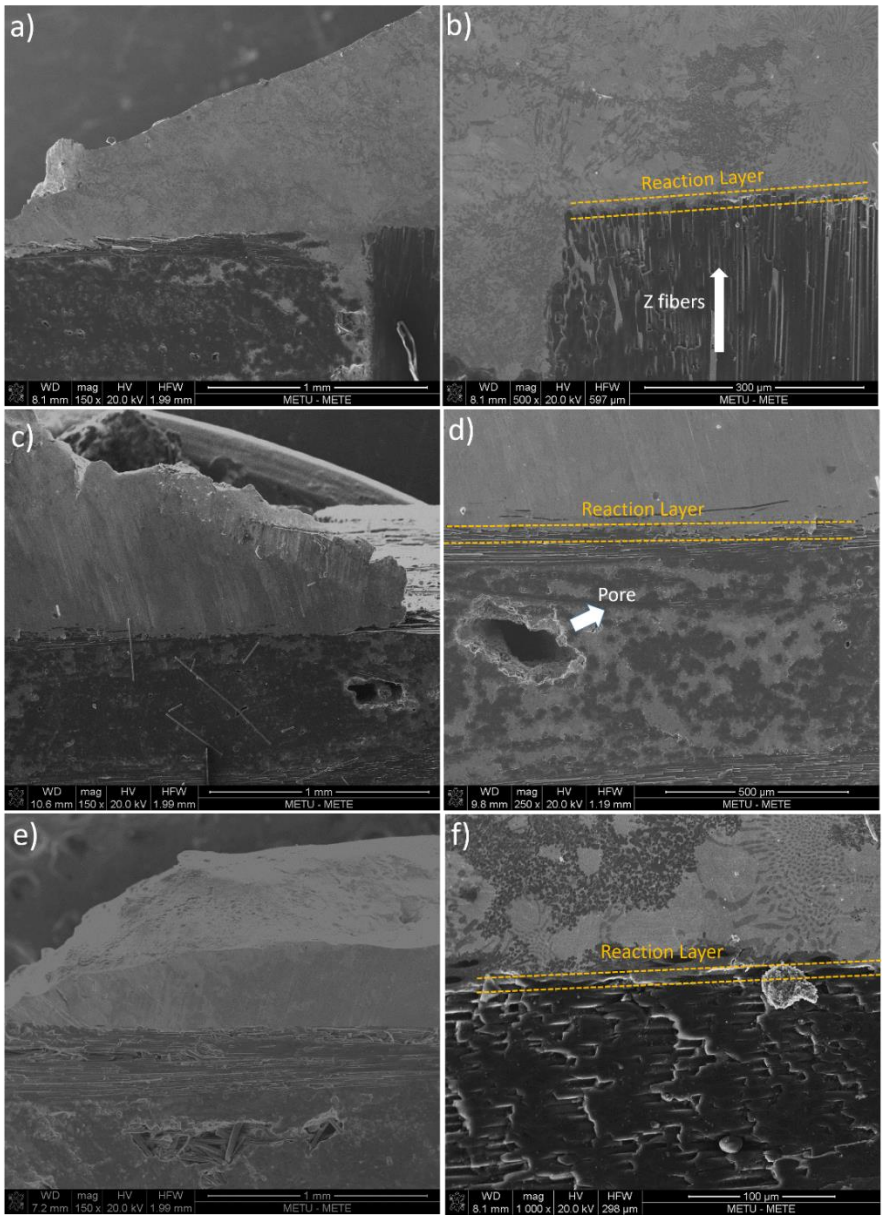

Figure 4.65 Cross-sectional views of the brazing filler alloy/ceramic composite surfaces after wetting experiments at 915 °C for 15 minutes a) 3D C/SiC composite b) reaction layer formation at the interface of the 3D C/SiC composite and brazing filler interlayer, c) 2D C/C-SiC composite, d) reaction layer formation at the interface of the 2D C/C-SiC composite and brazing filler interlayer, e) 2D C/C-SiC composite with CNT impregnation, f) reaction layer formation at the interface of the 2D C/C-SiC composite with CNT impregnation and brazing filler interlayer.

As it is seen in Figure 4.65(a), Ticusil brazing filler alloy appears to have penetrated into the 3D C/SiC composite surface during the wetting experiment. It fills the pores of the 3D C/SiC surface, which has a porous structure due to the reinforcement structure. Z fiber direction of the 3D C/SiC composite is seen in Figure 4.65(b).

For all composites, reaction layers are visible between the ceramic composite and the Ticusil filler alloy interlayer as shown in Figure 4.65. Comparing the reaction layers formed during the wetting experiments, it can be stated that the reinforcement structure does not affect the reaction layer formation. Furthermore, the reaction layer thickness values acquired from wetting experiments are identical to the reaction layer thicknesses obtained from brazing studies. As it was stated in Section 4.4.2, for both brazing and wetting tests, identical interfacial reaction layer formations were identified on all composite surfaces.

As it is presented in Figure 4.66, approximate spreading area and height values are calculated after the wetting experiment. According to Figure 4.66, the spreading area of the Ticusil brazing filler alloy for the 2D C/C-SiC without CNT impregnation is the lowest point comparing with other configurations. Fluidity is directly related to the reactions between the brazing filler alloy and the ceramic matrix composite. The fact that all types of composites have similar reaction layer formation indicates that the degree of decrease in the spreading of the filler alloy on the 2D C/C-SiC composite without CNT impregnation does not affect the reaction layer kinetics considerably.

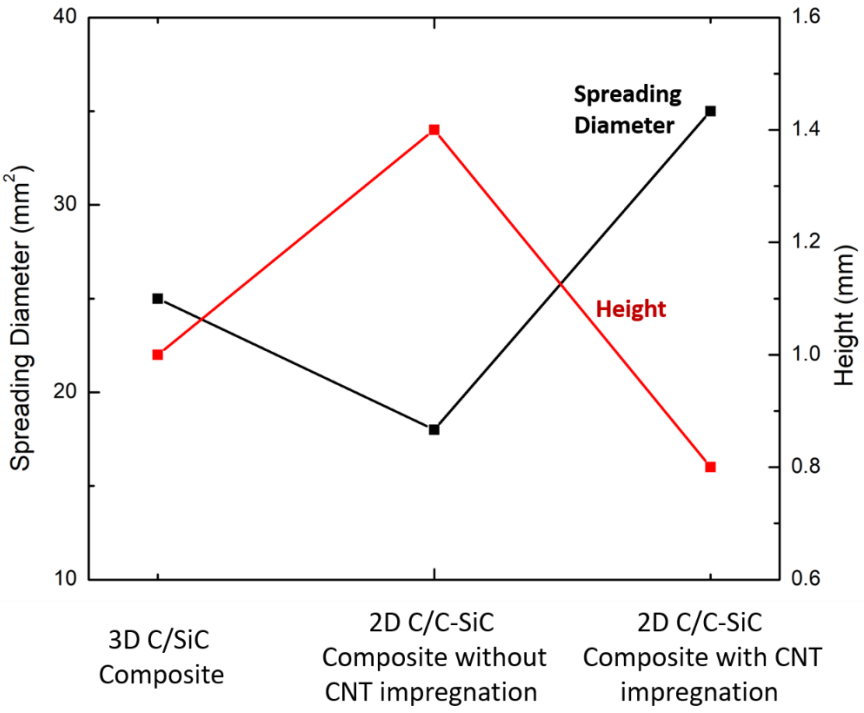

Figure 4.66 Fluidity of the Ticusil brazing filler alloy on different types of composites as presented by the spreading diameter and height of the droplet solidified after the wetting experiment.

4.4.2 Brazing Performance

CNT impregnated 2D C/C-SiC composite and C/C-SiC composite without CNT addition are brazed using Ticusil brazing filler alloy at 915 °C for 15 minutes to investigate the effect of the ceramic matrix composites with different thermal properties on the microstructural evolution and mechanical properties of the brazed joints. The microstructures of the brazed joints are given in Figure 4.67. The microstructural evolution of the interface for C/C-SiC composites with and without CNT impregnation displays similar behavior, as shown in the figure. The sole difference between the two types of composites is pore formation that appears at the brazed interlayer of the C/C-SiC composite without CNT impregnation.

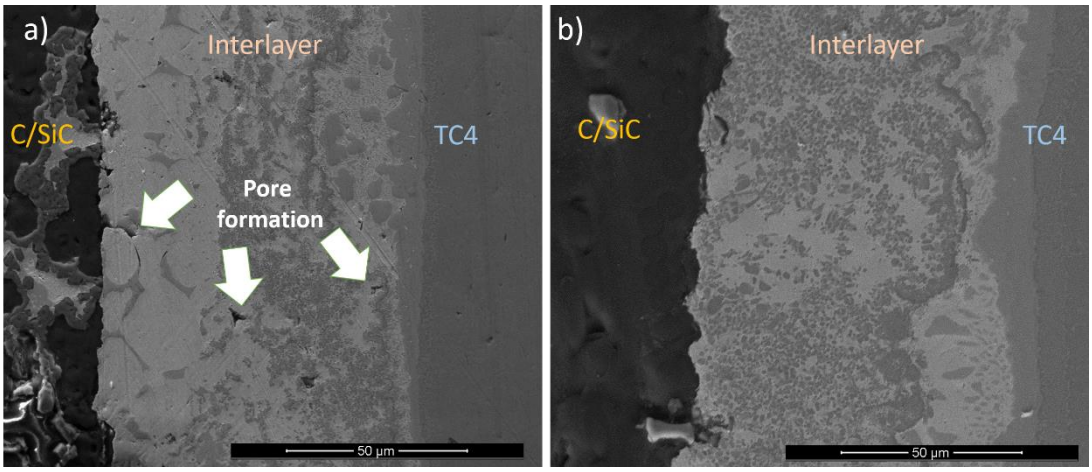

Figure 4.67 The microstructure of the interface between a) C/C-SiC composite without CNT impregnation and Ti6Al4V alloy, b) CNT Impregnated C/C-SiC composite and Ti6Al4V alloy.

Using the mechanical test results, the relationship between the reinforcement structure, thermal properties and shear strength of the brazed joints were examined. As shown in Figure 4.68, the joint with 3D C/SiC composite presents the highest shear strength of 33.2 MPa. 2D C/C-SiC composite without CNT impregnation and CNT impregnated 2D C/C-SiC composite have approximately 17 MPa and 21 MPa shear strength values, respectively.

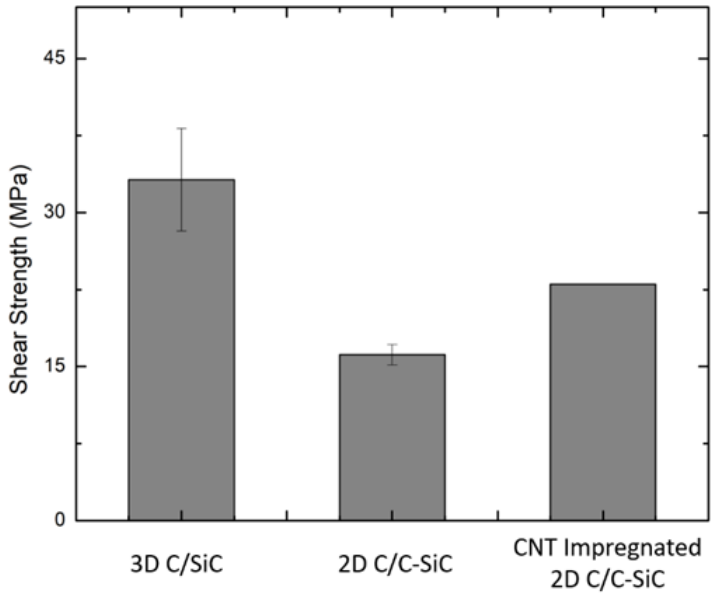

Figure 4.68 Mechanical property of the brazed joints between three different ceramic composites and Ti6Al4V alloy.

Finite element analysis has been carried out to investigate the effect of different thermal properties of the ceramic composites on the mechanical strength of the brazed joints. In addition to the thermal properties of the composites obtained experimentally (thermal expansion coefficient, thermal conductivity, heat capacity), elastic modulus and density of the composites were also used for the finite element analysis. During the analysis, differences in the reinforcement direction as well as phase formations at the interlayer and related microstructural changes were not included.

As it is seen in Figure 4.69 ceramic matrix composite part is under compressive stress during cooling after the brazing process. In contrast, the Ti6Al4V alloy part is subjected to tensile stress due to the thermal expansion mismatch of the two materials being joined by brazing. Moreover, according to the finite element analysis results, the maximum value of the residual stress reached was 45, 78, and 52 MPa for 3D

C/SiC composite, 2D C/C-SiC composite without CNT impregnation and CNT impregnated 2D C/C-SiC composite, respectively.

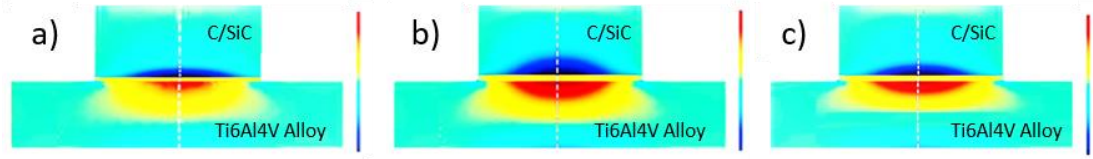

Figure 4.69 Residual stress distribution of the brazed joints upon cooling from the brazing temperature a) 3D C/SiC composite, b) 2D C/C-SiC composite without CNT impregnation, c) 2D C/C-SiC composite with CNT impregnation.

Both 3D and 2D ceramic matrix composite parts have much lower thermal expansion coefficient values compared to the Ti6Al4V alloy. Therefore, during the cooling step of the brazing process, the metallic alloy part shrinks more than the ceramic matrix composites. The ceramic composite side exhibits residual compressive stress in relation to this phenomenon, whereas the Ti6Al4V alloy exhibits residual tensile stress. Tensile stresses are distributed at the border of the ceramic composites to achieve internal stress equilibrium, whereas compressive stresses are created at the Ti6Al4V alloy component. As it is known, while ceramic-based materials are resistant to compressive loads, they are weak under tension. Therefore, residual stress effects are far more damaging to ceramic matrix composites than they are to Ti6Al4V alloys [142,144].

Although the interlayer microstructures of the CNT impregnated C/C-SiC composite and the C/C-SiC composite without CNT impregnation do not differ significantly (Figure 4.67), material property changes caused by CNT addition lead to distinct levels of residual stress distribution at the brazed joints. According to the finite element analysis and shear strength results, lower residual stress in the interlayer results in higher mechanical strength of the brazed joint. Furthermore, during the shear strength test, pores existing in the interlayer for the C/C-SiC composite without

CNT impregnation behave as stress concentration sides, further reducing the shear strength value alongside with the highest residual stress observed in this case.

As a type of carbon fiber-based materials, the material properties of the C/SiC composites depend on the carbon fiber volume fraction and reinforcement architecture. In order to evaluate the effect of reinforcement structure on the resulting brazing performance, 3D C/SiC composite and 2D C/C-SiC composite have been compared.

C/C-SiC composite is reinforced by 2D plain-woven carbon fiber fabrics. The ratio of the reinforcing material is in the range of 45–55% by volume. Figure 4.70 presents the structure of the 2D carbon fiber woven fabric schematically and three different surfaces of its composite form. SEM micrographs are accompanying the sketch to explain the detailed microstructure of the surfaces.

Figure 4.71 displays the detailed microstructure of the XY and XZ planes, as well as a schematic of the 3D orthogonal carbon fiber architecture used in 3D C/SiC composites.

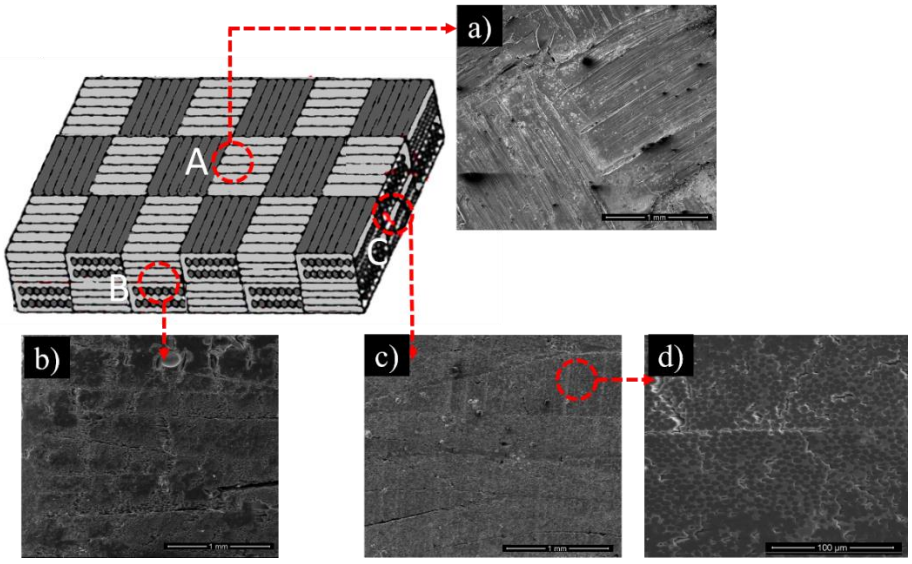

Figure 4.70 Sketch of the 2D plain woven C/C-SiC composite a) SEM micrograph of the surface A, b) SEM image of the surface B, c) SEM image of the surface C along fiber bundles, d) higher magnification image of the surface C.

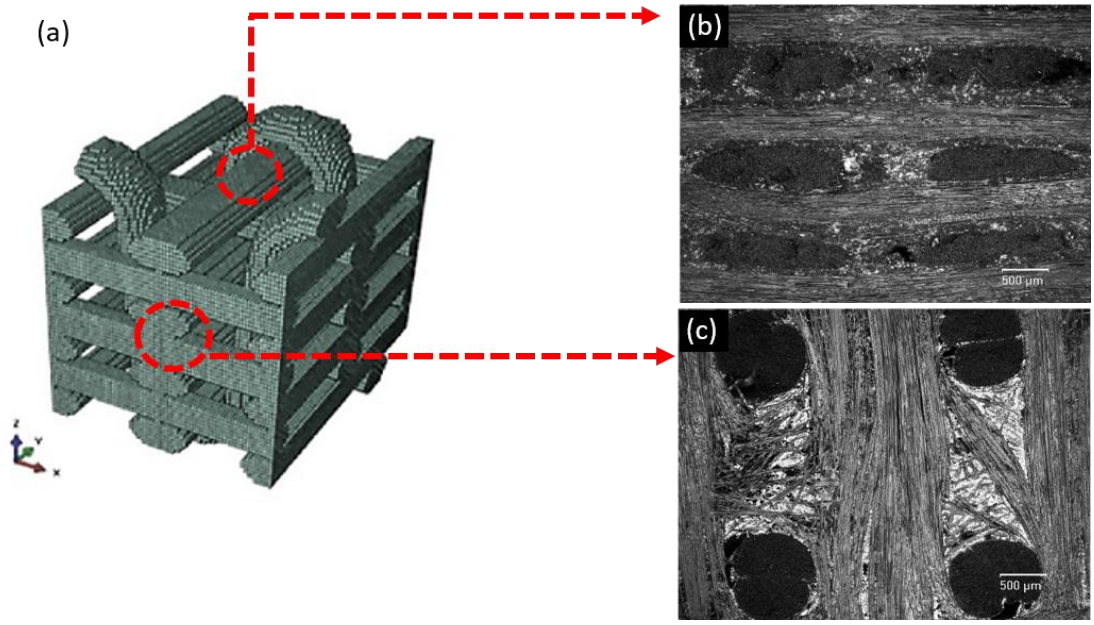

Figure 4.71 (a) Sketch of reinforcement architecture in 3D C/SiC composite (b) Micrograph of XY plane, (c) Micrograph of XZ plane.

Figures 4.70 and 4.71 present the reinforcement distribution difference between the 2D and 3D carbon fiber reinforced ceramic matrix composites. As shown in the micrographs given in Figure 4.70(a) and Figure 4.71(c), the volume fraction of the SiC matrix phase in the bonding direction for 2D plain woven C/C-SiC composite is lower than that of the XZ plane of the 3D C/SiC composite. For C/SiC composite and brazing filler interlayer, chemical reaction possibility resulting in reaction layer is higher in SiC phase than the carbon fibers [78]. As a result, the reinforcing phase (carbon fiber) arrangement has direct impact on the chemical reaction potential of the ceramic matrix composite and the brazing filler alloy as well as the corresponding joint strength. Furthermore, the microstructure of the 3D C/SiC composite comprises a greater pore structure in the XZ plane. Extra surface roughness and capillary pathways for the brazing filler material to follow are created by these pores [145-147]. Consequently, brazed joints between 3D C/SiC composite and Ti6Al4V show

better bonding and higher mechanical performance as a result of the above-mentioned thermal property, reinforcement architecture and microstructure advantages of the 3D composite structure when compared to those of the 2D ceramic matrix composites.

The effect of material characteristics and reinforcement structure of carbon fiber reinforced SiC matrix composites on brazing performance of the joints and wetting behavior have been investigated. The differences observed in fluidity and wetting characteristics due to variation in material properties and reinforcement structures revealed that observed differences are at an acceptable level which were obtained by experiments performed under optimum conditions for Ticusil alloy. The resultant reaction layer and interlayer morphologies are similar due to the comparable wettability characteristics of all three composite cases. It can be stated that the observed difference in mechanical properties resulted from the level of residual stresses due to material property differences and the defects existing at the joint interlayer.

CHAPTER 5

CONCLUSION

The use of Ag-Cu based brazing filler alloys to join two different materials, C/SiC composites and Ti6Al4V alloys, has been investigated. The effect of active Ti element content and additive particle size/amount in the filler alloy, as well as the reinforcing structure and material characteristics of the C/SiC composite, on the interface evolution mechanism and the consequent mechanical performance of the brazed joints, have been studied. Modeled wetting studies conducted under actual brazing parameters have been used to link the relationship between brazing performance and wetting behavior. Major findings and conclusions of the current study can be listed as follows;

- No Ti containing Cusil brazing filler alloy showed insufficient bonding at all brazing temperatures due to lack of adhesion and wetting of the C/SiC composite. Therefore, it could be declared that dissolution of the Ti atoms from the metallic base materials was not available in sufficient quantity to ensure a uniform reaction layer formation for wetting and subsequent adhesion of the C/SiC composite. Presence of Ti as an active element in the filler alloy seems to be crucial for proper joint formation.

- Cusil brazing filler alloy on Ti coated C/SiC ceramic composite also showed insufficient bonding revealing that Ti layer could not provide enough reactive elements for bond formation on the C/SiC composite side.

- Presence of 1.25 wt% Ti in the brazing filler alloy, namely Cusil-ABA, resulted in improved joint performance with a shear strength of 9.5 MPa. With the help of the Ti coating on the ceramic composite surface, the joint

brazed using Cusil-ABA at 875 ºC for 10 min presented further improved shear strength of 23.8 MPa. The interface contained Ti_3SiC_2 and Ti_5Si_3 reaction layer products resulting in strong interfacial bonds and improved joint properties.

- The interface evolution model of the C/SiC composite/Ti6Al4V alloy brazed joint included four different stages namely; brazing filler alloy melting, diffusion of atoms, reaction layer formation, growth and solidification of the reaction layers.

- The effect of active Ti element content on the wetting behavior of the molten brazing filler alloy has been investigated. It was shown that increasing the Ti content in the interlayer and/or at the interface enhanced the wetting behavior of the monolithic SiC ceramic and C/SiC composite surfaces considerably.

- Wetting experiments conducted on both monolithic SiC ceramic and C/SiC composite using the same brazing alloy revealed that the wetting characteristic of the brazing filler alloy is negatively affected by the chemical and structural heterogeneity as well as by the presence of carbon fibers on the surface.

- Introduction of Ti to the joint system either by adding it directly into the filler alloy or by coating as a thin layer on the ceramic composite surface, improved the wettability of the ceramic composite surface by the filler alloy and revealed contact angle values lower than 60°.

- Studies on the brazing of C/SiC composite to Ti6Al4V alloy at various temperatures (900-930 °C) and times (1-30 min) conducted using the brazing filler alloy with the highest Ti content (Ticusil) revealed that the reaction

layer thickness and the type of interlayer phases are a strong function of the brazing temperature and time.

- In order to improve the mechanical performance of the brazed joint, reaction layer thickness and existing phases in the interlayer should be optimized by controlling brazing temperature and time.

- In the case of the brazing filler alloy with the highest Ti content (Ticusil), at brazing temperatures higher than 915 °C and times longer than 15 min, the reaction layers contained brittle Ti_5Si_3 particles which are dispersedly embedded in residual Ti_2Cu.

- With increasing reaction layer thickness, shear strength of the brazed joints initially increases then decreases due to the escalated quantity of brittle phases. In this study, the highest shear strength of ~33 MPa has been achieved in the joints with the Ticusil filler alloy brazed at 915 °C for 15 min, where the reaction layer had an intermediate thickness of ~1 μm.

- Reaction layer thickness, which mainly depends on the brazing time, t, and temperature, T, could be estimated using the resulting empirical equation:

$$X = 2.13 \times 10^{28} \exp(-813.989 \times 10^{3}) / 8.314\ T) \times t^{0.5}$$

- Comparing the reaction layers formed during the brazing experiments and wetting experiments, it can be stated that the thickness of the reaction layers is similar at a temperature of 915 °C for Ticusil brazing filler alloy. Moreover, similar interfacial reaction mechanisms were observed on the C/SiC composite surfaces for both brazing and wetting experiments.

- The effect of particle size and content of the SiC additive on the wetting behavior of the additive containing Ticusil brazing filler alloy and the

performance of the resulting C/SiC composite/Ti6Al4V alloy joints were investigated. Studies revealed that the Ti element in the brazing filler alloy reacts with the additional SiC particles. SEM analysis results have proven that the nano level additive containing interlayer is more uniform compared to micron level additive containing one.

- The change in contact angle with time has been investigated for varying SiC additive particle size and concentration. Similar to no-additive containing brazing filler alloys, nano and micron level additive containing brazing filler alloys showed two distinct patterns in contact angle variation.

- The contact angle values increased as the SiC additive content increased, and the time for the dramatic contact angle decrease shifted to longer durations. Wetting behavior of the brazing filler alloy was affected negatively by increasing the content of both nano and micron level SiC additives beyond a certain level. However, the increase in the contact angle with the additive content was higher for micron level SiC particles.

- The shear strength of brazed joints increased first then decreased as the amount of both nano and micron level additives increases. The joint containing 2 wt% nano level SiC additive had the highest shear strength of 44.8 MPa. Although the observed contact angle values are nearly same for 2 wt% nano level (42°) and for 1 wt% micron-scale (37°) SiC addition, higher increment in the joint' mechanical performance was achieved with the nano level SiC additive due to the finer and more homogeneous reinforcement effect of the nanoparticles.

- Shear strength decreased considerably in the case of a 5 wt% nano level SiC addition. The molten brazing filler alloy mixed unevenly due to the agglomeration tendency of the nanoparticles resulting in delamination at the

interface and degradation in mechanical performance. Furthermore, an extreme nanoparticle content reduced the brazing filler's wettability, which is crucial for the formation of strong bonds in brazing operations.

- Larger additive size and higher additive content decreased the fluidity of the filler alloy remarkably suppressing its penetration ability to the C/SiC composite rendering a potentially weaker interaction and bonding at the brazed joint.

- The additive content and related wetting behavior should be tailored in order to provide optimal mechanical performance for both nano and micron level SiC additives. It can be stated that for both additive cases, the optimum contact angle for the highest joint performance was ~40°.

- The effect of reinforcement structure and material properties on brazing performance and wetting behavior of carbon fiber reinforced SiC matrix composites has been examined. Variation in reinforcing structures and material properties of the composites demonstrated minor differences in fluidity and wetting characteristics which were determined by experiments conducted under ideal conditions for Ticusil alloy.

- Composites reinforced with two different types of carbon fiber architectures, 3D and 2D, displayed identical wettability characteristics and thus morphologies in the reaction layer and interlayer.

- Carbon nanotube (CNT) impregnation to the matrix of the 2D C/C-SiC composites improved the wettability of its surface by the brazing filler alloy. Despite superior wetting, 2D C/C-SiC composites with or without CNT impregnation exhibited inferior mechanical properties, which can be

attributed to residual stresses generated by material property variations as well as defects at the junction interlayer.

In order to further enhance the performance of the brazed joints, following recommendations can be listed for future work;

- As well as the active element content in the brazing filler alloy, its type also affects the performance of the brazed joints. Therefore, it would be interesting to investigate the effect of different surface active elements such as Zr, Hf etc. on the wetting behavior and brazing performance.

- In addition to the effect of the presence of different types of surface-active elements in the brazing filler alloys, the effect of these elements on wetting behavior and brazing performance should be investigated further by coating them on the ceramic surfaces in various thicknesses and layer by layer conditions.

- In this study it has been revealed that active Ti element concentration and additive particles in the filler alloy are critical parameters; therefore, the effect of Ti coated additive particles in different size and content on the brazing performance can be investigated.

REFERENCES

[1] A. Okada, *Ceramic-Matrix Composites*, vol. 2–2. 2003.

[2] Y. Liu *et al.*, "Research on the interface properties and strengthening-toughening mechanism of nanocarbon-toughened ceramic matrix composites," *Nanotechnology Reviews*. 2020, doi: 10.1515/ntrev-2020-0017.

[3] J. Mukerji, "Ceramic matrix composites," *Def. Sci. J.*, 1993, doi: 10.14429/dsj.43.4292.

[4] J. Kim, "Tensile fracture behavior and characterization of ceramic matrix composites," *Materials (Basel).*, 2019, doi: 10.3390/ma12182997.

[5] D. K. Rajak, D. D. Pagar, R. Kumar, and C. I. Pruncu, "Recent progress of reinforcement materials: A comprehensive overview of composite materials," *J. Mater. Res. Technol.*, 2019, doi: 10.1016/j.jmrt.2019.09.068.

[6] S. Tülbez, Z. Esen, and A. F. Dericioglu, "Effect of CNT impregnation on the mechanical and thermal properties of C/C-SiC composites," *Adv. Compos. Hybrid Mater.*, 2020, doi: 10.1007/s42114-020-00155-3.

[7] S. Tülbez, "Processıng And Characterızatıon of Carbon Fiber Reınforced Silicon Carbıde (C/C-SiC) Matrıx Composites," Middle East Technical University, July, p. 2015, 2015.

[8] F. Raether, "Ceramic Matrix Composites – an Alternative for Challenging Construction Tasks," *Ceram. Appications*, vol. 1, no. 1, pp. 45–49, 2013.

[9] M. Patel, K. Saurabh, V. V. B. Prasad, and J. Subrahmanyam, "High temperature C / C – SiC composite by liquid silicon infiltration :," *Bull. Mater. Sci.*, vol. 35, no. 1. pp. 67–77, 2012.

[10] W. Krenkel and F. Berndt, "C/C-SiC composites for space applications and advanced friction systems," *Mater. Sci. Eng. A*, 2005, doi:

10.1016/j.msea.2005.08.204.

[11] W. Krenkel, “Carbon fiber reinforced CMC for high-performance structures,” *Int. J. Appl. Ceram. Technol.*, 2004, doi: 10.1111/j.1744-7402.2004.tb00169.x.

[12] W. Krenkel, *Ceramic Matrix Composites: Fiber Reinforced Ceramics and their Applications*. 2008.

[13] N. P. Bansal and J. Lamon, *Ceramic Matrix Composites: Materials, Modeling and Technology*. 2014.

[14] Y. Wang, Z. Chen, and S. Yu, “Ablation behavior and mechanism analysis of C/SiC composites,” *Journal of Materials Research and Technology*. 2016, doi: 10.1016/j.jmrt.2015.10.004.

[15] W. Krenkel, “Applications of fibre reinforced C/C-SiC ceramics,” *CFI Ceram. Forum Int.*, 2003.

[16] X. Yang, C. Zhao-hui, and C. Feng, “High-temperature protective coatings for C/SiC composites,” *Journal of Asian Ceramic Societies*. 2014, doi: 10.1016/j.jascer.2014.07.004.

[17] W. Krenkel and J. Georges Thébault, “Ceramic Matrix Composites for Friction Applications,” in *Ceramic Matrix Composites: Materials, Modeling and Technology*, 2014.

[18] J. Xiao, H. Y. Zhang, S. K. Gong, H. Bin Xu, and H. B. Guo, “High-temperature oxidation resistance of Si-coated C/SiC composites,” *Rare Met.*, 2019, doi: 10.1007/s12598-019-01209-2.

[19] X. Yin, L. Cheng, L. Zhang, and Y. Xu, “Oxidation behaviors of C/SiC in the oxidizing environments containing water vapor,” *Mater. Sci. Eng. A*, 2003, doi: 10.1016/S0921-5093(02)00644-5.

[20] C. Veiga, J. P. Davim, and A. J. R. Loureiro, “Proprties and applications of

titanium alloys," *Rev. Adv. Mater. Sci.*, vol. 32, pp. 133–148, 2012.

[21] R. R. Boyer, "An overview on the use of titanium in the aerospace industry," *Mater. Sci. Eng. A*, vol. 213, no. 1–2, pp. 103–114, 1996, doi: 10.1016/0921-5093(96)10233-1.

[22] M. Niinomi, "Titanium alloys," in *Encyclopedia of Biomedical Engineering*, 2019.

[23] G. Lütjering, "Influence of processing on microstructure and mechanical properties of (α + β) titanium alloys," *Mater. Sci. Eng. A*, vol. 243, no. 1–2, pp. 32–45, 1998, doi: 10.1016/s0921-5093(97)00778-8.

[24] X. Yang and C. R. Liu, "Machining titanium and its alloys," *Mach. Sci. Technol.*, 1999, doi: 10.1080/10940349908945686.

[25] J. Donachie and J. M, "Titanium – A Technical Guide," *ASM Int. 2nd Ed.*, 2000.

[26] L. M. Kang and C. Yang, "A Review on High-Strength Titanium Alloys: Microstructure, Strengthening, and Properties," *Advanced Engineering Materials*. 2019, doi: 10.1002/adem.201801359.

[27] S. Liu and Y. C. Shin, "Additive manufacturing of Ti6Al4V alloy: A review," *Mater. Des.*, vol. 164, p. 107552, 2019, doi: 10.1016/j.matdes.2018.107552.

[28] C. Veiga, J. P. Davim, and A. J. R. Loureiro, "Properties and applications of titanium alloys: A brief review," *Reviews on Advanced Materials Science*. 2012.

[29] I. V. Gorynin, "Titanium alloys for marine application," *Mater. Sci. Eng. A*, 1999, doi: 10.1016/s0921-5093(98)01180-0.

[30] R. A. Antunes, M. C. L. de Oliveiraa, and C. A. F. Salvador, "Materials selection of optimized titanium alloys for aircraft applications," *Mater. Res.*, 2018, doi: 10.1590/1980-5373-mr-2017-0979.

[31] D. G. Dixon, “Ceramic matrix composite-metal brazed joints,” *J. Mater. Sci.*, 1995, doi: 10.1007/BF00375261.

[32] V. Petley, S. Verma, K. Saravanan, M. Stalin, K. Raghavendra, and K. Venkateswarlu, “Evaluation of Metal–Ceramic Composite Joint Under Tensile Loads at Elevated Temperature,” *Trans. Indian Inst. Met.*, 2017, doi: 10.1007/s12666-017-1063-4.

[33] American Welding Society, “Brazing Handbook,” in *Brazing Handbook*, 2007.

[34] L. F. M. da Silva, A. Öchsner, and R. D. Adams, “Introduction to adhesive bonding technology,” *Handbook of Adhesion Technology: Second Edition*. 2018, doi: 10.1007/978-3-319-55411-2_1.

[35] M. W. Mahoney and C. C. Bampton, “Fundamentals of Diffusion Bonding,” in *Welding, Brazing, and Soldering*, 2018.

[36] H.-S. Lee, “Diffusion bonding of metal alloys in aerospace and other applications,” in *Welding and Joining of Aerospace Materials*, 2021.

[37] P. . Roberts, *Introduction to Brazing Technology*. 2016.

[38] A. B. Kilgore, M. L. Koehler, J. W. Metzler, and S. R. Sturges, “Welding, brazing, and soldering handbook,” *ASM Int.*, 1993.

[39] ASM Handbook Committee, “ASM Metals HandBook Volume 06 - Welding, Brazing, and Soldering,” *Mech. Des.*, 2019.

[40] J. Szczurek and J. Kowalewski, “Issues in vacuum brazing,” *Proc. 3rd Int. Brazing Solder. Conf.*, vol. 2006, pp. 326–333, 2006.

[41] T. Yamazaki, “Brazing,” *Yosetsu Gakkai Shi/Journal Japan Weld. Soc.*, 2015, doi: 10.1016/b978-075067757-8/50007-5.

[42] K. Mergia, “Joining of Cf/C and Cf/SiC Composites to Metals,” in *Nanocomposites with Unique Properties and Applications in Medicine and*

Industry, 2011.

[43] N. Eustathopoulos, “Wetting by liquid metals—application in materials processing: The contribution of the grenoble group,” *Metals (Basel).*, vol. 5, no. 1, pp. 350–370, 2015, doi: 10.3390/met5010350.

[44] N. Eustathopoulos, N. Sobczak, A. Passerone, and K. Nogi, “Measurement of contact angle and work of adhesion at high temperature,” 2005, doi: 10.1007/s10853-005-1945-4.

[45] G. Kumar and K. N. Prabhu, “Review of non-reactive and reactive wetting of liquids on surfaces,” *Advances in Colloid and Interface Science*. 2007, doi: 10.1016/j.cis.2007.04.009.

[46] N. Eustathopoulos, M. G. Nicholas, and B. B. Drevet, *Wettability at high temperatures*. 1999.

[47] N. Eustathopoulos, B. Drevet, and M. L. Muolo, “The oxygen-wetting transition in metal/oxide systems,” *Mater. Sci. Eng. A*, 2001, doi: 10.1016/S0921-5093(00)01790-1.

[48] N. Frage, N. Froumin, and M. P. Dariel, “Wetting of TiC by non-reactive liquid metals,” *Acta Mater.*, 2002, doi: 10.1016/S1359-6454(01)00349-4.

[49] O. Dezellus, S. Jacques, F. Hodaj, and N. Eustathopoulos, “Wetting and infiltration of carbon by liquid silicon,” 2005, doi: 10.1007/s10853-005-1950-7.

[50] P. Protsenko, J. P. Garandet, R. Voytovych, and N. Eustathopoulos, “Thermodynamics and kinetics of dissolutive wetting of Si by liquid Cu,” *Acta Mater.*, 2010, doi: 10.1016/j.actamat.2010.06.038.

[51] C. Rado, B. Drevet, and N. Eustathopoulos, “Role of compound formation in reactive wetting: The Cu/SiC system,” *Acta Mater.*, 2000, doi: 10.1016/S1359-6454(00)00235-4.

[52] A. Koltsov, F. Hodaj, and N. Eustathopoulos, “Brazing of AlN to SiC by a Pr silicide: Physicochemical aspects,” *Mater. Sci. Eng. A*, 2008, doi: 10.1016/j.msea.2007.11.092.

[53] R. Voytovych, F. Robaut, and N. Eustathopoulos, “The relation between wetting and interfacial chemistry in the CuAgTi/alumina system,” *Acta Mater.*, 2006, doi: 10.1016/j.actamat.2005.11.048.

[54] Q. Zhu *et al.*, “Enhanced mechanical properties and thermal cycling stability of Al2O3-4J42 joints brazed using Ag–Cu–Ti/Cu/Ag–Cu composite filler,” *Ceram. Int.*, 2021, doi: 10.1016/j.ceramint.2021.07.204.

[55] C. Valette, M. F. Devismes, R. Voytovych, and N. Eustathopoulos, “Interfacial reactions in alumina/CuAgTi braze/CuNi system,” *Scr. Mater.*, 2005, doi: 10.1016/j.scriptamat.2004.09.008.

[56] M. Singh, R. Asthana, and N. Sobczak, “Active Brazing of SiC-Base Ceramics to High-Temperature Alloys,” *J. Mater. Eng. Perform.*, 2020, doi: 10.1007/s11665-020-04934-3.

[57] E. I. Krasnov, E. I. Kurbatkina, A. A. Shavnev, V. M. Serpova, and A. N. Zhabin, “Application of The Actıve Brazıng Method For Connecting Fiber Materials With Ceramic Materials (review),” *Proc. VIAM*, 2020, doi: 10.18577/2307-6046-2020-0-10-63-72.

[58] W. B. Hanson, K. I. Ironside, and J. A. Fernie, “Active metal brazing of zirconia,” *Acta Mater.*, 2000, doi: 10.1016/S1359-6454(00)00256-1.

[59] Y. Lu, X. Zhang, J. Chu, X. Liu, and Z. Fang, “Study on active reactive brazing of C/SiC ceramic to Nb alloy,” *Xiyou Jinshu / Chinese J. Rare Met.*, 2008.

[60] R. Asthana and M. Singh, *Active metal brazing of advanced ceramic composites to metallic systems*. 2013.

[61] A. K. Ray, A. Kar, S. A. Kori, L. C. Pathak, and A. N. Sonnad, “Graphite-to-

304SS braze joining by active metal-brazing technique: Improvement of mechanical properties," *J. Mater. Eng. Perform.*, 2013, doi: 10.1007/s11665-012-0225-0.

[62] K. Suganuma, "Recent Advances in Joining Technology of Ceramics to Metals," *isij Int.*, 1990, doi: 10.2355/isijinternational.30.1046.

[63] F. Moret and N. Eustathopoulos, "Ceramic to metal direct brazing," *J. Phys.*, 1993, doi: 10.1051/jp4:19937162.

[64] J. Yang, J. Huang, Z. Ye, S. Chen, R. Ji, and Y. Zhao, "Influence of interfacial reaction on reactive wettability of molten Ag-Cu-X wt.%Ti filler metal on SiC ceramic substrate and mechanism analysis," *Appl. Surf. Sci.*, 2018, doi: 10.1016/j.apsusc.2017.12.106.

[65] R. F. Guo, P. Shen, J. Zang, Y. H. Ma, and Q. C. Jiang, "The influence of surface orientation on the wetting and reaction at the Al/MgAl2O4 interfaces," *Ceram. Int.*, 2019, doi: 10.1016/j.ceramint.2019.08.106.

[66] S. Hausner and B. Wielage, "Brazing of metal and ceramic joints," in *Advances in Brazing: Science, Technology and Applications*, 2013.

[67] R. Arróyave and T. W. Eagar, "Metal substrate effects on the thermochemistry of active brazing interfaces," *Acta Mater.*, 2003, doi: 10.1016/S1359-6454(03)00330-6.

[68] S. Li *et al.*, "A review on filler materials for brazing of carbon-carbon composites," *Reviews on Advanced Materials Science*. 2021, doi: 10.1515/rams-2021-0007.

[69] G. Elssner and G. Petzow, "Metal/Ceramic Joining," *isij Int.*, 1990, doi: 10.2355/isijinternational.30.1011.

[70] D. R. Simhan and A. Ghosh, "High vacuum active brazing of cBN with improved composite filler: Microstructure, interfaces and performance evaluation," *Vacuum*, 2021, doi: 10.1016/j.vacuum.2020.109803.

[71] S. Mishra, A. Sharma, D. H. Jung, and J. P. Jung, “Recent Advances in Active Metal Brazing of Ceramics and Process,” *Met. Mater. Int.*, vol. 26, no. 8, pp. 1087–1098, 2020, doi: 10.1007/s12540-019-00536-4.

[72] R. E. Loehman and A. P. Tomsia, “Reactions of Ti and Zr with AlN and Al2O3,” *Acta Metall. Mater.*, 1992, doi: 10.1016/0956-7151(92)90266-H.

[73] N. Y. Taranets and H. Jones, “Wettability of aluminium nitride based ceramics of different porosity by two active silver based brazing alloys,” *Mater. Sci. Eng. A*, 2004, doi: 10.1016/j.msea.2004.02.021.

[74] Eremenko Vn, Buyanov Yuı, And Panchenko Nm, “Polythermal And Isothermal Sectıons Of The System Tıtanıum-Copper- Sılver-2,” *Poroshkovaya Metall.*, 1970.

[75] O. Dezellus, R. Arroyave, and S. G. Fries, “Thermodynamic modelling of the Ag-Cu-Ti ternary system,” *Int. J. Mater. Res.*, 2011, doi: 10.3139/146.110472.

[76] R. Arróyave and T. W. Eagar, “Thermodynamic Assessment of the Ag-Cu-Ti System,” 2003.

[77] B. Cui, J. Hua Huang, J. Hui Xiong, and H. Zhang, “Reaction-composite brazing of carbon fiber reinforced SiC composite and TC4 alloy using Ag-Cu-Ti-(Ti+C) mixed powder,” *Mater. Sci. Eng. A*, vol. 562, pp. 203–210, 2013, doi: 10.1016/j.msea.2012.11.031.

[78] J. H. Xiong, J. H. Huang, H. Zhang, and X. K. Zhao, “Brazing of carbon fiber reinforced SiC composite and TC4 using Ag-Cu-Ti active brazing alloy,” *Mater. Sci. Eng. A*, 2010, doi: 10.1016/j.msea.2009.09.024.

[79] A. Elrefaey, “High-temperature brazing in aerospace engineering,” *Welding and Joining of Aerospace Materials*. pp. 345–383, 2011, doi: 10.1016/B978-1-84569-532-3.50011-3.

[80] Q. Zhang, L. Sun, Q. Liu, J. Zhang, T. Wang, and C. Liu, “Effect of brazing

parameters on microstructure and mechanical properties of Cf/SiC and Nb-1Zr joints brazed with Ti-Co-Nb filler alloy," *J. Eur. Ceram. Soc.*, 2017, doi: 10.1016/j.jeurceramsoc.2016.09.031.

[81] M. Way, J. Willingham, and R. Goodall, "Brazing filler metals," *Int. Mater. Rev.*, 2020, doi: 10.1080/09506608.2019.1613311.

[82] T. Watanabe, A. Yanagisawa, and T. Sasaki, "Development of ag based brazing filler metal with low melting point," *Sci. Technol. Weld. Join.*, 2011, doi: 10.1179/1362171811Y.0000000037.

[83] M. Brochu, M. D. Pugh, and R. A. L. Drew, "Joining silicon nitride ceramic using a composite powder as active brazing alloy," *Mater. Sci. Eng. A*, 2004, doi: 10.1016/j.msea.2003.10.276.

[84] A. Jain and Lucas-Milhaupt, "Brazing Technical Bulletin," 2008, [Online]. Available: www.lucasmilhaupt.com.

[85] O. M. Akselsen, "Advances in brazing of ceramics," *Journal of Materials Science*. 1992, doi: 10.1007/BF01117909.

[86] R. M. do Nascimento, A. E. Martinelli, and A. J. A. Buschinelli, "Review Article: recent advances in metal-ceramic brazing," *Cerâmica*, 2003, doi: 10.1590/s0366-69132003000400002.

[87] D. Giuranno *et al.*, "Studies of the Joining-Relevant Interfacial Properties in the Si-Ti/C and Si-Ti/SiC Systems," *J. Mater. Eng. Perform.*, 2020, doi: 10.1007/s11665-020-04655-7.

[88] J. H. Xiong, J. H. Huang, H. Zhang, and X. K. Zhao, "Brazing of carbon fiber reinforced SiC composite and TC4 using Ag-Cu-Ti active brazing alloy," *Materials Science and Engineering A*, vol. 527, no. 4–5. pp. 1096–1101, 2010, doi: 10.1016/j.msea.2009.09.024.

[89] J. H. Xiong, J. H. Huang, H. Zhang, and X. K. Zhao, "Joining of Cf/SiC composite and TC4 using Ag-Al-Ti active brazing alloy," *J. Mater. Eng.*

Perform., 2011, doi: 10.1007/s11665-010-9732-z.

[90] M. G. Nicholas, "Ceramic-Metal Interfaces," in *Surfaces and Interfaces of Ceramic Materials*, 1989.

[91] R. Beeranur, K. K. Waghmare, and R. kumar Singh, "Characterization of Vacuum Brazing of SS 304 and Alumina Ceramic with Active Brazing Alloy," *Procedia Mater. Sci.*, 2014, doi: 10.1016/j.mspro.2014.07.385.

[92] J. Yang *et al.*, "Investigation on viscosity, surface tension and non-reactive wettability of melting Ag-Cu-Xwt%Ti active filler metals," *J. Alloys Compd.*, 2019, doi: 10.1016/j.jallcom.2018.09.186.

[93] C. Xin, N. Li, and J. Yan, "Microstructural evolution in the braze joint of sapphire to Kovar alloy by Ti-Cu metallization layer," *J. Mater. Process. Technol.*, 2017, doi: 10.1016/j.jmatprotec.2017.05.016.

[94] O. Kozlova, M. Braccini, R. Voytovych, N. Eustathopoulos, P. Martinetti, and M. F. Devismes, "Brazing copper to alumina using reactive CuAgTi alloys," *Acta Mater.*, 2010, doi: 10.1016/j.actamat.2009.10.029.

[95] E. Lugscheider and W. Tillmann, "Methods for brazing ceramic and metal-ceramic joints," *Mater. Manuf. Process.*, 1993, doi: 10.1080/10426919308934826.

[96] R. Asthana, M. Singh, and N. Sobczak, "Wetting behavior and interfacial microstructure of palladium- and silver-based braze alloys with C-C and SiC-SiC composites," *J. Mater. Sci.*, vol. 45, no. 16, pp. 4276–4290, 2010, doi: 10.1007/s10853-010-4647-5.

[97] Y. Mao, L. Peng, Q. Deng, D. Nie, S. Wang, and L. Xi, "Wetting behavior and interfacial interactions of molten Cu50Ti alloy with hexagonal BN and TiB2 ceramics," *Ceram. Int.*, 2016, doi: 10.1016/j.ceramint.2016.03.090.

[98] M. A. I. A. Rahman *et al.*, "Effects of wetting time on properties of steel-aluminium brazed joint," *J. Teknol.*, 2016, doi: 10.11113/jt.v78.9147.

[99] H. Y. Chen, X. C. Wang, L. Fu, and M. Y. Feng, “Effects of surface microstructure on the active element content and wetting behavior of brazing filler metal during brazing Ti3SiC2 ceramic and Cu,” *Vacuum*, 2018, doi: 10.1016/j.vacuum.2018.07.043.

[100] J. Chen, X. Wang, X. Li, N. Li, and Q. Yang, “Effects of brazing temperature and holding time on wettability of brazing diamond and brazing interface analysis,” *Weld. World*, 2020, doi: 10.1007/s40194-020-00954-8.

[101] G. Lin, J. Huang, and H. Zhang, “Joints of carbon fiber-reinforced SiC composites to Ti-alloy brazed by Ag-Cu-Ti short carbon fibers,” *J. Mater. Process. Technol.*, 2007, doi: 10.1016/j.jmatprotec.2007.01.031.

[102] C. Cai, J. Xiong, J. Huang, and S. Chen, “Brazing of Cf/SiC and Ti alloy by using Ag-Cu-Ti active brazing alloy,” *Hanjie Xuebao/Transactions China Weld. Inst.*, 2011.

[103] Y. Cao, J. Yan, N. Li, Y. Zheng, and C. Xin, “Effects of brazing temperature on microstructure and mechanical performance of Al2O3/AgCuTi/Fe-Ni-Co brazed joints,” *J. Alloys Compd.*, 2015, doi: 10.1016/j.jallcom.2015.07.237.

[104] W. Han, M. Wan, R. Zhao, H. Kang, And Y. Rao, “Microstructural evolution and mechanical properties of brazed IN718 ultrathin-walled capillary structure using different particulate reinforced filler alloy,” *Chinese J. Aeronaut.*, 2021, doi: 10.1016/j.cja.2021.03.001.

[105] S. Saltik, Z. Esen, and A. F. Dericioglu, “Wetting behavior and reaction layer formation in C/SiC composite-titanium alloy joints,” *Adv. Mater. Process. Technol.*, vol. 00, no. 00, pp. 1–21, 2021, doi: 10.1080/2374068x.2021.1971001.

[106] R. E. Thrillwood, “Vacuum Brazing.,” *Eng.*, vol. 219, no. 11, pp. 1468–1471, 1979.

[107] R. Voytovych, L. Y. Ljungberg, and N. Eustathopoulos, “The role of

adsorption and reaction in wetting in the CuAg-Ti/alumina system," *Scr. Mater.*, vol. 51, no. 5, pp. 431–435, 2004, doi: 10.1016/j.scriptamat.2004.05.002.

[108] D. Fan, J. Huang, X. Zhao, J. Yang, S. Chen, and X. Zhao, "Joining of Cf/SiC composite to Ti-6Al-4V with (Ti-Zr-Cu-Ni)+Ti filler based on in-situ alloying concept," *Ceram. Int.*, vol. 43, no. 5, pp. 4151–4158, 2017, doi: 10.1016/j.ceramint.2016.12.030.

[109] J. Yang *et al.*, "Reactive wetting behavior and mechanism of AlN ceramic by CuNi-Xwt%Ti active filler metal," *Ceram. Int.*, 2020, doi: 10.1016/j.ceramint.2019.10.150.

[110] M. G. Nicholas, "Reactive metal brazing of ceramics," *Scand. J. Metall.*, 1991.

[111] J. S. Pimenta, A. J. A. Buschinelli, R. M. Do Nascimento, A. E. Martinelli, and U. Reisgen, "Brazing of metalized zirconia with titanium to Ti-6Al-4V alloy," *Cerâmica*, 2012, doi: 10.1590/S0366-69132012000200006.

[112] Y. Cao, J. Yan, N. Li, Y. Zheng, and C. Xin, "Effects of brazing temperature on microstructure and mechanical performance of Al2O3/AgCuTi/Fe-Ni-Co brazed joints," *J. Alloys Compd.*, vol. 650, pp. 30–36, 2015, doi: 10.1016/j.jallcom.2015.07.237.

[113] M. Wu, C. Z. Cao, R. Ud-Din, X. B. He, and X. H. Qu, "Brazing diamond/Cu composite to alumina using reactive Ag-Cu-Ti alloy," *Trans. Nonferrous Met. Soc. China (English Ed.*, 2013, doi: 10.1016/S1003-6326(13)62651-5.

[114] Y. Wang, W. Wang, J. Huang, R. Yu, J. Yang, and S. Chen, "Reactive composite brazing of C/C composite and GH3044 with Ag–Ti mixed powder filler material," *Mater. Sci. Eng. A*, 2019, doi: 10.1016/j.msea.2019.05.065.

[115] X. Song, Y. Zhao, S. Hu, J. Cao, W. Fu, and J. Feng, "Wetting of AgCu-Ti filler on porous Si3N4 ceramic and brazing of the ceramic to TiAl alloy,"

Ceram. Int., vol. 44, no. 5, pp. 4622–4629, 2018, doi: 10.1016/j.ceramint.2017.11.212.

[116] H. Xu, Y. Zhao, J. Yang, J. Huang, S. Chen, and Z. Ye, "Investigation on wetting behavior and mechanism of AgCu-Xwt.%Ti filler metal/AlN ceramic reactive wetting system: Experiments and first-principles calculations," *J. Alloys Compd.*, 2021, doi: 10.1016/j.jallcom.2021.159323.

[117] X. Huang, X. Li, and Y. Li, "Wetting kinetics and interfacial structure of AgCu alloy spreading on TB8 substrates," *Mater. Res. Express*, 2019, doi: 10.1088/2053-1591/ab2516.

[118] X. Song, J. Cao, X. Lin, and J. Feng, "Interfacial structure and properties of Si3N4/AgCu/TiAl brazing joints," *Xiyou Jinshu Cailiao Yu Gongcheng/Rare Met. Mater. Eng.*, 2011.

[119] X. Dai, J. Cao, Z. Chen, X. Song, and J. Feng, "Brazing SiC ceramic using novel B4C reinforced Ag-Cu-Ti composite filler," *Ceram. Int.*, vol. 42, no. 5, pp. 6319–6328, 2016, doi: 10.1016/j.ceramint.2016.01.021.

[120] J. Xiong, J. Huang, Z. Wang, G. Lin, H. Zhang, and X. Zhao, "Joining of Cf/SiC composite to Ti alloy using composite filler materials," *Mater. Sci. Technol.*, vol. 25, no. 8, pp. 1046–1050, 2009, doi: 10.1179/174328408X378889.

[121] J. H. Xiong, J. H. Huang, H. Y. Xue, H. Zhang, X. K. Zhao, and G. B. Lin, "Joining of Cf/SiC composite to Ti alloy using AgCuTi-W composite filler materials," *Hangkong Cailiao Xuebao/Journal of Aeronautical Materials*, vol. 29, no. 6. pp. 48–52, 2009, doi: 10.3969/j.issn.1005-5053.2009.6.010.

[122] Y. M. He, J. Zhang, C. F. Liu, and Y. Sun, "Microstructure and mechanical properties of Si3N4/Si3N4 joint brazed with Ag-Cu-Ti + SiCp composite filler," *Mater. Sci. Eng. A*, 2010, doi: 10.1016/j.msea.2010.01.065.

[123] W. Wang, D. Fan, J. Huang, C. Li, J. Yang, and S. Chen, "Microstructural

mechanism and mechanical properties of Cf/SiC composite/TC4 alloy joints composite-diffusion brazed with TiZrCuNi + TiCp composite filler," *Mater. Sci. Eng. A*, vol. 728, no. April, pp. 1–9, 2018, doi: 10.1016/j.msea.2018.04.091.

[124] X. R. Song, H. J. Li, and X. Zeng, "Brazing of C/C composites to Ti6Al4V using multiwall carbon nanotubes reinforced TiCuZrNi brazing alloy," *J. Alloys Compd.*, vol. 664, pp. 175–180, 2016, doi: 10.1016/j.jallcom.2015.12.242.

[125] G. Lin, J. Huang, H. Zhang, and X. Zhao, "Joints of Cf/SiC composite to Ti-alloy with in-situ synthesized TiC x improved brazing layers," *Mater. Trans.*, 2006, doi: 10.2320/matertrans.47.1261.

[126] G. B. Lin and J. H. Huang, "Brazed joints of Cf-SiC composite to Ti alloy using Ag-Cu-Ti-(Ti+C) mixed powder as interlayer," *Powder Metall.*, 2006, doi: 10.1179/174329006X113454.

[127] D. Liu, K. Zhao, Y. Song, L. Zhang, X. Song, and W. Long, "Effect of introducing carbon fiber into AgCuTi filler on interfacial microstructure and mechanical property of C/C-TC4 brazed joints," *Mater. Charact.*, vol. 157, no. July, p. 109890, 2019, doi: 10.1016/j.matchar.2019.109890.

[128] Y. Wang, W. Wang, J. Huang, S. Zhou, J. Yang, and S. Chen, "Composite brazing of C/C composite and Ni-based superalloy using (Ag-10Ti)+TiC filler material," *J. Mater. Process. Technol.*, 2021, doi: 10.1016/j.jmatprotec.2020.116886.

[129] D. Bridges, C. Ma, S. Zhang, S. Xue, Z. Feng, and A. Hu, "Diffusion and wetting behaviors of Ag nanoparticle and Ag nanowire pastes for laser brazing of Inconel 718," *Weld. World*, 2018, doi: 10.1007/s40194-017-0526-x.

[130] R. Eluri and B. K. Paul, "Silver nanoparticle-assisted diffusion brazing of 3003 Al alloy for microchannel applications," *Mater. Des.*, 2012, doi: 10.1016/j.matdes.2011.11.005.

[131] W. Wang, Y. Wang, J. Huang, R. Yu, J. Yang, and S. Chen, “Joining of Cf/SiC composite and stainless steel via Ag+Ti filler in-situ alloying,” *J. Mater. Process. Technol.*, 2019, doi: 10.1016/j.jmatprotec.2019.116295.

[132] J. John Williams and J. John, “Structure and high-temperature properties of Ti5Si3 with interstitial additions Recommended Citation,” 1999, [Online]. Available: https://lib.dr.iastate.edu/rtd/12494.

[133] M. P. Reddy *et al.*, “Enhanced performance of nano-sized SiC reinforced Al metal matrix nanocomposites synthesized through microwave sintering and hot extrusion techniques,” *Prog. Nat. Sci. Mater. Int.*, 2017, doi: 10.1016/j.pnsc.2017.08.015.

[134] F. Wang, L. Cheng, and S. Liang, “Effects of Pore on Thermal Diffusivity and Thermal Radiation Properties of C/SiC Composites at High Temperatures,” *Appl. Compos. Mater.*, 2019, doi: 10.1007/s10443-019-09787-1.

[135] J. Chen, Y. Wang, L. Cheng, and L. Zhang, “Thermal diffusivity of three-dimensional needled C/SiC-TaC composites,” *Ceram. Int.*, 2011, doi: 10.1016/j.ceramint.2011.05.046.

[136] L. Cheng, Y. Xu, Q. Zhang, and L. Zhang, “Thermal diffusivity of 3D C/SiC composites from room temperature to 1400 °C,” *Carbon N. Y.*, 2003, doi: 10.1016/S0008-6223(02)00382-2.

[137] K. Li *et al.*, “Effects of fabric architectures on the thermal expansion coefficient and the thermal diffusivity of carbon fiber reinforced silicon carbide composites,” *Kuei Suan Jen Hsueh Pao/ J. Chinese Ceram. Soc.*, 2008.

[138] C. W. Nan, G. Liu, Y. Lin, and M. Li, “Interface effect on thermal conductivity of carbon nanotube composites,” *Appl. Phys. Lett.*, 2004, doi: 10.1063/1.1808874.

[139] C. W. Nan, Z. Shi, and Y. Lin, “A simple model for thermal conductivity of

carbon nanotube-based composites," *Chem. Phys. Lett.*, 2003, doi: 10.1016/S0009-2614(03)00956-4.

[140] K. F. Chan, M. H. M. Zaid, M. S. Mamat, S. Liza, M. Tanemura, and Y. Yaakob, "Recent developments in carbon nanotubes-reinforced ceramic matrix composites: A review on dispersion and densification techniques," *Crystals*, 2021, doi: 10.3390/cryst11050457.

[141] X. C. Tong, "Thermally Conductive Ceramic Matrix Composites," in *Springer Series in Advanced Microelectronics*, 2011.

[142] A. G. Lanin, "Effect of residual stresses on the strength of ceramic materials (Review)," *Russian Metallurgy* 2012, doi: 10.1134/S0036029512040076.

[143] J. X. Zhang, R. S. Chandel, Y. Z. Chen, and H. P. Seow, "Effect of residual stress on the strength of an alumina-steel joint by partial transient liquid phase (PTLP) brazing," *J. Mater. Process. Technol.*, 2002, doi: 10.1016/S0924-0136(02)00010-9.

[144] H. Yang, L. Gao, R. Yuan, K. R. Kim, and J. Y. Jung, "Effect of residual stress on the bending strength of ground Al2O3/TiCN ceramics," *Mater. Chem. Phys.*, 2003, doi: 10.1016/S0254-0584(02)00520-5.

[145] K. Zhang, L. Zhang, R. He, K. Wang, K. Wei, and B. Zhang, "Joining of Cf/SiC Ceramic Matrix Composites: A Review," *Advances in Materials Science and Engineering*. 2018, doi: 10.1155/2018/6176054.

[146] C. Li, Z. Wang, X. Si, J. Qi, J. Feng, and J. Cao, "Review on the Research of the Joining of Lightweight Metals and Ceramics," *Jixie Gongcheng Xuebao/Journal of Mechanical Engineering*. 2020,

[147] E. Wulf, H. Bachmann, K. Möhwald, R. Eifler, and H. J. Maier, "The influence of brazing temperature and surface roughness on the wettability of reactive brazing alloys," *Int. J. Mater. Res.*, 2014, doi: 10.3139/146.111022.

CURRICULUM VITAE

PERSONAL INFORMATION

Saltık, Simge

EDUCATION

Degree	Institution	Year of Graduation
MS	METU Metallurgical and Materials Engineering	2015
BS	METU Metallurgical and Materials Engineering	2012
High School	Edirne Anatolian Teacher's Training High School	2007

WORK EXPERIENCE

Year	Place	Enrollment
2012-2013	Atılım University, Metallurgical and Materials Engineering	Research Assistant
2013-2016	METU, Metallurgical and Materials Engineering	Research Assistant
2016-2018	ROKETSAN, Advanced Materials and Technologies Department	Engineer
2018-2020	ROKETSAN, Advanced Materials and Technologies Department	Specialist Engineer
2020-2021 August	ROKETSAN, Advanced Materials and Technologies Department	Senior Engineer
2021 August-present	ROKETSAN, Advanced Materials and Technologies Department	Technical Leader

FOREIGN LANGUAGES

Advanced English, Elementary German

PUBLICATIONS

1. Tulbez S, Esen Z, Dericioglu A (2020) Effect of CNT impregnation on the mechanical and thermal properties of C/C-SiC composites. Adv Compos Hybrid Mater. *doi: 10.1007/s42114-020-00155-3.*
2. Saltık S, Esen Z, Dericioglu A (2021) Wetting Behavior and Reaction Layer Formation in C/SiC. Adv. Mater. Process. Technol. *doi: 10.1080/2374068x.2021.1971001*

CONFERENCES

1. **Simge Tülbez,** Arcan F. Dericioğlu, *Effect of Pyrolysis Temperature on the Efficiency of C/C-SiC Composite Production,* IMMC 2014, 17th International Metallurgy and Materials Congress, September 2014, Istanbul, TURKEY.

2. Aylin Güneş, **Simge Tülbez,** Arcan F. Dericioğlu, *Processing and Characterization of Glass Flake-Reinforced Thermoplastic Polymer Matrix Bio-Inspired Bulk Lamellar Composites*, IMMC 2014, 17th International Metallurgy and Materials Congress, September 2014, Istanbul, TURKEY.

3. **Simge Tülbez,** Arcan F. Dericioğlu, *Processing and Characterization of Carbon Fiber Reinforced Silicon Carbide (C/SiC) Matrix Composites*, TMS 2015, 144th Annual Meeting and Exhibition, Orlondo, FL, USA.

4. **Simge Tülbez,** Arcan F. Dericioğlu, *Optimization of Pyrolysis and Liquid Silicon Infiltration Parameters for the Processing of C/C-SiC Composites,* IMMC 2016, 18th International Metallurgy and Materials Congress, October 2016, Istanbul, TURKEY.

5. Emel Erdal, **Simge Tülbez,** Arcan F. Dericioğlu, *Synthesis of BaHF Ceramics by Microwave Heating*, IMMC 2016, 18th International Metallurgy and Materials Congress, October 2016, Istanbul, TURKEY.

6. **Simge Tülbez,** Ziya Esen, Arcan F. Dericioğlu, *Investigations on Alternative Matrix Materials Towards the Efficiency of SiC Formation in C/SiC Ceramic Composites,* IMMC 2018, 19th International Metallurgy and Materials Congress, 25-27 October 2018, Istanbul, TURKEY.

7. **Simge Tülbez,** Arcan F. Dericioğlu, *Interfacial Reaction Kinetics and Microstructural Evolution of C/SiC Composıtes To Titanıum Alloy Joints*, HT-CMC10, 19th International Conference on Ceramic Matrix Composites, 22-26 September 2019, Bordeux, FRANCE.

8. **Simge Tülbez,** Ziya Esen, Arcan F. Dericioğlu, *Effect of Brazing Parameters on The Microstructural and Mechanical Characteristics of Ceramic Matrix Composite/Titanium Alloy Brazed Joints*, IMMC 2021, 20th International Metallurgy and Materials Congress, September 2021, TURKEY.